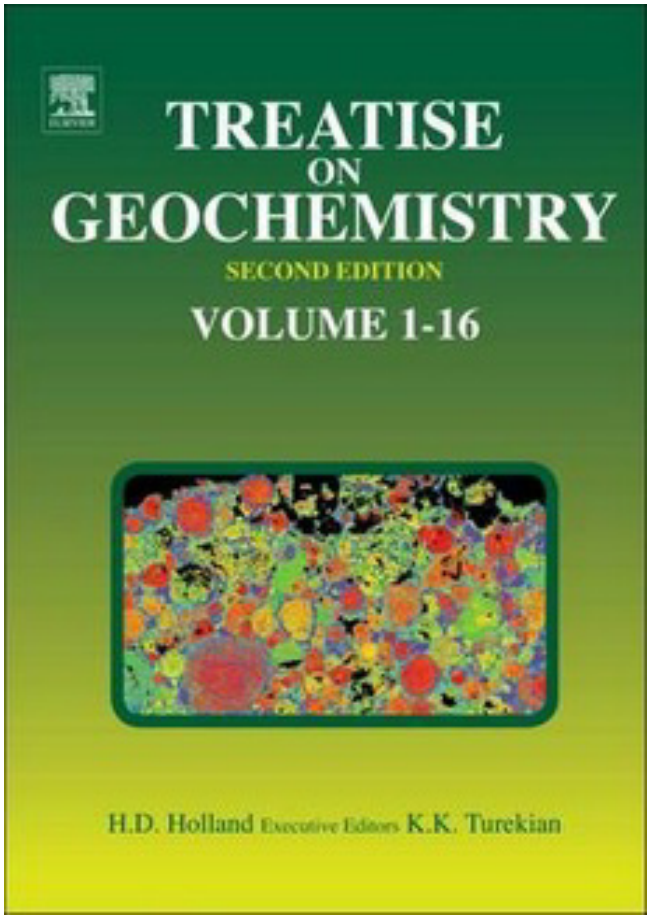

Saunders J.A., Hofstra A.H., Goldfarb R.J. and Reed M.H. (2014) Geochemistry of Hydrothermal Gold Deposits. In: Holland H.D. and Turekian K.K. (eds.) Treatise on Geochemistry, Second Edition, vol. 13, pp. 383-424. Oxford: Elsevier.

13.15 Geochemistry of Hydrothermal Gold Deposits

JA Saunders, Auburn University, Auburn, AL, USA
AH Hofstra, U.S. Geological Survey, Denver, CO, USA
RJ Goldfarb, U.S. Geological Survey, Denver, CO, USA
MH Reed, University of Oregon Eugene, OR, USA

13.15.1 Introduction

The geochemistry of the three most significant hydrothermal gold deposit types, epithermal, Carlin-type, and orogenic, is described in this article. The geologic characteristics of these deposits are discussed in detail elsewhere (Cline et al., 2005; Goldfarb et al., 2005; Simmons et al., 2005), and their general geotectonic settings and relationship to other important deposit types are summarized in Figure 1.

Another important hydrothermal gold deposit type, porphyry copper–gold deposits, is not discussed here. Among the three deposit classes considered, the high-sulfidation epithermal and probably most low-sulfidation epithermal deposits are genetically linked to coeval magmas and magmatic

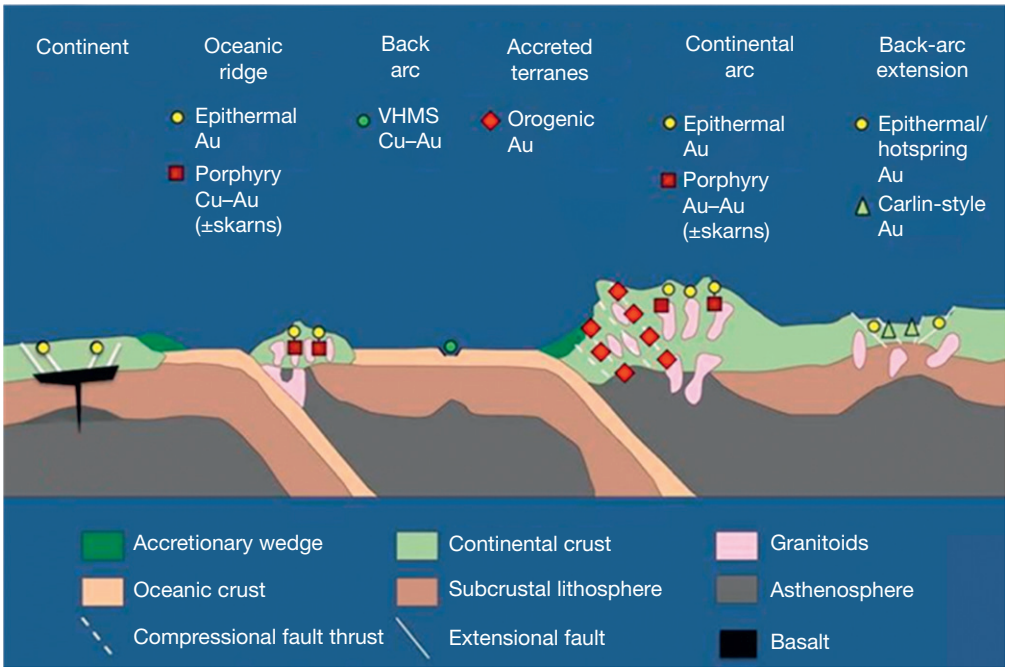

Figure 1 Diagrammatic illustration showing the geotectonic settings of the gold deposits discussed here and some associated ores types (Groves et al., 1998).

fluids, although it is clear that there is a large component of meteoric water in the ore-forming solutions (Saunders et al., 2008). Carlin-type deposits (CTD) might also have a magmatic fluid source although the magmatic connection is still seriously debated (Cline et al., 2005; Emsbo et al., 2006). Magmatic fluids are not involved in the third deposit class considered here, orogenic gold, which formed from metamorphic fluids released along active collisional or compressive plate boundaries (Goldfarb et al., 2005; Groves et al., 1998). Together, deposits of these three ore types account for ~75% of the gold mined globally from lodes.

Since the time of Boyle's (1979) description of the geochemistry of the entire spectrum of gold deposits, there have been some significant advances in knowledge based in part on new geochemical analytical techniques. These include multielement inductively coupled plasma optical emission spectrometry (ICP-OES) and ICP mass spectrometry (ICP-MS) analysis; high-precision and *in situ* stable and radiogenic isotopic analyses; development of stable isotopic techniques for zinc, copper, selenium, and iron; new geochronologic tools such as single-crystal zircon U–Pb and $^{40}Ar/^{39}Ar$ analyses; and laser ablation (LA)-ICP-MS of minerals, and single fluid inclusions to measure dissolved species. The new analytical techniques have led to a better understanding of the geochemistry not only of the ores and fluids but also of the ore-forming processes, which can now be well constrained by computer modeling founded on a wealth of new thermodynamic data.

13.15.2 Epithermal Deposits

13.15.2.1 Introduction

The term epithermal was coined by Lindgren (1933) to refer to deposits formed near the surface in genetic connection with igneous rocks at temperatures and pressures that he inferred to be less than 200 °C and ~100 bars. The term is still applied to ore settings where a link to a magmatic fluid source is implied by the proximity of the ores to contemporaneous volcanic or intrusive rocks, but, in practical terms, epithermal ores are distinguished by particular assemblages of ore minerals and wall rock alteration minerals and by ore textures and structures that indicate a shallow crustal setting. They are most commonly mined for gold and silver, although copper, lead, and zinc are also abundant in many such ores. Modern fluid inclusion microthermometry (Hedenquist and Henley, 1985; Nash, 1972; Simmons et al., 2005) has extended the temperature range of epithermal ores to about 300 °C and indicates typical pressures up to many hundreds of bars.

Epithermal precious-metal ores occur widely in Tertiary and younger rocks throughout the Pacific Rim and in other Phanerozoic orogenic belts worldwide. The shallow setting of epithermal ores leads to their relatively rapid erosion and skews the ages of known deposits to Cretaceous and younger, but many older deposits are known. They are tied to volcanism in a variety of geotectonic settings and exhibit a wide range of mineralogical and geochemical characteristics. Epithermal ores have been classified a number of different ways but most recognize that there are two end-member deposit types: (1) deposits that occur above coeval magmas, typified by advanced argillic alteration with gold, enargite, covellite and pyrite, and fluid inclusions of moderate to high salinity; and (2) deposits in veins, breccias, and stockworks that typically flank a magmatic center, where gangue minerals such as adularia, sericite, and carbonates occur with ores containing electrum, acanthite, and silver-bearing sulfosalts, as well as locally abundant selenide and telluride minerals, all with fluid inclusions of low salinity. Between these end-members are epithermal vein ores commonly dominated by sulfides of

zinc, lead, copper, and silver with additional silver and gold in electrum, and fluid inclusions of moderate salinity. In the terminology of Hedenquist et al. (2000) and Sillitoe and Hedenquist (2003), the first category mentioned earlier is termed high-sulfidation (HS) and the second is called low-sulfidation (LS), and the transitional ore type between these two is termed intermediate sulfidation (IS). In this article, focused on gold ores, the geochemistry of the two end-member types is described because gold is the economically dominant precious metal in these two forms of mineralization. Although the authors apply the 'sulfidation' classification terms here because they have been widely adopted, alternative classifications that distinguish the same categories using descriptive schemes are also widely used, as outlined by Simmons et al. (2005).

13.15.2.2 Low-Sulfidation Epithermal Deposits

The global abundance of LS ores may reflect the numerous geotectonic settings where they form. Most LS ores formed in settings where earlier subduction enriched the lithospheric mantle above the subducted plate with volatiles and metals. Partial melting of this subduction-enriched mantle wedge produced magmas that yielded porphyry and epithermal mineralization (e.g., Richards, 2009; Saunders and Brueseke, 2012). The LS ores are typically hosted by basalt–rhyolite calc-alkaline volcanic rocks in predominantly extensional environments in intra-arc, near-arc, and back-arc postcollisional rifts (Sillitoe and Hedenquist, 2003). The LS ores are generally similar in age to the nearby or host volcanic rocks (Hames et al., 2009; Izawa et al., 1990; Leavitt et al., 2004; Tohma et al., 2010). New high-precision geochronology suggests that ore formation was of relatively short duration, perhaps as brief as a few thousand to a few tens of thousands of years (Heinrich, 2006; Saunders, 2010; Simmons and Brown, 2006; Tohma et al., 2010). Some large LS deposits (Ladolam, Porgera, and Cripple Creek) formed in association with alkaline rocks in a variety of convergent-margin extensional settings, as opposed to well-developed rifts, and have some geologic characteristics somewhat atypical of most LS deposits (Richards, 1995; Sillitoe and Hedenquist, 2003).

The diversity of geotectonic and magmatic processes responsible for forming LS ores in a single setting is well illustrated by the Miocene–Pliocene deposits of the northern Great Basin of the USA. John (2001) showed that these LS ores are contemporaneous with two different host petrogenetic magma suites that reflect variations in the geotectonic setting: (1) continental rift-related bimodal rhyolite and basalt that is K-rich tholeiite and (2) a subduction-related andesite > dacite, oxidized high-K, calc-alkaline volcanic assemblage. The LS Sleeper, National, Midas, and Mule Canyon deposits are hosted by the bimodal suite, whereas LS deposits such as the Comstock Lode and Tonopah and HS ores such as Goldfield and Paradise Peak are in the subduction-related andesite assemblage (John, 2001). Saunders et al. (1996, 2008) and Kamenov et al. (2007) proposed that the 16–14 Ma LS ores in northern Nevada and southwestern Idaho associated with the bimodal volcanic assemblage were genetically related to the initial emergence of the Yellowstone hotspot mantle plume. John (2001) concluded that these LS ores were more directly related to the Northern Nevada Rift (NNR) but also proposed that the NNR was formed by the Yellowstone hotspot.

There are important exceptions to the general rule that LS ores are formed during regional extension. For example, the Plio-Pleistocene McLaughlin deposit formed in a transpressive setting within the San Andreas fault system (Sherlock et al., 1995; Sillitoe and Hedenquist, 2003). In summary, LS ore formation may have deep roots, apparently initiated by partial melting of a 'prepared' lithospheric mantle (Richards, 2009; Saunders and Brueseke, 2012).

13.15.2.2.1 Trace elements and mineral associations

The LS gold deposits are commonly enriched in Ag, As, Au, Hg, Sb, Se, Te, and locally Tl, a group of elements generally known as the 'epithermal suite.' Base metals, Cu, Pb, and Zn, are also locally abundant and some ores become relatively enriched with the base metals at deeper levels in veins and thus resemble the IS ore type. In addition, Mo, Sn, V, and W may be enriched in LS ores and in their altered wall rock (Jensen and Barton, 2000; John et al., 2003; Simmons et al., 2005). In the northern Great Basin of the USA, chalcopyrite is particularly abundant in the highest grade LS ores (Saunders et al., 2011a). This is true also in the bonanza LS gold ores at Hishikari (**Figure 2**; Izawa et al., 1990; Nagayama, 1993; Shikazono and Nagayama, 1993), Kushikino (Matsuhisa et al., 1985), and Koryu (Shimizu et al., 1998a, 1998b). At Hishikari, there is a stronger statistical correlation between Au and Cu than there is between Au and Ag (Nagayama, 1993). HS ores are also very much enriched in Cu, as discussed in the succeeding text. Because of the abundance of telluride and selenide minerals in some LS ores, Lindgren (1933) separated them into separate epithermal subclasses. Typically tellurides and selenides do not occur together, but there are exceptions such as at the Prasolovskoye deposit, Kunashir Island, Kuril island arc (So et al., 1995). In the telluride ores of Colorado, calaverite ($AuTe_2$), sylvanite ($AuAgTe_4$), krennerite [$(Au,Ag)Te_2$], petzite (Ag_3AuTe_2), hessite (Ag_2Te), native gold or electrum, and tetrahedrite are the main ore minerals, but native Te and tellurides of Fe, Ni, Pb, and Hg are also locally abundant (Saunders, 1988, 1991; Saunders and May, 1986). An interesting geochemical and mineralogical association in Colorado, as well as worldwide for LS telluride-rich ores, is the ubiquitous presence of the V-bearing mica roscoelite. In a study of several Colorado LS telluride ores, Saunders (1986) showed that the ores were very similar irrespective of whether they formed during Laramide subduction or later rifting. Saunders (1986) also showed that the country rocks that hosted the ores were highly variable in their composition and age and thus apparently were not the source of the precious metals, Te, or V. However, Jensen and Barton (2000) recognized a correlation between the amount of mafic wall rock and V content of veins and alteration minerals. Saunders et al. (2008) concluded that the host rocks were not the source of Au, Ag, and Se in the bonanza LS ores of the northern Great Basin; the precious metals and Se apparently are derived from deeper mafic magmatic sources based on Pb isotope data (Kamenov et al., 2007). However, country rocks in the upper crust apparently did contribute some major chemical constituents in the ores (e.g., silica, Na, K, Ca, and Al; Saunders et al., 2008).

Figure 2 (Left) Photograph of banded Ryosen no. 6 vein, Hishikari deposit, Japan, which is up to 2 m thick. (Right) Photograph of the Colorado Grande vein at the Midas deposit, Nevada, which is approximately 1 m thick in the image. Note fragments of wall rocks encrusted by silica in the vein.

13.15.2.2.2 Ore fluid characteristics

Studies of fluid inclusions trapped in gangue minerals show that LS ores, or at least the gangue minerals, typically formed at 150–300 °C, from dilute solutions, typically 0.1 to ~5.0% NaCl equivalent (Hedenquist and Henley, 1985; Nash, 1972; Simmons et al., 2005). The more telluride-rich LS examples typically have slightly higher dissolved salt contents of 5–9% NaCl equivalent (Ahmad et al., 1987; Saunders, 1988, 1991; Saunders and May, 1986). However, telluride-rich ore-forming fluids are often CO_2 rich, which depresses the melting point of ice in the inclusions such that the salinity value will be erroneously high unless the CO_2-clathrate melting temperature is used to determine the salinity (Hedenquist and Henley, 1985). The fluid inclusion observations often show that the ore-forming solutions were boiling, which is an effective mechanism for depositing precious metals from solution (Spycher and Reed, 1989) and is also commonly observed in geothermal systems at depth (e.g., Hedenquist, 1991). The low salinities of fluid inclusions are largely consistent with H–O isotope ratio measurements, which show that the vein-forming solutions are predominantly heated groundwaters with some degree of oxygen isotopic exchange with the surrounding country rocks, as occurs in active geothermal systems (Hedenquist, 1991; Simmons et al., 2005). In fact, at the <1 Ma Hishikari deposit (**Figure 2**), where veins formed at ~200–220 °C (Etoh et al., 2002; Izawa et al., 1990), 70 °C water is still discharging along the vein structure. In contrast to the predominant meteoric-water source in the ore-forming fluids, detailed sulfur isotope studies (Jensen, 2003; John et al., 2003; Shelton et al. 1990; So and Yun, 1996; Yuningsih et al., 2011; Zhang and Spry, 1994) on LS epithermal ores suggest that sulfur in sulfide minerals associated with precious-metal minerals has a magmatic source (e.g., $\delta^{34}S$ values in the −5 to +5‰ range) or perhaps a mixture of magmatic and host-rock sulfur (Castor et al., 2003).

13.15.2.2.3 Hydrothermal alteration

Hydrothermal alteration in LS deposits can be subdivided into (1) K-feldspar or sericite- and chlorite-altered wall rock bordering veins at depth; and (2) the overlying draping blanket of pervasive intermediate and advanced argillic alteration and silicification. The latter is produced by downward percolating near-surface waters acidified by oxidized H_2S gases and by CO_2 condensation, both accompanied by cooling of silica-rich waters. At the district scale, there is additional regional propylitic alteration (not specifically related to precious-metal mineralization) consisting of chlorite, epidote, and calcite that is particularly evident in volcanic host rocks.

Hydrothermal alteration associated with LS ores is interpreted as a product of complex water–rock–vapor interactions. For example, acid volatiles released from a cooling magma chamber or boiling solutions at depth are incorporated into the heated groundwater comprising the geothermal system where an epithermal vein forms. This decreases the pH of the geothermal waters and can lead to local acid argillic alteration or even complete destruction of the host rocks at very low pH, such as in the mud pots of advanced argillic alteration at Yellowstone National Park. This local advanced argillic alteration, which forms the common steam-heated blankets in the LS epithermal environment, should not be confused with the pervasive advanced argillic alteration intimately associated with HS ores discussed in the succeeding text. In LS ores, advanced argillic alteration is caused by oxidation of H_2S at and above the water table to H_2SO_4 (Hedenquist, 1991). Hydrothermal alteration of the country rock may be produced prior to ore deposition by lower-pH solutions than those that deposit the precious metals. For example, there is widespread pervasive alteration of the volcanic rocks at Cripple Creek, Colorado (Jensen and Barton, 2000), but lamprophyre breccia fragments coated with ore and gangue minerals, such as calaverite, petzite, dolomite, and quartz, deep in the Cresson

diatreme at Cripple Creek (−2200 level in the 1930s mining), are virtually unaltered, suggesting that ore-forming solutions were not very corrosive at a relatively low temperature of ~185 °C (Saunders, 1988). The Bessie G Au–Ag–Te deposit in Colorado is another example of very weak hydrothermal alteration associated with LS ore-forming solutions. At Bessie G, the host rocks for the vein are Mesozoic siltstones and sandstones, and associated silicification extends only a few centimeters into the wall rocks (Saunders and May, 1986). It is likely that hydrothermal alteration of wall rocks provides most of the chemical constituents to form the non-ore minerals in the veins (Saunders et al., 2008). For example, at the Sleeper deposit in Nevada, glassy rhyolites hosting the ore were the source of high concentration of silica in ore-forming fluids that deposited opal (**Figure 3**) in the high-grade veins (Saunders and Schoenly, 1995). In contrast, the Mule Canyon deposit in Nevada, hosted predominantly by basalts, lacks significant amounts of silica in the ores (John et al., 2003). Saunders et al. (2008) observed that some very adularia-rich LS epithermal veins in Nevada, such as those at Jumbo, Tenmile, and Sandman, were hosted by metapelites and proposed that these were the source for the Al, Si, and K. Leaching of Al from wall rocks requires low-pH geothermal waters presumably caused by absorption of acid volatiles from below. However, most LS ores appear to have formed from near-neutral pH solutions. This apparent disparity can best be explained by widespread boiling in fractures that leads to a significant pH increase (Drummond and Ohmoto, 1985; Spycher and Reed, 1989) primarily because of loss of CO_2. Thus, boiling causes platy calcite formation (Simmons and Christensen, 1994), precious-metal precipitation by H_2S loss, base metal precipitation by pH increase, and deposition of silica, adularia, and sericite.

The general geochemistry of LS ore-forming fluids is fairly well established (see Reed, 1997; Saunders and Schoenly, 1995; Spycher and Reed, 1989). Ore-forming solutions are typically near-neutral pH, consistent with deposition of adularia, sericite, and/or carbonate, moderately reducing (pyrite-stable), and contain significant amounts of H_2S and minor CO_2. Gold and silver in these ore-forming fluids typically form stable aqueous complexes with H_2S(aq) and its deprotonated equivalent, bisulfide (HS^-). The H_2S(aq) is the quintessential 'soft Lewis acid' and, consequently, makes strong covalent bonds with soft Lewis bases, such as Au, Ag, Hg, As, Sb, Te, and Se (Langmuir, 1997; Saunders et al., 2008). The implications of this are threefold: (1) H_2S-rich fluids will dissolve significant amounts of Au and Ag, although how much is debated (see Brown, 1986; Saunders, 2010; Saunders and Schoenly, 1995; Simmons and Brown, 2006); (2) H_2S in the ore-forming fluid causes the epithermal suite of elements to travel together; and (3) high levels of dissolved H_2S suppresses the solubility of base metals such as Fe, Pb, Zn, and Cu (Saunders and Schoenly, 1995). A number of physicochemical processes can lead to Au precipitation from a neutral pH, moderately reduced, H_2S-rich ore-forming fluid, including boiling, mixing with cooler and more dilute groundwaters, reaction with wall rocks, particularly iron minerals, oxidation, and simple cooling. All of these processes may be important locally in LS ores and, in some cases, more than one may induce ore mineral precipitation. Boiling (Drummond and Ohmoto, 1985; Romberger, 1988; Saunders and Schoenly, 1995; Spycher and Reed, 1989) can be the paramount process in LS ore formation, particularly when the solutions are significantly undersaturated with respect to gold (Brown, 1986; Spycher and Reed, 1989).

Figure 3 Photograph of an opal-electrum band encrusted by later silica-only bands from the Sleeper deposit, Nevada. In detail, the bands consist of three-dimensional dendrites of electrum formed by aggregation of colloids; top of the image is toward the vein center (see Saunders, 1990, 1994). Scale bar = 0.5 cm

Taylor (2007) posed the question as to whether Au-rich epithermal deposits form mainly due to gold-enriched sources, such as fluids or magmas, or from exceptionally efficient mechanisms or processes of Au precipitation. Saunders (2010) argued for the latter possibility, at least in the formation of bonanza epithermal ores, based on new data indicating how short-lived epithermal ore-forming processes can be. Nevertheless, in support of the former, Saunders and Schoenly (1995) found that ore-forming solutions at the Sleeper deposit may have contained as much as several ppm of dissolved gold, which was about three orders of magnitude higher than observed in the geothermal solution from Ohaaki-Broadlands, New Zealand (Brown, 1986). If one assumes a boiling geothermal system is generally part of an LS epithermal ore-forming system (but not necessarily directly related to ore deposition; e.g., Saunders et al., 2008), then what additional requirement is needed to make a bonanza epithermal deposit and not just a low-grade or barren geothermal system? Perhaps the answer lies in understanding controls on the formation of gold- and volatile-rich, shallow magmas that episodically release their metalloids and volatiles within the porphyry environment. Increasingly, there appears to be a connection between hydrothermal processes in the deeper porphyry setting and much shallower epithermal setting (e.g., Hedenquist and Lowenstern, 1994; Heinrich, 2005; Heinrich et al., 2004).

13.15.2.2.4 Geochemistry of the Midas LS deposit, Nevada

The Midas deposit of northern Nevada consists of LS epithermal veins that are chosen here as a representative example of LS epithermal systems because of its excellent documentation and its characteristics that exemplify LS ores. Details of the general geology the Midas district and veins are summarized here from Goldstrand and Schmidt (2000), Leavitt et al. (2004), Leavitt and Arehart (2005), Riederer (2007), and Chitwood (2012). Further, the Midas deposit has experienced little post-ore faulting or erosion. It is also considered a world-class deposit,

containing a resource of ~125 t Au and 1250 t of Ag (Leavitt et al., 2004). Although there had been some gold production in the district in the early 1900s (~3 t), it was not until the early 1990s that the large veins were discovered at Midas. Not long after, Saunders et al. (1996) and John (2001) proposed that Midas was just one of a clan of mid-Miocene bonanza epithermal deposits in the northern Great Basin, including National, Sleeper, Mule Canyon, Buckskin National, DeLamar, and Ivanhoe that formed during the volcanism attending the initial emergence of the Yellowstone hotspot.

From a geochemical standpoint, Midas and similar deposits of the northern Great Basin contrast to some extent with LS ores worldwide because of their Se enrichment. Lindgren (1933) recognized the importance of these Se-rich ores and proposed they were a subclass of epithermal ores. Although the mid-Miocene northern Great Basin LS ores are enriched in Se, this does not relate specifically to the Yellowstone hotspot and/or NNR. Saunders and Brueseke (2012) pointed out that similar Se-rich bonanza LS ores occur in the Eocene Republic district of Washington and the Plio-Pleistocene epithermal ores of Japan. Thus, Se-rich LS epithermal ores do not necessarily relate to a mantle plume, but perhaps require rifting-induced partial melting of a fertile lithospheric mantle wedge (Saunders and Brueseke, 2012) that is enriched in Se. Alternatively, John et al. (2003) suggested that black shales could be the source of Se at the Mule Canyon LS deposit of northern Nevada.

Midas exhibits many geologic characteristics common to LS bonanza veins, such as (1) well-defined vein structures typically exhibiting fine to coarse banding caused by successive ore and gangue mineral deposition on vein walls (**Figure 2**) indicating multiple episodes of precious-metal deposition; (2) electrum as the principal ore mineral; (3) general lack of sulfides coprecipitated with precious metals during bonanza ore formation, although chalcopyrite and pyrite are common locally; (4) local ore mineral textures consistent with colloid aggregation and physical transport of colloids in the ore-forming solutions (e.g., Saunders et al., 2011b); (5) fluid inclusion and other evidence (e.g., pyrite replacing marcasite, formation of bladed calcite that typically then gets replaced by silica, adularia precipitation, and elevation controls on ore zones) that hydrothermal solutions boiled at the time of ore deposition; and (6) ore veins and host volcanic rocks are close in age. The Midas district lies along the eastern edge of the NNR, but also it and the nearby mid-Miocene Ivanhoe LS epithermal district lie along the northwestern extension of the Carlin Trend that contains numerous Eocene world-class, sediment-hosted gold deposits described in the succeeding text (John, 2001; Leavitt et al., 2004).

The bonanza veins at Midas are hosted by an assemblage of mid-Miocene bimodal volcanic and sedimentary rocks, including mafic dikes, sills, and lava flows; rhyolitic tuffs, including air-fall, ash-flow, and vitrophyres, and flows; and carbonaceous and locally tuffaceous siltstone (Goldstrand and Schmidt, 2000; Leavitt et al., 2004). The $^{40}Ar/^{39}Ar$ geochronology by Leavitt et al. (2004) and Hames et al. (2010) has shown that volcanism at Midas initiated with eruption of apparently pre-ore basalts from $16.32 + 0.17$ to $15.51 + 0.07$ Ma, which were overlain by rhyolitic flows and tuffs (~15.6 Ma). Bonanza veins formed at ~15.4 Ma at Midas and the nearby Ivanhoe district. A post-ore rhyolitic tuff overlying the mineralized rock has an age of 15.2 Ma. The similarity in age of the rhyolitic rocks at Midas to the ores led Leavitt et al. (2004) to propose that rhyolites contributed both heat and metals to drive the ore-forming solutions. However, Pb isotope data presented by Saunders et al. (2011c) suggests that Pb in electrum at Midas was derived from a mafic rock source, perhaps a deeper magma chamber that was the source of the mafic sills, dikes, and flows exposed in underground workings in the district.

Major veins at Midas include the Colorado Grande and Discovery, along with the Gold Crown vein that is a footwall split off the Colorado Grande vein. Recent drilling and underground workings have encountered additional, much more silver-rich and smaller veins to the east of the main producing veins (Chitwood, 2012). Most of the production from Midas to date has come from the Colorado Grande vein, which has a strike length of ~1.5 km and is typically 1–2 m wide (**Figure 2**). A longitudinal section through the Colorado Grande vein shows that mineralization is confined to a vertical interval of ~600 m (**Figure 4**). This elevation control is typical in epithermal deposits and is seen elsewhere in northern Great Basin, such as at the Sleeper deposit, and has been attributed to the boiling level (Nash et al., 1995; Saunders, 1994).

The bottom of the zone is controlled by initiation of boiling due to the drop in pressure as ore-forming solutions move from deeper levels, whereas the top represents the elevation where ore-forming solutions were depleted. There is some evidence that the spent ore-forming solutions discharged at the surface, as some siliceous sinter is preserved in the Midas district (Leavitt et al., 2004) and in the Ivanhoe district 15 km to the southeast (Wallace, 2003).

The Midas veins exhibit typical banded black and white encrustation textures closely resembling those at the Hishikari and many other epithermal deposits (**Figures 2** and **5**). At Midas, black-colored bands (**Figure 5**) host most of the ore minerals as they do in the 'ginguro' (silver-black) ore at Hishikari and other Japanese LS deposits (e.g., Izawa et al., 1990). The principal gangue minerals in the Midas veins are quartz, chalcedony, adularia, calcite, and fluorite (Goldstrand and Schmidt, 2000; Leavitt and Arehart, 2005), and calcite has the bladed appearance common to boiling hydrothermal systems (Simmons and Christensen, 1994) and is only locally replaced by silica. The most significant ore minerals identified at Midas veins are naumannite (Ag_2Se), aguilarite (Ag_4SeS), chalcopyrite, electrum (**Figure 6**), and locally fischesserite (Ag_3AuSe_2). Clausthalite (PbSe) and rare Cu– and Cu–Fe selenides have also been identified, along with more common galena, sphalerite, and pyrite (Goldstrand and Schmidt, 2000). Within the individual ginguro bands, naumannite at Midas commonly exhibits self-organized dendritic textures similar to those at the Sleeper deposit (Saunders, 1994), which along with local textural evidence from the naumannite particles (Goldstrand and Schmidt, 2000; Saunders et al., 2011b), indicate that naumannite was physically transported and deposited as colloids or nanoparticles. This is also observed at deposits in the nearby Ivanhoe, Jarbidge, National, and Seven Troughs districts (Saunders et al., 1996, 2011b). Aggregates of naumannite colloids recrystallize, anneal, and grow into coarser-grained minerals, much as aggregates of silica and electrum colloids can (Saunders 1990, 1994). Thus, what is commonly observed are relatively coarse-grained phases such as those in **Figure 6**.

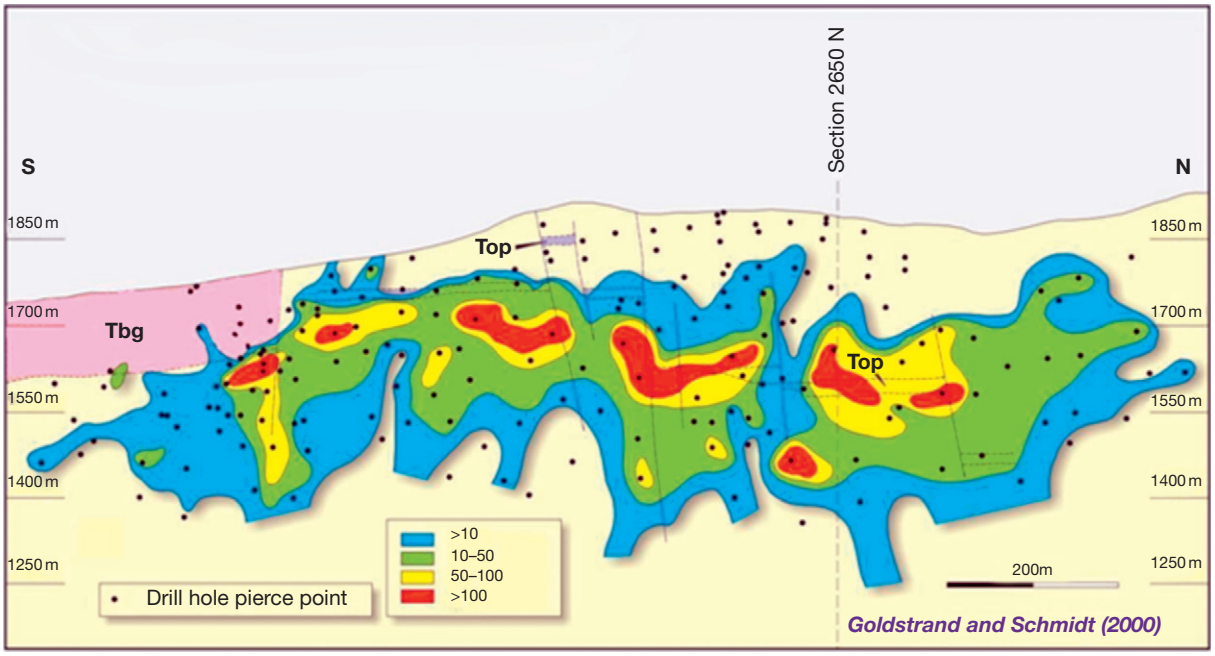

Figure 4 Longitudinal section through the Colorado Grande vein at Midas showing g t^{-1} Au × vein thickness (m) (reproduced from Goldstrand PM and Schmidt KW (2000) Geology, mineralization, and ore controls at the Ken Snyder Gold–Silver Mine, Elko County, Nevada: In: John DA and Wallace AR (eds.) *Geology and Ore Deposits 2000*: *The Great Basin and Beyond*, pp. 265–287. Reno, NV: Geological Society of Nevada).

Figure 5 Photograph of the black 'ginguro' bands of the Discovery vein at the Midas deposit, Nevada. Black ginguro bands contain mostly dendritic naumannite, electrum, and minor sulfide minerals. Vein width shown here is 0.5 m.

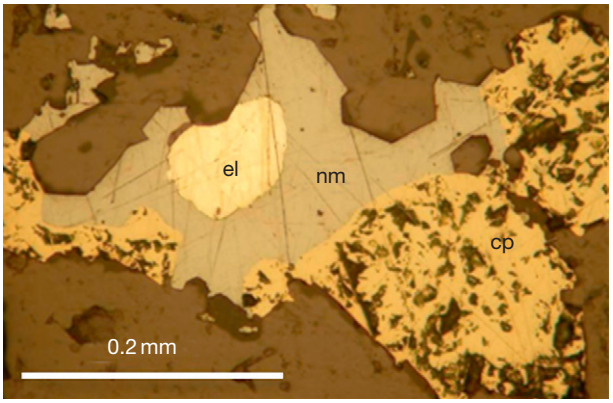

Figure 6 Photomicrograph (reflected light) of the principal ore minerals in the Colorado Grande vein: chalcopyrite (cp), naumannite (nm), and electrum (el).

Electrum and coexisting naumannite–aguilarite account for the bulk of the precious metals in the Midas veins currently being mined, and they are closely associated with chalcopyrite (**Figure 6**), which is similar to the National and Ivanhoe districts, the Silver City district, Idaho (Saunders et al., 2011a), and the Japanese LS ores. Silver-to-gold ratios are variable through the main veins but typically range from 10 to 15:1 (Saunders, unpublished data). Semiquantitative electrum analyses by Riederer (2007) showed that Au:Ag ratios of the alloy were typically in the 40:60–60:40 range. Geochemically, trace elements in veins, for the most part, mirror their principal mineral constituents. For example, Redak (2005) studied the geochemistry of the Colorado Grande vein, plotted longitudinal sections of the distribution of Au, Ag, Se, As, Cu, and Hg in the vein, and showed that they all tended to show the same elevation control as gold in the longitudinal section of Goldstrand and Schmidt (2000; **Figure 4**). Redak (2005) concluded that gold was strongly correlated with Ag, Se, and Hg. Earlier statistical analyses of the Colorado Grande samples by Goldstrand and Schmidt (2000) showed a strong positive correlation between Au, Ag, Se, and Cu, which is similar to what was observed at Hishikari (Nagayama, 1993). Leavitt and Arehart (2005) evaluated the geochemical trends of major,

minor, and trace elements in the Colorado Grande and Gold Crown veins, but did not include gold in their statistics. In general, geochemical trends reported by Leavitt and Arehart (2005) are similar to the earlier studies, but they did note a slight increase in Hg and As at the top of the veins. Leavitt and Arehart (2005) found no increase in base metals with depth in the veins, which commonly occurs in some LS and IS systems (Simmons et al., 2005).

Fluid inclusion studies, most recently by Riederer (2007), indicate that the ore-forming fluids at Midas were in the range of 200–260 °C and were relatively dilute (<1.7% NaCl equiv.), which is similar to many other epithermal systems (Hedenquist and Henley, 1985). The dilute fluids suggest meteoric-water dominance, which is consistent with interpretations from light-stable isotope data elsewhere in northern Nevada, such as Buckskin National (Vikre, 1985), Mule Canyon (John et al. 2003), and Sleeper (Saunders et al., 2008), that indicated most of the ore-forming solutions consisted of exchanged heated meteoric water. Because ore-forming fluids at Midas were near-neutral pH, based on the presence of calcite and adularia gangue minerals and moderately reducing (pyrite-stable), they would likely have transported dissolved precious metals as aqueous complexes with H_2S(aq) and bisulfide (HS^-; e.g., Seward, 1973; Spycher and Reed, 1989). Boiling of such a fluid is very effective in precipitating precious metals (Brown, 1986; Spycher and Reed, 1989).

As discussed in the preceding text, hydrothermal alteration associated with epithermal mineralization can be quite variable and often provides little exploration aid for vectoring toward mineralization (Simmons et al., 2005). However, Leavitt and Arehart (2005), building on the earlier work by Goldstrand and Schmidt (2000), conducted a detailed investigation of hydrothermal alteration at Midas and showed that it could be used as an exploration aid. It is important to remember that the fluids causing much of the hydrothermal alteration are not necessarily the same solutions that deposit the precious metals. For example, the precious-metal depositing fluid interpreted for Midas would not have been particularly reactive toward the wall rocks. However, if the heated groundwater entering the hydrothermal system at Midas had absorbed acid volatiles released from a degassing magma chamber at depth or from a deeper boiling hydrothermal solution, then alteration would be expected to be more intense. Indeed, Leavitt and Arehart (2005) showed that hydrothermal alteration at Midas was apparently centered about the Colorado Grande and Gold Crown veins, which are the principal structures. Leavitt and Arehart (2005) noted an extensive zone of weak propylitic alteration, consisting of calcite, chlorite, pyrite, and smectite, which becomes more intense nearer the veins and where epidote appears as an alteration mineral. Closer to the veins, smectite gives way to illite, the Fe:Mg ratio in chlorite increases, pervasive K-alteration leads to adularia formation, and silicification is noted. Argillic alteration of wall rocks is common in the upper parts of the Midas vein system, where it overprints earlier alteration events. Alteration halos surrounding the veins extend a few tens of meters from the main veins, and the recognition of alteration patterns has aided in the exploration in the district (Leavitt and Arehart, 2005). However, hydrothermal alteration varies with the lithology of the wall rocks and over time at Midas.

Potassic alteration resulted in gains in K, S, Se, P, Ag, As, Sb, Hg, and W and losses in Ca, Mg, and Cr in mafic rocks. In rhyolites, potassic alteration led to an increase in S, Ba, Mg, Mn, P, Se, Ag, Sb, Cu, W, and Bi and losses in Na, Fe, and Zn. Finally, potassic alteration of felsic volcaniclastic rocks increased S, Al, Ti, Mg, P, Sr, Cr, Cu, and W and depleted Fe, Na, and Ca. The formation of the banded bonanza veins appears to have coincided with potassic alteration (Leavitt and Arehart, 2005; Leavitt et al., 2004).

13.15.2.3 High-Sulfidation Epithermal Ores

The gold–copper deposits of Summitville (CO, USA) and of the Nansatsu District (southwestern Kyushu, Japan) are typical examples of the acid-sulfate covellite–enargite–gold ore type described in early studies by Steven and Ratte (1960), Saito and Sato (1978), Stoffregen (1987), and Izawa and Cunningham (1989). The ores have been called Nansatsu-type (Urashima, 1975), Nansatsu-Summitville-type, acid-sulfate Cu–Au, and HS. The Nansatsu and Summitville deposits are two of a large number of HS epithermal deposits (see Hedenquist et al., 1994), which include the historic deposit at Goldfield, Nevada (Ransome, 1909; Vikre, 1989), and the recently developed deposits at Pascua, Chile (Chouinard et al., 2005a, 2005b), and Yanacocha, Peru (Teal and Benavides, 2010). All are hosted by volcanic rocks and shallow subvolcanic intrusions that are intensely altered to assemblages of quartz, quartz–alunite, and quartz–kaolinite where the rocks were permeated by acidic fluids along fractures and breccia bodies. Some of the cavities opened by acid attack are filled with native sulfur and ore minerals, characteristically including pyrite, enargite, luzonite, covellite, and gold-rich electrum. Barite and native gold are also common associates in cavities and in late veins.

The occurrence of many HS epithermal deposits at shallow depths above commonly Au-rich porphyry copper deposits and the contemporaneity of the two (e.g., Arribas et al., 1995; Longo et al., 2010) clearly link the genesis of the two ore types, as others have outlined (e.g., Sillitoe, 2010). There is also a clear kinship of this acid-sulfate epithermal ore type with many late-stage vein and breccia systems superimposed on porphyry copper deposits, such as the Butte, Montana, covellite–enargite ore with advanced argillic alteration (Meyer et al., 1968) and similar veins at El Salvador, Chile (e.g., Gustafson and Hunt, 1975).

13.15.2.3.1 Hydrothermal alteration

The HS epithermal type ores are defined by the accompanying intense advanced argillic alteration, which at its most intense consists almost entirely of quartz. The rock may be up to 95 wt% SiO_2; all other primary constituents have been leached, leaving a spongy texture where original phenocrysts are removed. The quartz-rich alteration is bordered by advanced argillic assemblages always including alunite and kaolinite and variably including natroalunite, dickite, pyrophyllite, zunyite ($Al_{13}Si_5O_{20}(OH)_{18}Cl$), and diaspore. Further, kyanite and topaz are common in metamorphosed HS deposits like Brewer, South Carolina, in the Carolina Slate Belt of SE USA.

The zoned alteration at Summitville, described by Steven and Ratte (1960) and Stoffregen (1987), is clearly developed, providing a good example as a standard of comparison. The

Summitville host rock is a quartz latite characterized by large oligoclase and sanidine phenocrysts that, when leached out, yield a highly porous rock called 'vuggy silica' (Steven and Ratte, 1960) with centimeter-scale cavities, some of which are occupied by ore minerals. The near-vertical bodies of vuggy silica (Stoffregen, 1987) consist of quartz with small amounts of rutile, anatase, and residual zircon, all of which resist acid attack as shown by persistence of original concentrations of Ti, Zr, and Hf in the altered rock (see succeeding text). Vuggy silica is surrounded on a scale of meters successively by alteration zones identified as quartz–alunite, quartz–kaolinite, illite–kaolinite, and chlorite–montmorillonite (**Figure 7**).

In the quartz–alunite zone, phenocryst cavities are filled by pink to white alunite in a groundmass entirely replaced by quartz. At the outer edges of the alunite zone, kaolinite joins alunite in the feldspar replacements and then becomes the dominant Al-bearing mineral over widths of centimeters to a meter. The kaolinite zone yields outward to illite-dominated alteration, where feldspars are replaced by illite and quartz in a tan to gray argillic groundmass. Further outward, in the illite–montmorillonite zone, primary sanidine persists, but most primary plagioclase is altered to illite–montmorillonite, as is the gray to tan groundmass. At a distance of many meters from the vuggy silica, the groundmass is green from montmorillonite and locally chlorite, and although sanidine is unaltered, plagioclase is clay-altered to various degrees.

In the Kasuga, Iwato, and Akeshi deposits of the Nansatsu district, the minerals and zoning of alteration of the host andesite are the same as at Summitville for all zones, but with added dickite, pyrophyllite, diaspore, and Mg-chlorite in the kaolinite zone at Iwato. Structurally, the alteration in the Nansatsu ores lies in flattened subhorizontal amoeboid bodies on a scale of 100–200 m in diameter (Hedenquist et al., 1994; Izawa and Cunningham, 1989) in contrast to the vertically elongated deposit at Summitville.

The same minerals and zoning occur in other HS epithermal deposits, including the giant gold deposits of the Yanacocha district, Peru, where the tabular quartz-rich alteration zone is gently dipping, 100–200 m wide, and broadly conforming to volcanic layering, but locally cutting stratigraphy with a subvertical attitude (Longo et al., 2010). Bordering the quartz alteration, the sequence of 10–100 m wide alteration zones is again dominated by alunite, kaolinite, illite, smectite, and chlorite–smectite. Similarly, at Pascua, Chile, Chouinard et al. (2005a, 2005b) described masses of vuggy silica aligned along vertical structures and breccia but laterally coalesced over many hundreds of meters. The vuggy silica masses are all bordered laterally and vertically by alunite ± kaolinite, dickite, and pyrophyllite, all of which is capped by apparently steam-heated quartz–kaolinite alteration, which also contains chalcedony, opal, sulfur, and rare alunite.

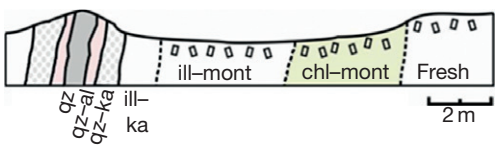

Figure 7 Cross section of the alteration envelope on a Summitville ore zone. Cu–Au mineralization is centered in the vuggy silica (qz), which is bordered by zones of quartz–alunite (qz-al), quartz–kaolinite (qz-ka), illite–kaolinite (ill-ka), illite–montmorillonite, chlorite–montmorillonite, and fresh rock. Small rectangles represent occurrence of primary sanidine. This schematic view is based on mapping of a pit exposure at the 3514 m elevation (M. Reed, unpublished data).

The changes in rock composition upon intense hydrothermal alteration have been well characterized in the Summitville deposit. The bulk-rock compositions of altered Summitville quartz latite are depicted in **Figure 8**, which shows compositions tabulated by Steven and Ratte (1960) and by Getahun (1994), calculated on a volume basis (g cm^{-3}), to determine chemical gains and losses (Sales and Meyer, 1948). The data show a complete leaching of Ca and Na in the quartz (vuggy silica), quartz–alunite, and quartz–kaolinite zones and far into the montmorillonite–chlorite zone, reflecting destruction of plagioclase. In the alunite zone, concentration spikes of Na, Ba, K, Sr, Pb, and P reflect incorporation of those elements into alunite and its analogues, such as woodhouseite (phosphate–sulfate). Titanium concentration is not changed in the altered rock, reflecting its residence in insoluble rutile and anatase. Zircon and Hf are similarly unaffected, owing to their occurrence in refractory zircon. Iron is removed from vuggy silica except where later pyrite fills porosity. Magnesium is removed from vuggy silica and alunite zones where primary biotite and hornblende are destroyed, but is apparently only slightly affected in the kaolinite zone where it likely forms colorless Mg-chlorite (Hedenquist et al., 1994). Magnesium and Ca are likely added to the rock in outer alteration zones where carbonates form.

Alumina is completely removed from quartz zone but is essentially unchanged in other zones, showing that alumina from the vuggy silica zone is not remobilized to the kaolinite zone or laterally beyond. Gray and Coolbaugh (1994) found slightly elevated Al_2O_3 on a weight basis in some kaolinite zones, but not in others, although the weight basis precludes a clear conclusion regarding aluminum gains and losses.

13.15.2.3.2 Trace elements and mineral associations

Primary ore minerals fill open space in intensely altered vuggy silica where primary rock minerals were fully leached away before precipitation of the ore minerals. The common ore minerals are enargite/luzonite, covellite, pyrite, gold-rich electrum, and native gold. Description of electrum and gold textures in relation to enargite/luzonite, covellite, and pyrite is rare, apparently owing to the fine-grained nature of gold and its incorporation into pyrite (see succeeding text). Assay data show a positive correlation of Cu with Au in sulfide ore, although textures show that gold precipitated after enargite/luzonite in some ores, such as Lepanto (Hedenquist et al., 1998), where the electrum occurs with a postenargite assemblage including tennantite, chalcopyrite, sphalerite, and galena. Tennantite and chalcopyrite are also common ore minerals; for example, at Summitville, Stoffregen (1987) found that the shallow enargite–covellite ores zone downward to tennantite–chalcopyrite, which were also in vuggy silica. In most settings, minor amounts of galena and sphalerite occur along with the copper minerals.

Vein or pore-filling barite with gold is a common late ore form, cutting or overlapping gold ores dominated by pyrite or enargite–pyrite. For example, Longo et al. (2010) describe late

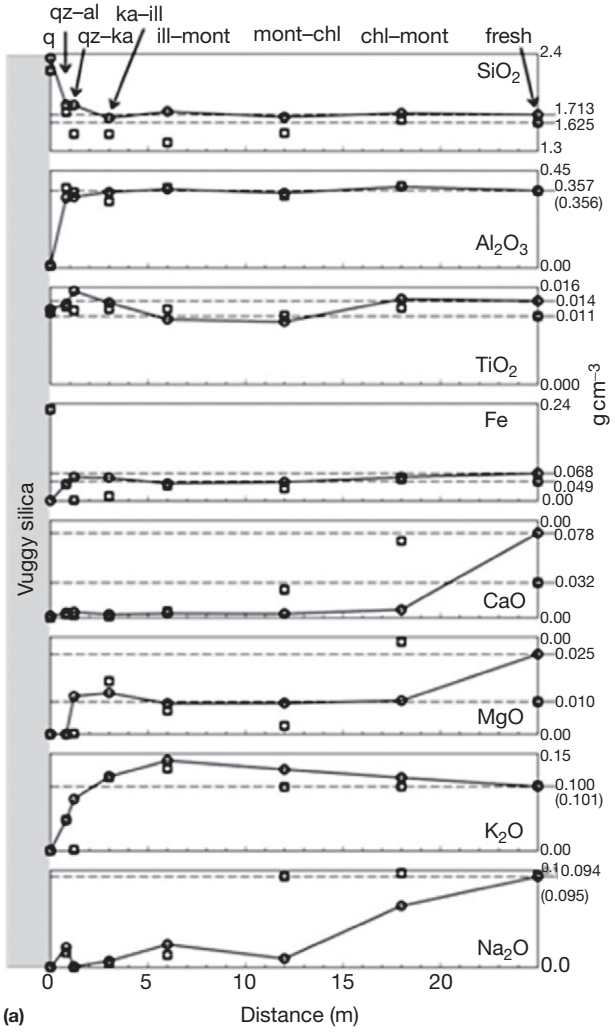

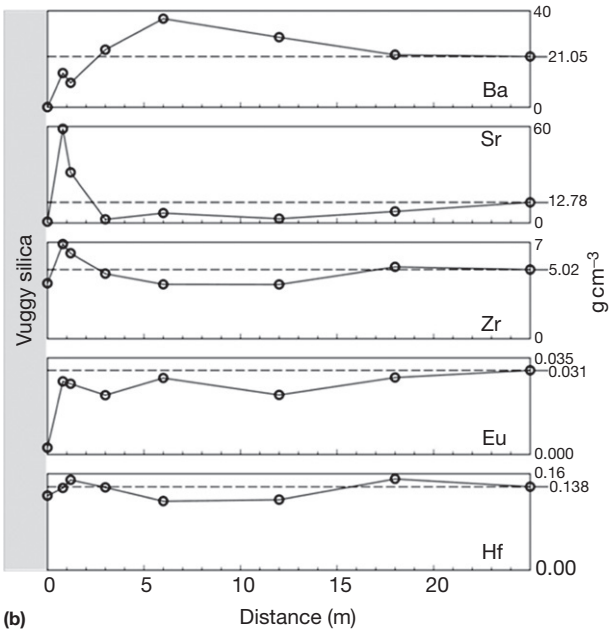

Figure 8 (Continued)

pyrite–tennantite–covellite–gold ± barite ± orpiment ± sulfur in unoxidized ore at Yanacocha, and at shallow depth, they report late gold intergrown with barite or quartz in vugs and fractures. At Goldfield, Nevada, Vikre (1989) described ore zones containing euhedral barite with quartz, pyrite, enargite/luzonite, famatinite, bismuthinite, gold, and kaolinite, all of which follow early quartz–pyrite–gold ore. Similarly, at Paradise Peak, early quartz–pyrite–marcasite–sulfur breccia with Au concentrations $\leq$1.8 ppm is cut by a black porous quartz-matrix breccia containing barite, gold, silver, marcasite, stibnite–bismuthinite, cinnabar, and sulfur but nearly lacking Cu sulfosalts (John et al., 1989; Sillitoe and Lorson, 1994).

Ore texture descriptions by Chouinard et al. (2005a, 2005b) for Pascua, Chile, relate precipitation of gold, pyrite, and enargite together in an alunite–pyrite–enargite assemblage that fills vuggy silica in a single ore stage. One distinctive pyrite textural type with a dull luster and intergrown alunite hosts economically significant amounts of Au. The same pyrite contains inclusions of calaverite, gold, and electrum and is included within enargite that also hosts grains of gold, electrum, gold tellurides, stibnite, cassiterite, and other phases containing Sn, Zn, Bi, Cu, and Sb. These observations at Pascua establish contemporaneity of Cu, Au, and As precipitation from a fluid in the enargite–pyrite mineralization stage, as opposed to or in addition to a later stage characterized by tennantite–tetrahedrite and chalcopyrite, as at Lepanto (Hedenquist et al., 1998), or as a later stage with barite, as outlined above.

13.15.2.3.3 Ore-fluid composition

Fluid inclusion homogenization temperatures and isotope fractionation between minerals in HS epithermal Au deposits indicate temperatures mostly in the range of 200–350 °C at depths of about 200–600 m, inferred from coexisting vapor and liquid inclusions in quartz and from geologic reconstructions of the paleosurface. At Julcani, Peru, sulfur isotope ratios for coexisting pyrite ($\delta^{34}S = -1$ to $+2$‰) and alunite ($\delta^{34}S = +22$ to $+25$‰) indicate temperatures from 210 to 290 °C with a mean of 260 °C (Rye et al., 1992). At Pascua, coexisting S isotope ratios in pyrite ($\delta^{34}S = -3.4$ to -5.3‰) and alunite ($\delta^{34}S = +15$ to $+20$‰) indicate temperatures ranging from 245 to 305 °C

Figure 8 (a) Bulk chemical analyses (g cm^{-3}) of Summitville alteration zones, plotted against distance (m) from the center of a vuggy silica zone (left end). Circles show analyses from Getahun (1994). Squares show analyses from Steven and Ratte (1960), but they are matched to alteration types shown in circles, not to distance from vuggy silica. Dashed lines indicate composition of fresh quartz latite in the two studies; where the two nearly overlap the numerical value of the one not plotted is shown in parentheses beneath the other. Notice that fresh rock (far right) MgO and CaO differ substantially in the two analyses, probably reflecting unrecognized added carbonate in the Getahun (1994) samples. For other elements, the spread in the fresh rock compositions shown by the vertical separation of the dashed lines indicates variation in parent rock composition that provides a basis for understanding a likely uncertainty in gains and losses in alteration owing to natural variation and to limitations of sample size. The strongly elevated concentrations of CaO and MgO shown by squares at 17 m probably reflect addition of those elements in forming carbonates, whose presence is indicated by 1.22 wt% CO_2 in that sample. (b) Selected trace elements in the altered rocks shown in **Figure 9(a)**.

(Deyell et al., 2005). At Lepanto, Hedenquist et al. (1998) determined a range of 210–250 °C for pyrite–alunite pairs. Similar isotope findings, although less well constrained, for Summitville (Bethke et al., 2005; Rye et al., 1992) and the Nansatsu deposits (Hedenquist et al., 1994) indicate similar temperatures.

A large number of measurements of liquid-rich fluid inclusions in the Nansatsu vein and vug-filling quartz, most of which is texturally post-ore, have homogenization temperatures (T_h) ranging from 160 to 240 °C and most are accompanied by vapor-rich inclusions (Hedenquist et al., 1994). Even if the T_h values in the post-ore quartz underestimate mineralization temperatures, the coexisting vapor-rich inclusions indicate boiling, yielding pressures corresponding to depths beneath the water table ranging from 150 to 400 m.

At Julcani, Peru, Deen et al. (1994) measured a large number of fluid inclusions in quartz, enargite, apatite, wolframite, and siderite. The homogenization temperatures for inclusions in enargite and ore-stage quartz largely overlap in the range of 240–300 °C. Homogenization temperatures for wolframite inclusions cluster near 315 °C. Deen et al. (1994) report no vapor-rich inclusions, indicating that maximum ore zone pressures must exceed 100 bars at the high temperatures, indicating an open system paleodepth exceeding 1000 m. They also cite a geomorphic reconstruction of the paleosurface indicating an ore zone paleodepth exceeding 600 m.

Fluid salinities in Julcani inclusions (Deen et al., 1994) range from 17 wt% NaCl (equiv.) in early wolframite to about 7 wt% in late stage and distal quartz and siderite. Ore-stage enargite lies between these in the range of 10–14 wt% NaCl (equiv.). Deen et al. (1994) interpret these findings, in combination with the isotopic evidence for meteoric-water dilution of magmatic fluids, to indicate that the course of mineralization was accompanied by mixing of magmatic fluids with meteoric waters. Similar conclusions for temperature and meteoric-water dilution are described by Hedenquist et al. (1998) for Lepanto on the basis of fluid inclusion and isotope measurements, although salinities at Lepanto are in the range of 1–3 wt% NaCl (equiv.).

Aside from Nansatsu, where abundant coexisting populations of liquid- and vapor-dominated fluid inclusion assemblages in late post-ore quartz indicate boiling (Hedenquist et al., 1994), most fluid inclusion studies reveal little boiling or occasional boiling in HS systems. For example, in a study of late enargite–pyrite veins at Roşia Poieni, Romania, Kouzmanov et al. (2010) identified coexisting liquid and vapor inclusions only in some quartz and pyrite, but in other texturally distinguished pyrite and quartz, they found liquid brine-only fluid inclusion assemblage with 35 wt% NaCl (equiv.) and homogenization temperatures of 290–340 °C. The boiling assemblages yield homogenization temperatures of 250–284 °C in fluids of ~1 wt% NaCl (equiv.), corresponding to pressure on the order of 50 bars, which are temperatures and pressures similar to those in the Nansatsu deposits.

13.15.2.3.4 Light-stable isotopes

The abundance of alunite and kaolinite facilitates the use of isotope ratios of H, O, and S, useful in establishing the sources and compositions of fluids responsible for hydrothermal alteration in HS epithermal gold systems. HS ore fluids are dominated by sulfuric acid formed from disproportionation of magmatic SO_2, according to the reaction:

$$SO_2(\text{aq or g}) + H_2O(\text{aq}) = 1\frac{1}{2}H^+(\text{aq}) + \frac{3}{4}SO_4{}^{2-}(\text{aq}) + \frac{1}{4}H_2S(\text{aq}) \rightarrow \text{(R1)}.$$

The products of the disproportionation reactions are variably diluted by meteoric waters (Deyell et al., 2005; Rye et al., 1992). The following Summitville isotopic data from Rye et al. (1992) typify their findings for many deposits:

1. $\delta^{34}S$ (alunite) = +13 to +25‰. The heavy values distinguish the sulfur in alunite as directly exsolved from a magma, as opposed to derivation from oxidized H_2S boiled from a hydrothermal fluid, as is typical for steam-heated acidic fluids. The heavy alunite reflects heavy sulfate sulfur, which reflects isotope fractionation upon partitioning of ~+2‰ magmatic sulfur between light H_2S and heavy sulfate at a sulfide/sulfate ratio of 4 (±2).
2. The O and H in fluids, calculated from alunite: $\delta^{18}O = 0$ to +8‰, and $\delta D = -35$ to −65‰. The lighter H correlates with the lighter O, together indicating admixed meteoric water with magmatic SO_2 and H_2O.
3. The O and H in fluids, calculated from wall rock kaolinite: $\delta^{18}O = +4$ to +7‰, and $\delta D = -60$ to −95‰. The large negative δD indicates meteoric-water dilution of fluids similar to those that produced alunite.

For the Nansatsu deposits, Hedenquist et al. (1994) provide analyses of pyrite, enargite, covellite, and native sulfur, all of which occur in gold ore, wherein some vug fillings contain enargite and pyrite together with gold. In the native sulfur and sulfide minerals collectively, $\delta^{34}S = -5$ to 0‰, which Hedenquist et al. (1994) infer to indicate magmatic sulfur. Alunite in these deposits has $\delta^{34}S = +24$ to +34‰, resembling the findings for Summitville, and together with the sulfide data, indicates an aqueous sulfide/sulfate ratio of ~3. A substantial number of analyses of O and H isotopes in residual silica, alunite, and clays (mostly kaolinite, pyrophyllite, and Al-chlorite) at Kasuga and Iwato yield ratios indicative of mixed magmatic and meteoric waters as inferred at Summitville. The data also indicate that the Nansatsu clays formed with more meteoric-water involvement than in the alunite alteration.

13.15.2.3.5 Reaction of volcanic gas condensate with quartz latite

Isotopic data combined with the open cavity textures observed in vuggy silica led Hedenquist et al. (1994) and Stoffregen (1987) to suggest that magmatic gas condensed into groundwater at shallow levels, reacted with the host rock, and was later followed by metal-bearing fluids that permeated the porous rock, which was created by the acid leaching. To examine the geochemical constraints on how the alteration pattern exemplified by the Summitville system forms as a proxy for the geochemical processes in most HS systems, a volcanic gas condensate was numerically reacted with the quartz latite of South Mountain in a computational model of alteration, following the methods of Reed (1997) and using thermodynamic data described by Reed and Palandri (2006). The volcanic gas is modified from the Augustine Volcano Spine 1D sample

analysis (Symonds et al., 1994) by a 5× dilution and an increased Na_2SO_4 concentration, yielding a fluid with an initial pH of 0.86 at 270 °C and 55 bars.

The initial fluid precipitates native sulfur, which is followed by quartz precipitation as the rock reacts with the evolving fluid (Figure 9(a)). With increasing amount of rock reaction, and thus decreasing water/rock ratio, the succession of key alteration minerals following quartz is alunite, kaolinite, pyrite, barite, anhydrite, muscovite, hematite, chlorite, feldspars, and calcite. This succession matches the observed sequence (Steven and Ratte, 1960; Stoffregen, 1987) and can be broken into an outwardly zoned alteration series of quartz, quartz–alunite, quartz–alunite–kaolinite, quartz–kaolinite–muscovite (illite), and propylitic (quartz, chlorite, feldspars, and calcite).

The precipitation of calcite with the chlorite and feldspars (Figure 9(b)) reflects its stability at neutral pH (5.7 at the ambient temperature), where its precipitation consumes CO_2 from the magmatic gas. Steven and Ratte (1960) report whole-rock CO_2 concentration of 1.22 wt% in the chlorite–montmorillonite zone, reflecting carbonate minerals observed in that alteration type and also reflecting a Ca enrichment they find relative to the primary rock. In other words, apparently some Ca leached from plagioclase in the inner zones precipitates in the chlorite–montmorillonite zone.

Across the alteration halo, the pH steps upward from 0.86 to 6.06, as the reaction with rock neutralizes the acid. In the quartz and quartz–alunite intervals, aqueous Al^{3+} reaches a concentration of $10^{-2.2}$ molal (160 ppm) at pH 1.0 (Figure 9(c)). Subsequent precipitation of kaolinite with rising pH removes 99% of the aqueous Al^{3+} where pH has risen to 1.7. The high solubility of Al-bearing and all other minerals except quartz at pH less than 1.5 allows total leaching of rock forming elements from the quartz alteration zone, yielding the highly porous vuggy silica that is subsequently filled by covellite, enargite, pyrite, and electrum.

13.15.2.3.6 Ore deposition

The ore minerals in most HS epithermal Au deposits filled open space or breccia matrices, fractures, or cavities in acid-leached wall rock, as opposed to replacement of wall rock

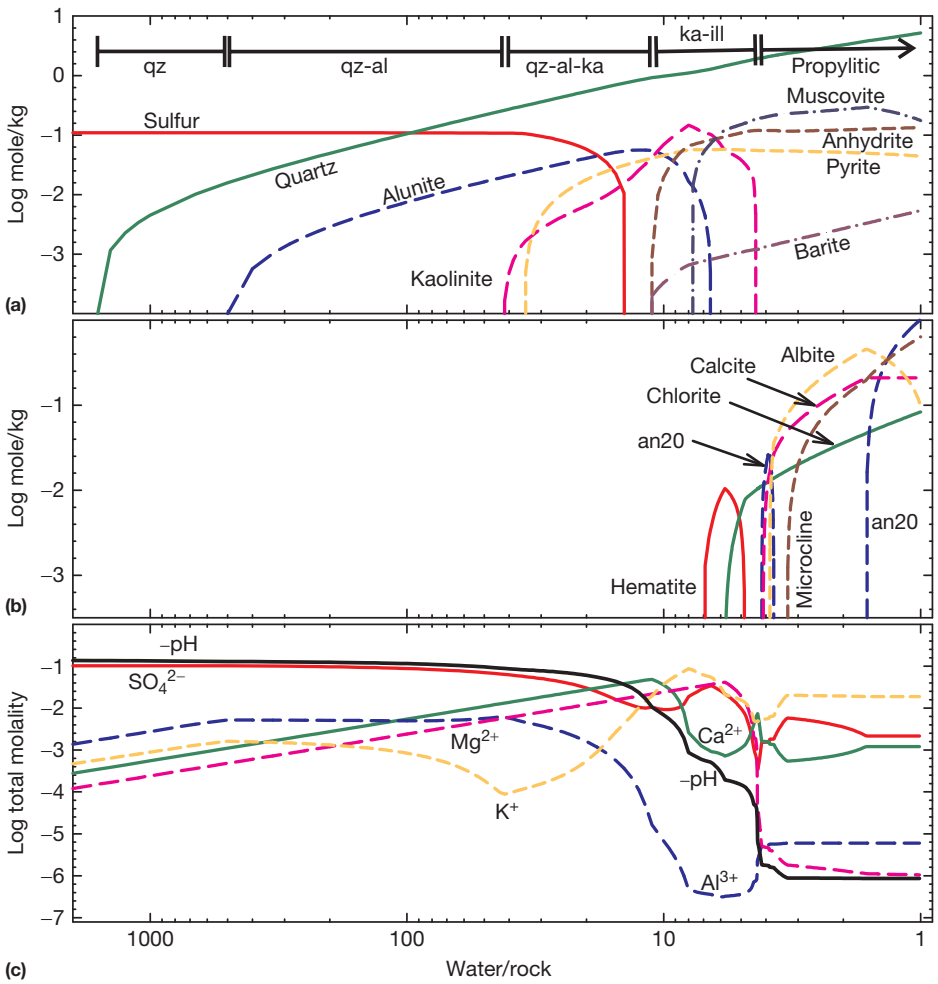

Figure 9 Computed reaction of a diluted volcanic gas condensate with quartz latite at 270 °C. The water/rock ratio is determined from the initial mass of water divided by the mass of rock. (a) Major minerals (abbreviation 'an20' refers to plagioclase with 20% anorthite component). Mineral alteration zones corresponding to the Summitville alteration envelopes are marked, wherein muscovite is equivalent to illite, and the term 'propylitic' notably includes the chlorite, feldspar and calcite assemblage shown in graph (b). (c) pH and total molalities of component species.

along with alteration minerals. In HS systems, ore minerals may precipitate where hypogene fluids boil, conductively cool, mix with cold groundwater, or mix with a reactive fluid, such as an acidic and Fe-rich magmatic condensate residual from the wall rock alteration stage (as above). An exception to open space-filling ore is the stage I ore at Pueblo Viejo, Dominican Republic (Kesler et al., 1981; Muntean et al., 1990), where Au and pyrite precipitated together upon sulfidation of wall rock iron by the hydrothermal fluids, as occurs in orogenic gold deposits (e.g., Reed, 1997).

The measurements of fluid inclusion salinities and isotopic ratios of H and O demonstrate that boiling and meteoric-water dilution of ascending magmatic fluids are active in HS epithermal ore-forming systems. These processes were evaluated in a series of numerical chemical equilibrium model calculations of simple cooling, boiling, cooler water mixing, and acidic water mixing, each one starting from a magmatic fluid at 325 °C. The starting fluid is derived, in part, from fluid inclusion compositions and equilibrium constraints applied in a model of wall rock alteration in the magmatic-hydrothermal system of Butte, Montana (Reed et al., 2013). The starting fluid Au aqueous concentration is at the low end of the range (0.1–5.0 ppm Au) found by Kouzmanov et al. (2010) for fluid inclusions in enargite and pyrite at Roşia Poieni, Romania. The results of three of the model runs (Figures 10–12) illustrate the essential chemical processes.

Progressive mixing of the 325 °C starting fluid with 5 kg of 25 °C meteoric water causes quartz, enargite, covellite, pyrite, sulfur, Au-rich electrum, stibnite, proustite, galena, and sphalerite to precipitate (Figure 10(a) and 10(b)), as pH changes from 2.5 at 325 °C to 2.1 at 75 °C (Figure 10(c)). Sulfide precipitation is driven by several factors (Reed and Palandri, 2006) that function despite the acidic pH: (1) decreasing temperature drives metal chloride complex dissociation; (2) dilution reduces the concentration of metal-complexing chloride; and (3) the sulfide minerals become intrinsically less soluble at lower temperature. The acidic pH favors pyrite plus covellite and enargite over the lower-sulfur alternatives, chalcocite (and bornite and chalcopyrite) and tennantite, illustrated by the following reaction (see Reed and Palandri (2006)

$$2\,\mathrm{CuS(cv)} + \mathrm{H_2O(aq)} = \mathrm{Cu_2S(cc)} + \frac{1}{4}\mathrm{SO_4^{2-}(aq)} + \frac{1}{2}\mathrm{H^+(aq)} + \frac{3}{4}\mathrm{H_2S(aq)} \rightarrow \quad \text{(R2)}$$

for more details) that shows increased H^+ activity favors covellite (cv) over chalcocite (cc).

In the cold meteoric-water dilution, aqueous Au^+ is complexed almost entirely by AuHS, which holds a minimum of 85% of the Au; $AuCl_2^-$ and $AuCl_3^{2-}$ contain the remainder (Figure 10(d)). Strong dominance of the Au bisulfide applies over all of the acidic pHs and temperatures up to at least 350 °C, despite the much greater concentration of H_2S than HS^- (Figure 10(d)) owing to the acidic pH. The large aqueous sulfide concentration in the HS ore fluids is sufficient, despite the low pHs, to assure enough HS^- to form AuHS instead of chloride complexes. Thus, gold precipitation is controlled by the following gold precipitation reaction:

$$8\,\mathrm{AuHS\,(aq)} + 4\,\mathrm{H_2O\,(aq)} = 8\,\mathrm{Au^\circ} + 7\,\mathrm{H_2S\,(aq)} + \mathrm{HSO_4^-(aq)} + \mathrm{H^+(aq)} \rightarrow \quad \text{(R3)}$$

which is written to the dominant species in the solution. The equilibrium constant for this reaction increases by 13 orders of magnitude between 300 and 100 °C, largely owing to the increased intrinsic stability of gold with decreasing temperature; thus, simple temperature decrease plays a key role in precipitating electrum. Despite the much larger aqueous Ag concentration than Au (Figure 10(c)), the computed electrum is gold-rich (Figure 10(b)), as observed in the natural setting, because the gold end-member is intrinsically quite stable relative to silver, and the temperature decrease has a stronger effect on the gold reaction than it does on the corresponding silver reaction involving aqueous Ag chloride.

The effects of cooling and acidic conditions on ore mineral precipitation, as outlined earlier in the text for the cold water mixing, apply similarly to boiling and to mixing with an acidic Fe-rich magmatic condensate residual from the wall rock alteration (Figures 11 and 12), both of which were computed for the same starting fluid used for cold water mixing. Boiling yields covellite and electrum, but little pyrite until temperatures cool below 175 °C (Figure 12). Electrum precipitates at a higher temperature upon boiling than in cold water mixing because a large quantity of aqueous H_2S is displaced to the gas phase, driving reaction R3 to the right, precipitating gold. The displacement of S to the gas phase also precludes precipitation of native sulfur in the mineral assemblage.

Mixing of the magmatic fluid with a 100 °C residual acidic Fe-rich fluid from the wall rock reaction calculation in the preceding text (at a water/rock ratio of 36) yields abundant pyrite with covellite and smaller amounts of enargite and alunite (Figure 12) at high temperature. Pyrite and covellite are joined by sulfur, stibnite, electrum, and barite at lower temperature, but not by galena and sphalerite, which form upon cold water mixing (Figure 10(a)). The pH changes from 2.5 at 325 °C to 0.9 at 135 °C. The more acidic pH at low temperature prevents precipitation of galena and sphalerite; however, the added barium from the wall rock fluid enables barite to form with the low-temperature ore assemblage. Similarly, aluminum in the wall rock-derived fluid forms alunite mixed with pyrite and covellite at high temperature. The low pH in this system results in substantial sulfur precipitation, more than for cold water mixing or boiling, which produced none.

The ore deposition calculations illustrate that cooling, cold water mixing, boiling, and acidic water mixing all yield the observed ore mineral assemblages. Given the wide variation in the details of natural assemblages and their relative timing as outlined above and the similarly various computed assemblages, depending on the processes and the details of fluid compositions, it is likely that mixing, boiling, and cooling all play roles in HS epithermal Au systems over time. In all of the ore precipitation processes, Pb, Zn, and most of the Ag remain in the solution at temperatures above 200 °C (e.g., Figure 10(d)), thus providing for their transport to a distal setting, where they may precipitate in base metal–silver veins.

In summary, HS epithermal Au deposits form at temperatures of 240–340 °C, where magmatic SO_2 disproportionates to yield sulfuric acid and H_2S that mix with meteoric water in a subvolcanic environment at depths of 200–1000 m. The sulfuric acid fluids leach all of the major constituents but silica from the host rock, thereby creating porosity that is subsequently

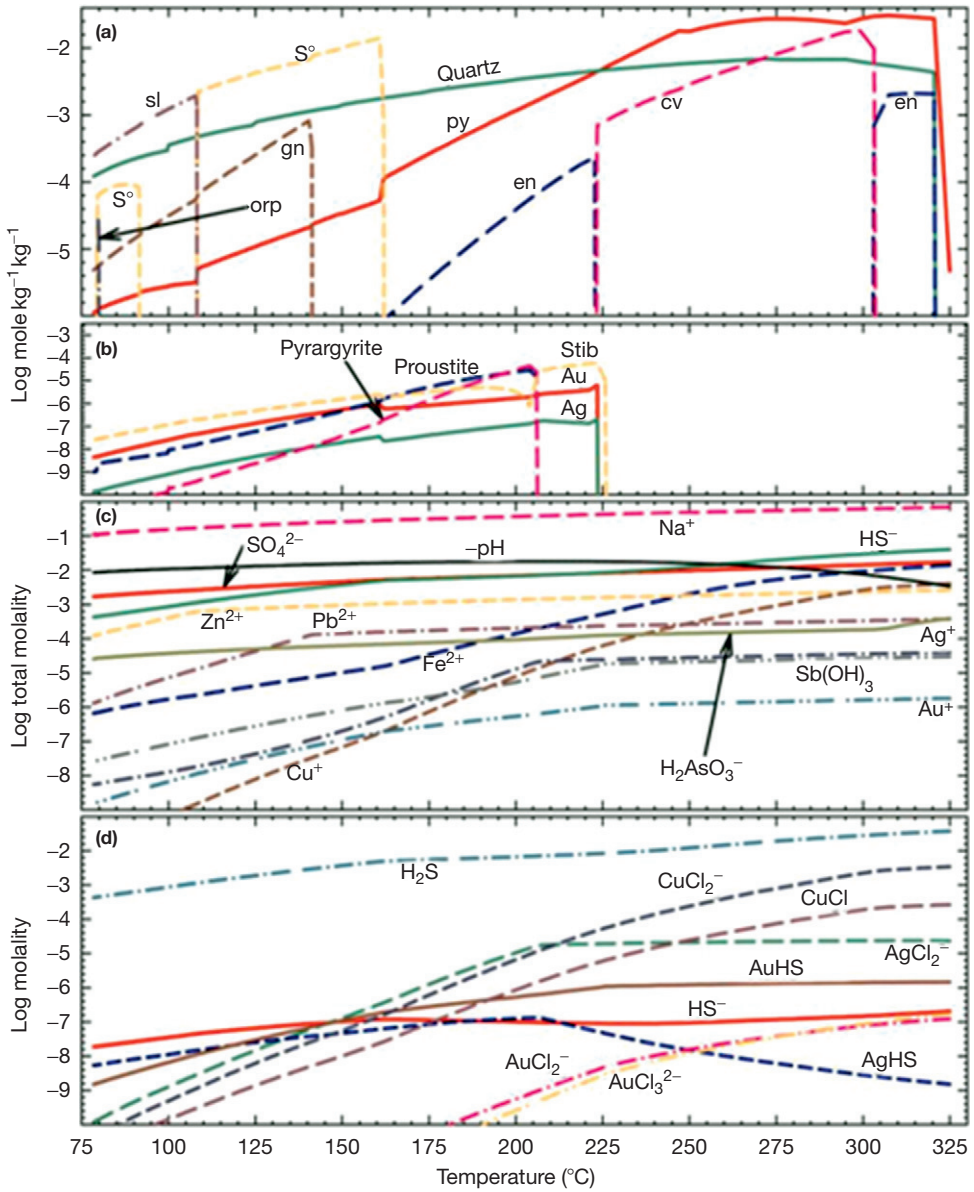

Figure 10 Model results for mixing of 325 °C magmatic fluid with 25 °C water with consequent temperature decrease, dilution, and reaction. At the low temperature end, 5 kg of cold water had been added to 1 kg of magmatic fluid. (a and b) Log of rate of mineral precipitation in units of moles per kilogram of initial water per kilogram of admixed cold water. (c) Total molalities of aqueous components. For Na+, the downward slope of the curve with decreasing temperature shows the effect of dilution alone on concentration. The steeper slopes of other curves (e.g., Cu^{+}, Fe^{2+}, and Au^{+}) reflect precipitation of those elements in minerals. (d) Molalities of sulfide species and the dominant individual complexes of Cu, Au, and Ag with HS^{-} and Cl^{-}. Chlorides of Cu and Ag and a bisulfide of Au dominate. Mineral abbreviations are as follows: al, alunite; bar, barite; cv, covellite; en, enargite; gn, galena; orp, orpiment; py, pyrite; pyro, pyrophyllite; sl, sphalerite; and stib, stibnite.

permeated by copper- and gold-bearing fluids that precipitate enargite/luzonite, covellite, pyrite, and electrum in the pore space. The metal-bearing fluids are apparently shallow derivatives of the same fluids that produce porphyry copper mineralization at depth, as argued by Hedenquist et al. (1998) based mainly on their findings on the HS epithermal ores of the Lepanto system and the subjacent Far Southeast porphyry copper deposit, Luzon, Philippines. Copper and gold precipitate where fluids cool upon boiling, mixing with meteoric waters, or mixing with residual acid-sulfate fluids in the porous host rock. The prevalence of covellite, pyrite, and enargite, as opposed to chalcopyrite, indicates acidic conditions in the ore precipitation zone, but not so acidic as to prevent sphalerite, galena, and tennantite–tetrahedrite from forming in some settings.

Although the acidic conditions are probably partly residual from the earlier period of acid-sulfate leaching, it is likely that the metal-bearing fluid is also acidic owing to its derivation by cooling of a metal-bearing porphyry copper fluid as explained by Reed et al. (2013), who propose that a late aliquot of the same fluid that forms the potassic and sericitic alteration in porphyry copper deposits likely also forms the vein deposits of pyrite, covellite, enargite, and chalcocite in Butte and similar

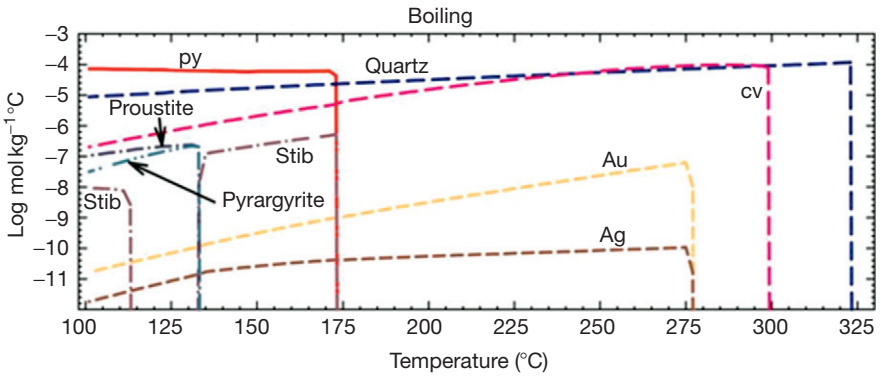

Figure 11 Model results of mineral precipitates from boiling of a 325 °C magmatic fluid from 325 to 100 °C, expressed as the rate of mineral precipitation per degree per kilogram of initial water. See caption to **Figure 10** for mineral abbreviations. The ore mineral assemblage is dominated by covellite and electrum at high temperature, but little enargite and pyrite and no sulfur. Electrum precipitates at a higher temperature (275 °C) upon boiling than it does by mixing, reflecting the removal of sulfur to the gas phase, which liberates Au from $AuHS^0$. The pH remains acidic throughout the run, from 2.4 at 325 °C to 1.2 at 100 °C, which, in combination with sulfur loss to the gas phase, precludes precipitation of galena and sphalerite at low temperature, in contrast to cold water mixing effect (**Figure 10**).

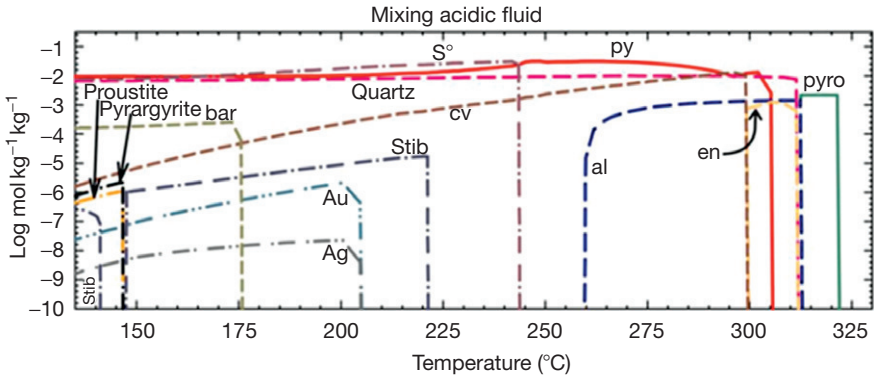

Figure 12 Model results of mineral precipitates from mixing of a 325 °C magmatic fluid with an acidic and Fe-rich 100 °C diluted magmatic gas condensate that had reacted with quartz latite wall rock (**Figure 9**). The ordinate units are log moles of mineral per kilogram of initial water per kilogram of admixed acidic water. See caption to **Figure 10** for mineral abbreviations. The pyrophyllite and alunite at high temperature reflect Al leached from altered rock. This run forms more sulfur than the others, reflecting the more acidic conditions, and electrum precipitates at a lower temperature, reflecting the effect of acid in displacing reaction R3 to the left.

deposits. The particular qualities of pH and metal concentrations of that fluid depend on its ascent history, including extent of wall rock reaction, and its P–T path with or without consequent phase separation. When that fluid arrives in the shallow environment, it may boil, mix with groundwater, or cool by conduction, yielding variations in the ore mineral assemblages and variations in the relative timing of assemblages. The acidic conditions that define the ore type, however, always yield advanced argillic alteration surrounding ores that include pyrite, covellite, enargite, sulfur, and gold.

13.15.2.4 New Ideas about the Geochemistry of Epithermal Deposits

In the past few decades, it has been increasingly apparent that there is a genetic link between some epithermal ores and porphyry ore deposits (e.g., Hedenquist and Lowenstern, 1994; Saunders, 1991; Saunders and May, 1986; Sillitoe, 1997), and thus the geochemistry of the 'porphyry to epithermal transition' should be evaluated using a system-wide approach. The recognition by Heinrich et al. (1999) that a low-density, gold-rich magmatic fluid separates from a much denser magmatic fluid has led to a shift in understanding the geochemical processes related to how magmas release metals to the much shallower epithermal systems (Heinrich 2005; Heinrich et al., 2004; Williams-Jones and Heinrich, 2005; see also **Chapter 13.1**). Thus, the hypothesis of vapor-phase transport of precious metals by supercritical, low-density magmatic fluids offers an attractive mechanism for the formation of LS epithermal deposits, but further investigations of this hypothesis, including laboratory experiments, are needed. New Pb and Re–Os isotopic studies on ore minerals, such as electrum (Kamenov et al., 2007; Saunders et al., 2011c; **Figure 13**), provide evidence for a deep magmatic source of gold in LS ores in the Great Basin of the USA and that mafic magmas are the most likely source of the precious metals (Hames et al., 2009; Kamenov et al., 2007; Saunders et al. 2008). If vapor-phase transport of metals and metalloids are

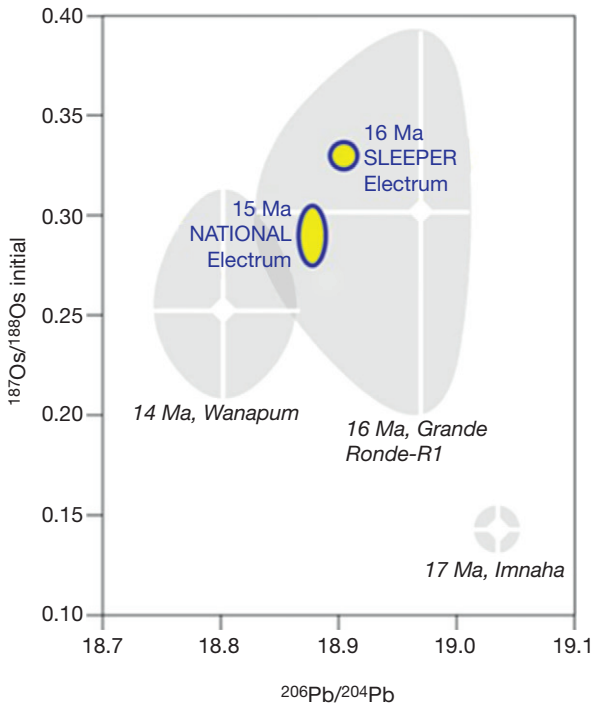

Figure 13 Plot of the initial Os and Pb isotopic composition of Sleeper and National (NV) electrum (data are from Kamenov et al. (2007) and Saunders et al. (2011c)) relative to the range of values from Columbia River basalt flows Wanapum, Grande Ronde, and Imnaha (data from Chamberlain and Lambert, 1994; Chesley and Ruiz, 1998).

important for the formation of LS epithermal ores, then the volatility of these elements should be considered and that too is only recently being evaluated (Saunders et al., 2008; Saunders and Brueseke, 2012). Lindgren (1933) and Saunders (1990, 1994) showed from the interpretation of electrum and silica textures that gold colloids played an important role in forming some bonanza LS epithermal ores such as at the National deposit in Nevada. Saunders (1994) and Saunders and Schoenly (1995) proposed that the electrum colloids form due to boiling of the ore-forming fluids. The new isotopic data of Kamenov et al. (2007) and Saunders et al. (2011c; **Figure 13**) led to a provocative new hypothesis; it can be argued that gold, silver, and copper nanoparticles, which are smaller than colloids, nucleated at much deeper levels than the epithermal environment, locked in a primitive isotopic signature in the process, and traveled to the site of epithermal ore formation as nanoparticles (Kamenov et al., 2007; Saunders, 2012; Saunders et al., 2008, 2011a, 2011b). In this new and relatively untested hypothesis, the same low-density supercritical Cu–Au–Ag-rich fluid found by Heinrich et al. (1999) is interpreted to be close to saturation with respect to electrum, naumannite (Ag_2Se), and chalcopyrite and that perhaps cooling from ~900 to ~700 °C leads to saturation or supersaturation with respect to the aforementioned minerals and they form nanoparticles at a relatively high temperature and deep setting. Recently, Kouzmanov et al. (2010) found indirect evidence of solid precious-metal nanoparticles trapped in fluid inclusions in enargite from a HS epithermal system. Further, Henley et al. (2011) and Berger and Henley (2011) discuss the process of magmatic-vapor expansion and the formation of HS gold mineralization at El Indio, Chile. More research on the role of vapor transport of metals and nanoparticles in hydrothermal ore formation appears to be warranted, including laboratory experiments to test this hypothesis. However, for now, one possible implication is that perhaps epithermal ore-forming processes are not restricted to the shallow crust as has been previously assumed.

13.15.3 Carlin-Type Gold Deposits

13.15.3.1 Introduction

CTD are epigenetic, disseminated, auriferous pyrite deposits enriched in As, Sb, Hg, and Tl that are typically hosted in calcareous sedimentary rocks. They are named after a deposit near Carlin, Nevada, that spurred exploration for similar deposits around the world. In these deposits, gold ore commonly occurs at intersections between faults and permeable reactive strata typically below an impermeable caprock and generally exhibits a central high-grade zone of carbonate dissolution and argillic alteration with micron-sized disseminated pyrite. Pervasively silicified rock, called jasperoid, is generally present within or near ore. In unsilicified rocks, many open fractures and pores are often lined with macroscopic crystals of orpiment, realgar, and calcite. In jasperoid, most fractures and vugs are lined with drusy quartz and may contain kaolinite, stibnite, barite, or calcite (Cline et al., 2005).

The three largest concentrations of CTD are in the western USA and in two areas in southern China (**Figure 14**). The amount of gold present in CTD in north-central Nevada (5500 t) is enormous and is exceeded only by the Witwatersrand in South Africa. The CTD in the Dian-Qian-Gui area and West Qinling belt in southern China each contains about an order magnitude less gold (400 t), but is not as thoroughly explored.

Gold ore is mined by both open-pit and underground operations, with lower ore grades in the former (less than 1 g t^{-1}) and higher ore grades in the latter (more than 34 g t^{-1}). Because most of the gold resides in pyrite, it must be oxidized in a roaster or autoclave to recover gold with cyanide solutions. Natural weathering and oxidation of the pyritic ores eliminates this step and permits direct recovery of gold by cyanide heap leach methods.

The geochemistry of CTD ore formation, described herein, is fairly well understood. In several districts, chemical and isotopic data constrain the source of ore fluid components and the age of mineralization enabling development of genetic models that relate mineralization to the geotectonic evolution of the region. However, the evidence collected from different districts permit multiple interpretations regarding the source of gold (magmatic or sedimentary) and the role of magmatic, metamorphic, and meteoric fluids in gold transport and deposition. Thus, no single model adequately explains the origin of every district.

Recent models for Nevada CTD call upon magmatic (Muntean et al., 2011) or sedimentary (Large et al., 2011a, 2011b) sources for gold and transport to the site of ore deposition by magmatic or metamorphic/meteoric fluids, respectively. Evidence from CTD in the West Qinling belt suggests

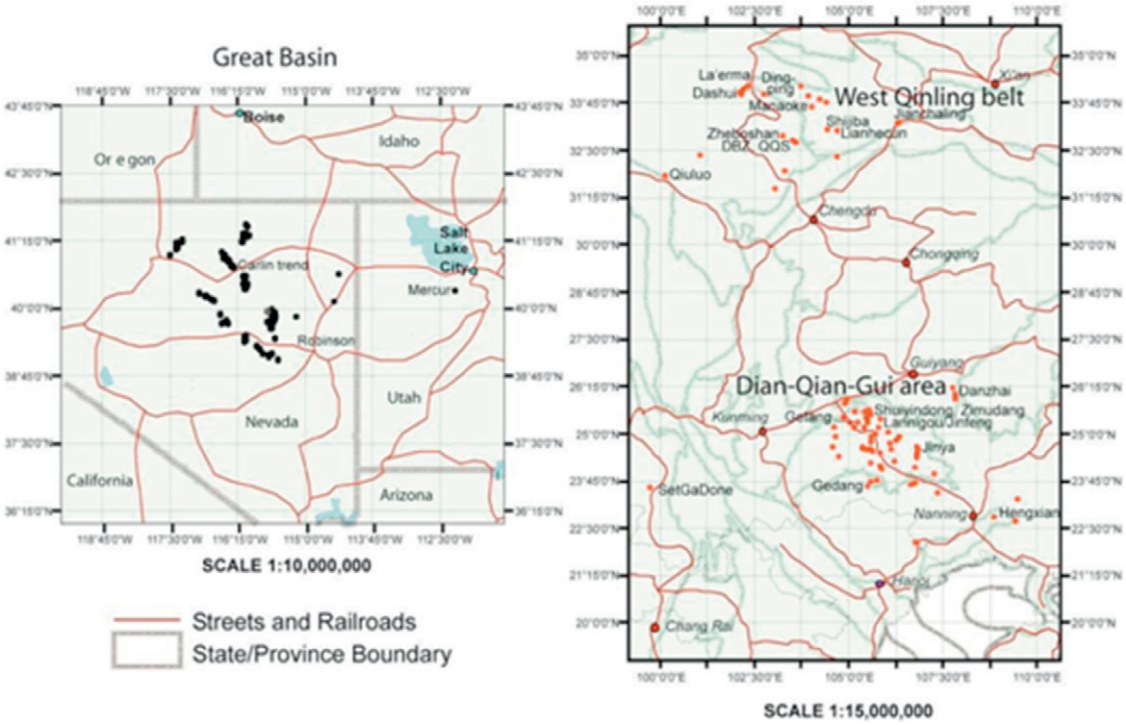

Figure 14 Location of Carlin-type deposits (CTD) (black or red dots) in the Great Basin, western USA, and in the West Qinling belt and Dian-Qian-Gui area of southern China.

they may be epizonal analogues of nearby mesozonal orogenic gold deposits with gold transport by metamorphic fluids (Hofstra et al., 2005; Mao et al., 2002). Likewise, evidence from CTD in the Dian-Qian-Gui area is consistent with an epizonal orogenic model (Hofstra et al., 2005; Hu et al., 2002; Su et al., 2009a, 2009b). If correct, then one might view the so-called CTD in China as simply epizonal orogenic gold deposits that have developed in a specific tectonostratigraphic setting.

13.15.3.2 Age and Geologic Setting of CTD

Many, but not all, CTD in Nevada are essentially the same age and cospatial with late Eocene dikes and thermal halos, aeromagnetic anomalies, and concealed subduction-related magmatic centers (Ressel and Henry, 2006), which were emplaced during slab rollback in an extensional tectonic regime. However, the CTD generally lack, or fail to fit into, alteration zonation patterns typically developed around epizonal porphyry intrusions (Cline et al., 2005). They generally occur in Paleozoic carbonate rocks deposited near the platform margin (Cook, 2005) along reactivated high-angle fault systems that may be inherited from Neoproterozoic rifting and formation of the western continental margin of North America (Lund, 2008). These faults were reactivated during subsequent extensional and contractional orogenies and served to localize Paleozoic hydrothermal dolomite and sedimentary exhalative deposits (SedEx) of Zn, Ba, and Au mineralization, as well as Mesozoic and Cenozoic plutons and related hydrothermal ore deposits (Emsbo et al., 2006). CTD typically occur below a less permeable caprock consisting of shaley slope or basin facies rocks that were either thrust over the platform margin during the early Mississippian Antler orogeny or overlain by Mississippian shales deposited in the adjacent foredeep (Hofstra and Cline, 2000). In the West Qinling belt, orogenic gold deposits occur in metamorphosed Devonian and Carboniferous siliciclastic rocks of the accretionary prism, and CTD occur in Triassic Songpan–Ganzi basin flysch or Neoproterozoic–Permian miogeoclinal rocks along the northern margin of the Precambrian Yangtze craton that were deformed by a south-verging foreland fold-and-thrust belt (Mao et al., 2002). Both gold deposit types are inferred to have formed after peak deformation, metamorphism, and magmatism (c.245–220 Ma) during the final stages of contraction (Mao et al., 2002), transpression (Vielreicher et al., 2002), or postcollisional uplift and extension of the Triassic Qinling collisional orogen. In contrast, in the Dian-Qian-Gui area, CTD are hosted in Cambrian to Middle Triassic age platform carbonate (±terrestrial basin), transitional, and basinal siliciclastic rocks, and locally in mafic intrusions (diabase and gabbro) or Late Permian Emeishan volcaniclastic rocks along the southwest margin of the Yangtze craton. Field relationships and unconventional isotopic dates suggest the deposits are Cretaceous in age (Hu et al., 2002; Su et al., 2009a, 2009b), although a new Re–Os isochron date of 193 ± 13 Ma on arsenian pyrite and a ^{40}Ar–^{39}Ar date of 194.6 ± 2 Ma on sericite from Jinfeng both indicate an older age (Chen et al., 2007; Gu et al., 2010).

13.15.3.3 Ore and Gangue Minerals

In all CTD, there are pre-ore hydrothermal breccias, followed by a main ore stage where fluids dissolve or replace minerals in

the host rocks, and subsequently there is a late ore stage when changes in temperature, fluid mixing, or phase separation (boiling) cause minerals to precipitate in open fractures and vugs (Figure 15).

Most of the gold in the ores resides in pyrite that replaces Fe-bearing minerals in the host rocks and commonly forms rims on pre-ore pyrite (Figure 16). Hence, pyrite is the principal ore mineral in CTD. Native gold is quite rare and generally is only visible in supergene goethite pseudomorphs of main ore-stage pyrite. In some deposits, gold also occurs in marcasite or arsenopyrite, jasperoidal quartz, and organic carbon. Main ore-stage silicate minerals include quartz, dickite, kaolinite, illite, illite–smectite, smectite, and chlorite. Pre-ore carbonate minerals are generally dissolved or replaced during the main ore stage, but hydrothermal calcite, dolomite, ankerite, and siderite also precipitated during main stage ore formation.

Vug or fracture-filling minerals of the late ore stage include pyrite, marcasite, orpiment, realgar, native arsenic, stibnite, cinnabar, lorandite ($TlAsS_2$), galkhaite [$(Cs,Tl)(Hg,Cu,Zn)_6(As,Sb)_4S_{12}$], sphalerite, tellurides, quartz, dickite, calcite, barite, and adularia (Figure 17). In a few deposits, millimeter-sized native gold is present in vugs or calcite veinlets. Micron-sized gold has been observed in late ore-stage marcasite and cinnabar.

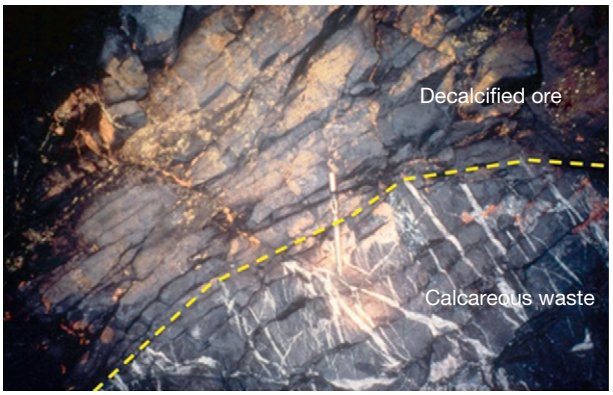

Figure 15 Photograph of decalcification front in Ordovician–Silurian Hanson Creek Limestone, Jerritt Canyon. Pre-ore calcite veins in limestone are absent in decalcified limestone. Fractures in ore are filled with orpiment and realgar. Pen for scale.

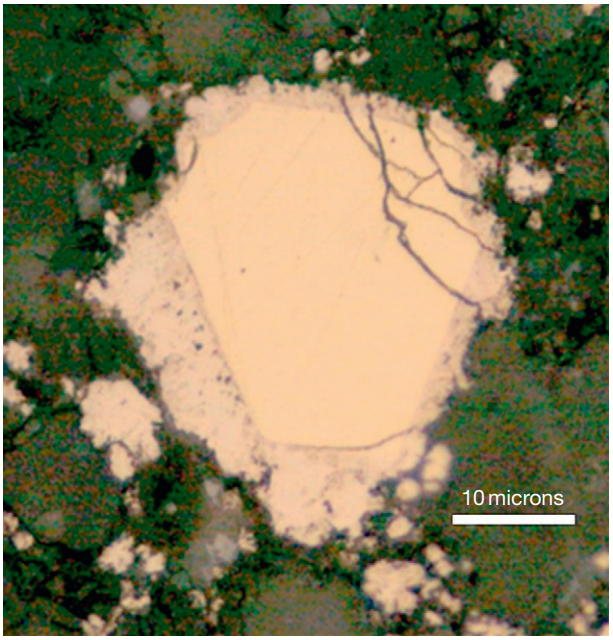

Figure 16 Reflected light photomicrograph of zoned euhedral pre-ore-stage pyrite with rim of ore-stage pyrite, Deep Star deposit, Carlin Trend. Ore-stage pyrite is more fine grained, anhedral, and darker than pre-ore pyrite.

13.15.3.4 Geochemistry of Rocks and Pyrite

The application of multivariate statistical techniques, such as factor analysis or cluster analysis, to whole-rock multielement geochemical data has proved useful in the identification of element associations of geologic significance (Hofstra and Cline 2000; Hofstra et al., 2011). Element associations for rock samples from CTD determined by these methods often correspond to the marine carbonate (CO_2, Ca, Sr, Mg, and Mn), terrigenous detritus (Al, Ti, K, REE), and organic (V, Ni, Mo, Se, and Zn) components of the host sedimentary rocks. For example, Figure 18 profiles the correlation of organic carbon, organic component factor scores, key elements, and the $\partial^{34}S_{sulfide}$ composition of the Popovich Formation, which is an important host for gold in the northern Carlin Trend. Carlin-type element associations identified in this manner include silicification with stibnite (Si and Sb) or precipitation of main ore-stage pyrite and late ore-stage orpiment, realgar, cinnabar, and lorandite (Au, As, Sb, Hg, and Tl). Depending on the pre- and post-ore history of the district, element associations due to other igneous and hydrothermal events may also be apparent, such as SedEx mineralization, felsic or mafic dikes, contact metamorphic aureoles, or base metal mineralization. Such differences are important and make it possible to distinguish preexisting geochemical suites from those imposed by Carlin-type hydrothermal systems. Likewise, multivariate statistical analyses of micro-analytical scans (e.g., LA-ICP-MS) across pyrite present in the ore can aid identification of the trace element associations present in diagenetic pyrite (V, Ni, Co, Cu, Mo, and Se) and main ore-stage pyrite (Au, As, Sb, Hg, Tl, ±(Cu, Pb, Te)) (Cline et al., 2005; Large et al., 2009).

To identify elements that were immobile, introduced, or depleted and to measure mass losses or gains associated with alteration and mineralization, the whole-rock multielement compositions of barren, unaltered host rocks and ore-grade equivalents can be compared on an isocon diagram (Grant, 1986; Hofstra and Cline, 2000). An isocon diagram for the Carlin deposit (Figure 19(a)) shows that SiO_2, Al_2O_3, Fe_2O_3, K_2O, TiO_2, and P_2O_5 were immobile; CaO, CO_2, MgO, Na_2O, and MnO were depleted; and S, As, Sb, Tl, Hg, and Au were introduced. The concentration of immobile elements in the ore is enriched by as much as 50% due to mass loss associated with dissolution of carbonate minerals and argillization of albite in the silty laminated limestone host rock. Where this approach has been properly applied to other CTD, evidence for analogous gains and losses is generally detected (e.g.,

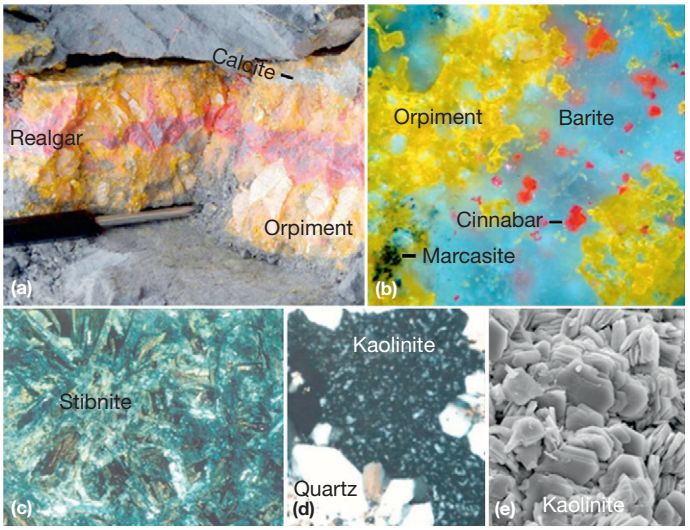

Figure 17 Images of late ore-stage minerals: (a) orpiment, realgar, and calcite in decalcified limestone (Getchell); (b) orpiment, marcasite, and cinnabar cemented by barite, Jerritt Canyon; (c) Stibnite rosette, Jerritt Canyon; (d) Drusy quartz and kaolinite, Deep Star (Thompson, 2005); (e) SEM image of kaolinite, Deep Star mine.

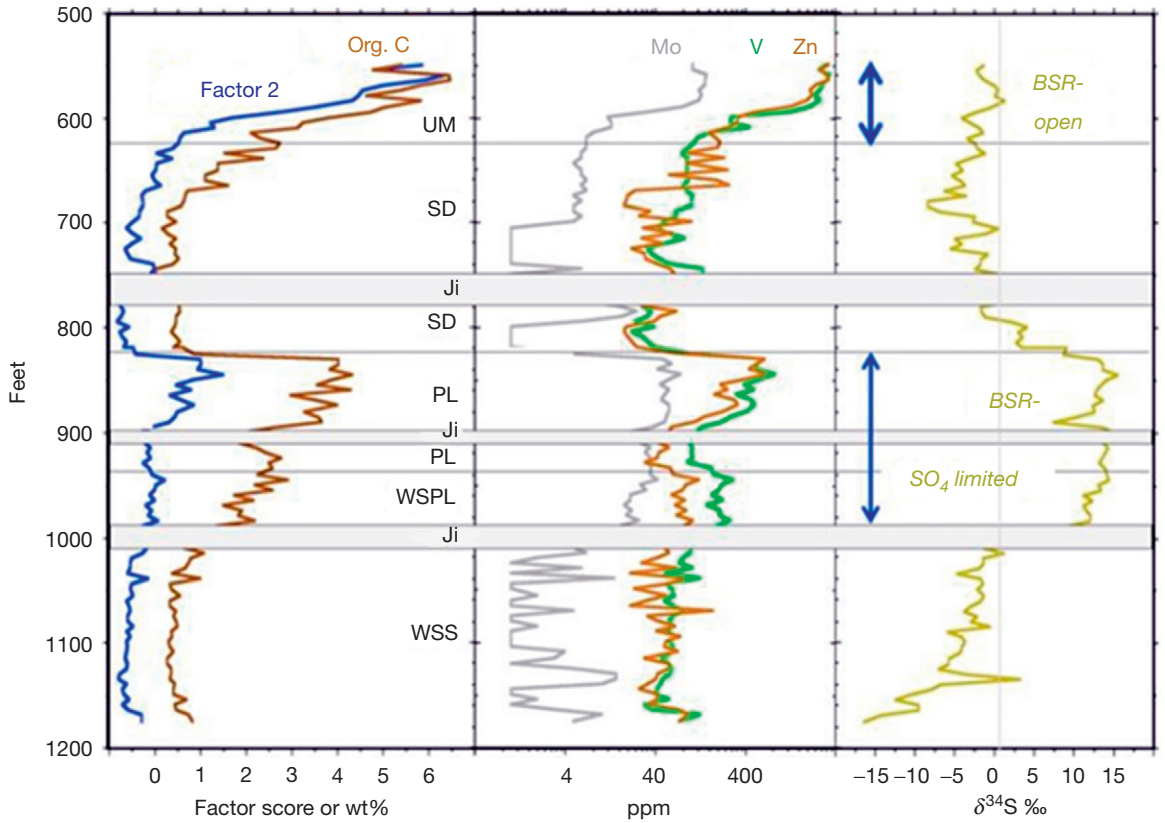

Figure 18 Downhole profile of metals and $\partial^{34}S_{sulfide}$ in strata (UM upper mud unit, SD soft sediment unit, PL planar unit, WSPL upper wispy planar subunit, and WSS lower wispy unit) of the Devonian Popovich Formation, from Hofstra et al. (2011). Factor 2 element suite comprised Ni, Cu, V, Zn, Cd, organic C, Mo, Y, and Cr. While Se was not determined, studies by Large et al. (2011a, 2011b) indicate it is part of the metalliferous black shale element suite. Sulfur isotope data are suggestive of bacterial sulfate reduction (BSR) in open and sulfate-limited marine environments. Intervals intruded by Jurassic dikes (Ji) are masked in gray.

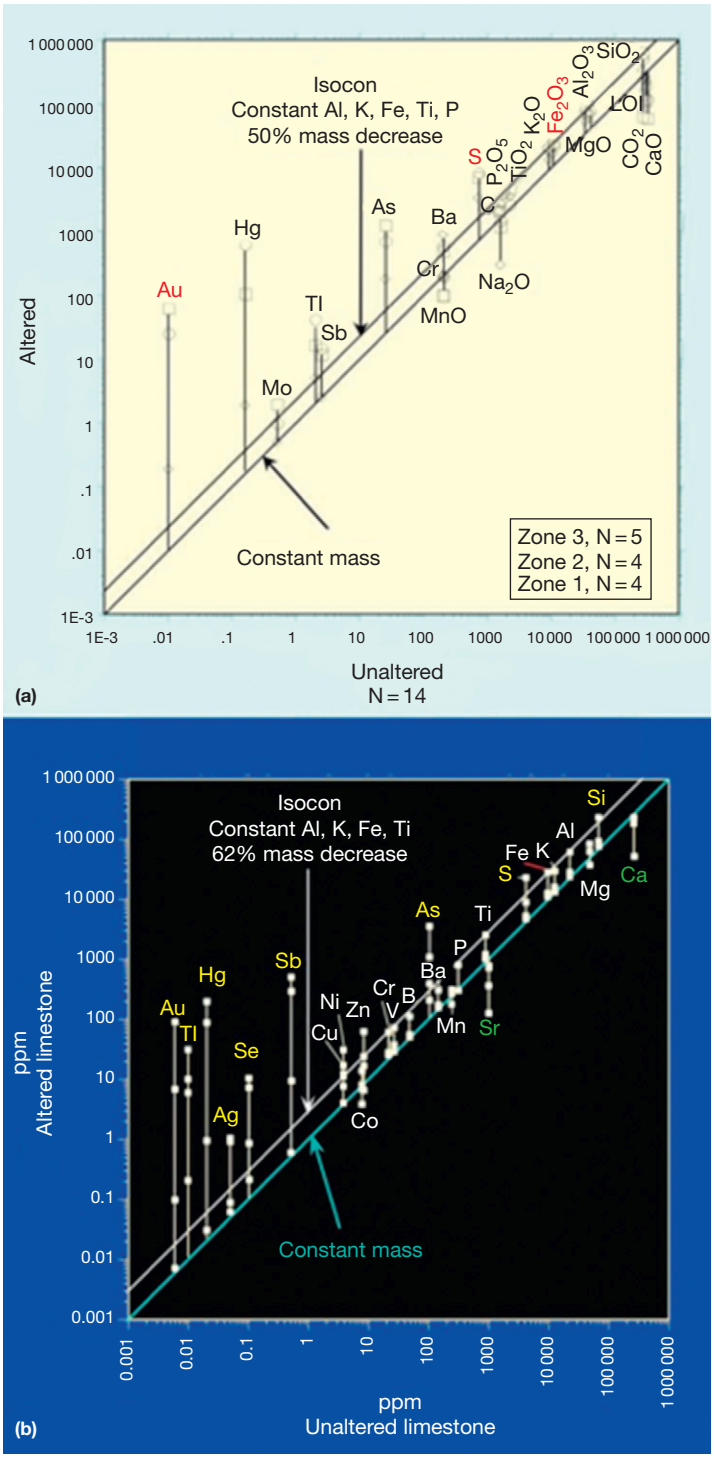

Figure 19 Isocon diagrams showing element mobility in (a) Silurian–Devonian Roberts Mountains Fm. at Carlin (data from Bakken, 1990) and (b) Ordovician–Silurian Hanson Creek Fm. at Jerritt Canyon (data from Hofstra, 1994). Elements that plot above or below the isocon are, respectively, introduced or depleted. In each deposit, the immobility of Fe and the introduction of S and Au are clear evidence of gold precipitation by sulfidation of host-rock iron.

Jerritt Canyon, Figure 19(b)). The immobility of Fe and the introduction of S, Au, As, Sb, Hg, and Tl, evident on the isocon diagrams, require that the Au- and trace element-rich pyrite in the ore precipitated where H_2S in ore fluids reacted with Fe-bearing minerals in the host rocks (sulfidation; Hofstra et al., 1991), discussed further in the succeeding text. Although less common, isocon diagrams for samples collected from the margins of a few deposits show that Fe locally was introduced, which suggests ore fluids locally mixed with external Fe-bearing fluids (Cail and Cline, 2001; Kesler et al., 2003).

In many early studies of CTD, multielement analyses were not conducted, and only a small suite of trace elements were determined on ore-grade material. In such cases, an alternative approach is to scale the trace element concentrations in the ore (e.g., >1 ppm Au) to their average concentrations in the crust (Clarke values; Levinson, 1974). Element enrichment plots constructed with such data from 31 CTD in Nevada (Figure 20) show elements that form sulfide complexes generally are enriched more than one hundred times their Clarke values (Au, As, Sb, Hg, and Tl), whereas those that form chloride complexes (Ag, Pb, Zn, and Cu) or oxyanions (Mo and W) are not as enriched (<100 × Clarke). The strong enrichment of the so-called Carlin suite of trace elements in the deposits is a direct reflection of the importance of sulfide complexing in ore fluids. Trace element data from CTD in the West Qinling belt and Dian-Qian-Gui area of southern China

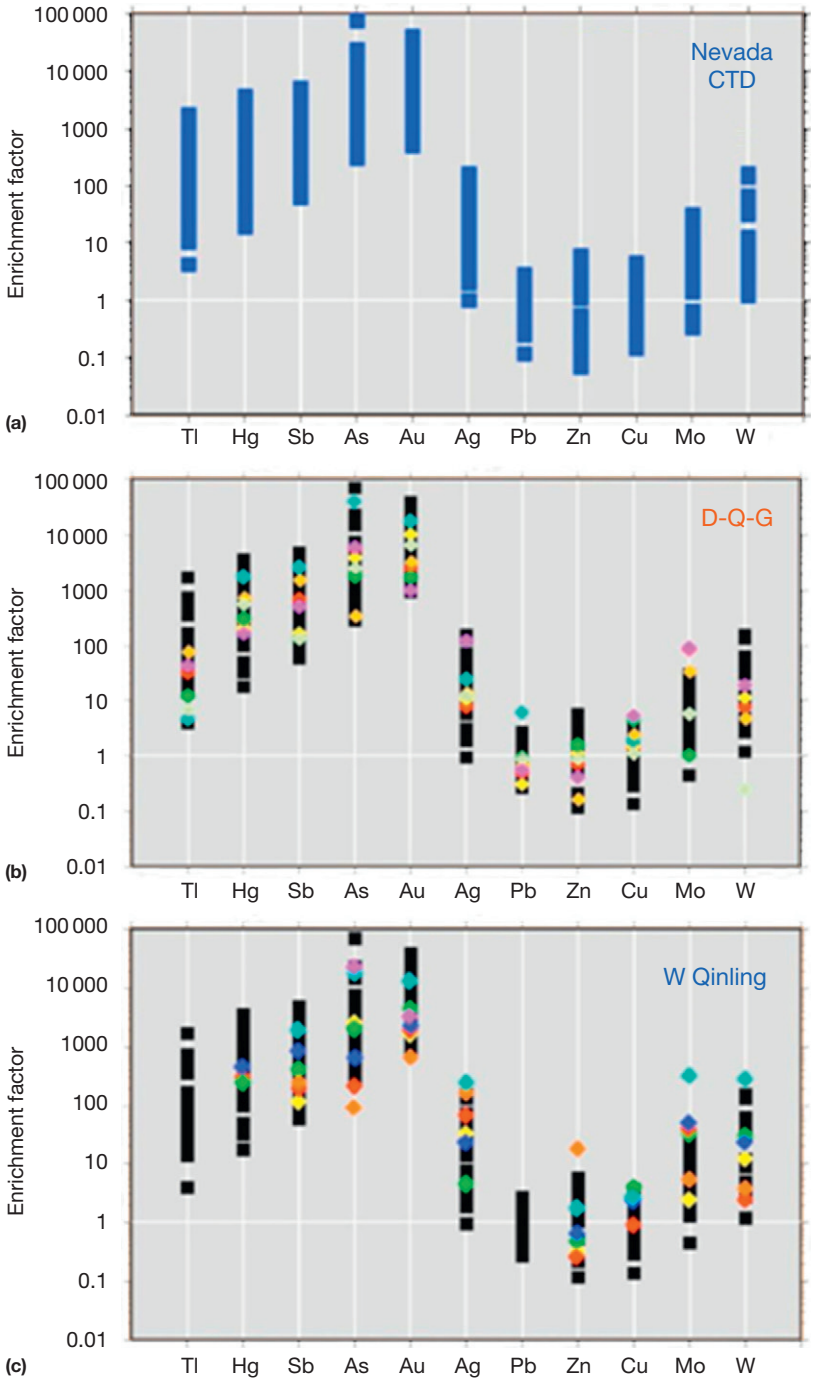

Figure 20 Trace element enrichment plots for ore (≥1 ppm Au) relative to average crust in (a) 31 Nevada Carlin-type deposits (CTD) from each significant gold district. In (b) and (c), data from seven CTD in the Dian-Qian-Gui area and five CTD in the West Qinling belt (colored diamonds) are shown relative to data from CTD in Nevada (black bars). The results suggest that the chemistry of ore fluids in each area was very similar.

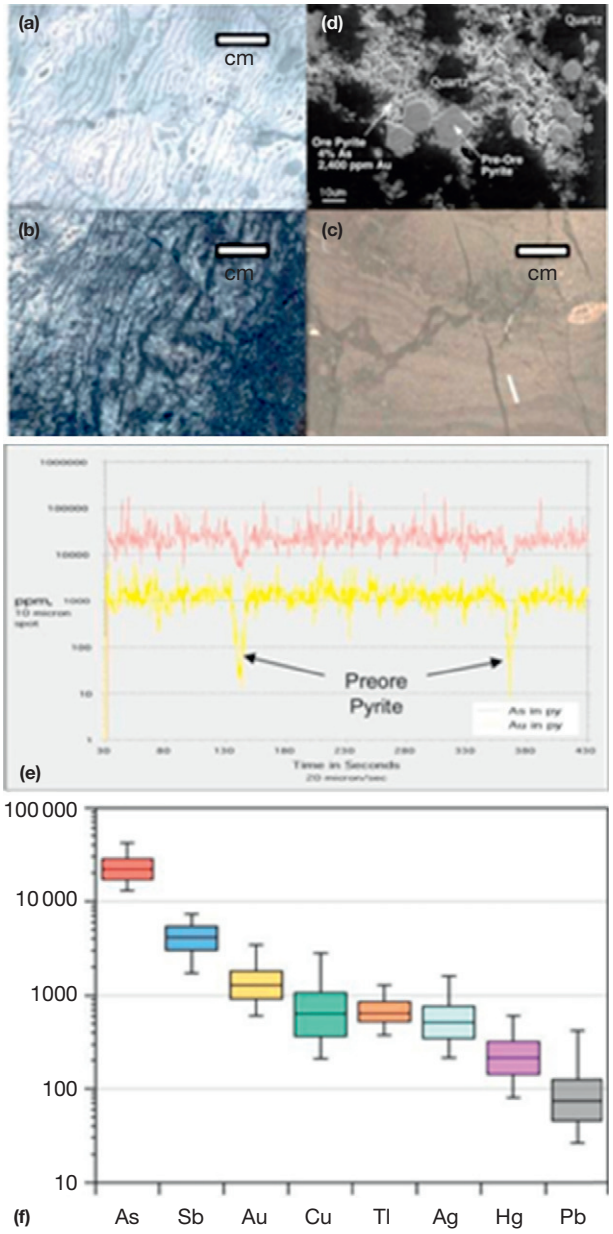

Figure 21 (a–d) Photographs from Emsbo et al. (2003) of (a) barren hydrothermal zebra texture dolomite in Devonian Bootstrap Limestone; (b) sulfidized dolomite with dark, fine-grained ore pyrite replacing ferroan dolomite; and (c) internal sediment in a breccia cavity with layers containing ore pyrite. The white line marks a laser ablation (LA) trace across one layer shown in (e). (d) Scanning electron microscope (SEM) backscatter image of euhedral pre-ore and bright anhedral ore pyrite. (e) Profile of arsenic (red) and gold (yellow) concentrations in pyrite along the 8 mm LA induction-coupled plasma (ICP)-mass spectrometer (MS) trace. The dips in As and Au correspond to the position of coarse-grained pre-ore pyrite grains. (f) Bar and whisker plot for nine elements detected in ore pyrite along the trace. The 10th, 25th, 50th, 75th, and 90th percentile values are indicated.

exhibit nearly identical enrichments (**Figure 20(b)** and **20(c)**) and likewise must have formed from H_2S-rich fluids at conditions similar to those of CTD in Nevada.

At the large (220 t Au), high-grade (24.7 g t^{-1}) Meikle deposit in the Carlin Trend of Nevada, evidence of carbonate dissolution and sulfidation is exceedingly clear because the ore occurs in an unusual ferroan dolomite host rock (Emsbo et al., 2003; **Figure 21(a)** and **21(b)**). LA-ICP-MS microanalyses of ore pyrite that replaced ferroan dolomite (**Figure 21(b)** and **21(c)**) provide a clear indication of the relative concentrations of trace elements (As > Sb > Au > Cu > Tl > Ag > Hg > Pb; **Figure 21(e)** and **21(f)**). Microanalyses of ore pyrite from other CTD show that its composition varies from deposit to deposit, both within and between different mining districts. For example, a greater abundance of Te and Cu is present in ore pyrite from certain deposits and districts (e.g., Barker et al., 2009). The sulfur isotopic composition of ore pyrite in CTD also varies. For example, in the northern Carlin Trend, the $\partial^{34}S$ of ore pyrite from the high-grade Meikle deposit and the central high-grade part of the enormous Betze-Post deposit is about 10‰ (Emsbo et al., 2003), whereas values in the Screamer section on the margin of Betze-Post are near 0‰ (Kesler et al., 2005; Hofstra et al., 2011; **Figure 22**). Likewise, $\partial^{34}S$ of ore pyrite in the Getchell trend is near 0‰, whereas in the Jerritt Canyon district it is near 10‰ (Cline et al., 2005). These relationships suggest that the source of the H_2S in ore fluids varied significantly within and between mining districts.

13.15.3.5 Composition of Ore Fluids

Studies of fluid inclusions in ore-stage quartz from Nevada CTD commonly indicate homogenization temperatures of 180–240 °C, salinities of 3–6 wt% NaCl (equiv.), and CO_2 contents of 1–4 mol%. After correction for the amount of CO_2 present (see succeeding text), salinities may actually be less than 3 or 4 wt% NaCl (equiv.). Ion chromatographic analyses of inclusion fluid extracted from orpiment, realgar, and stibnite generally show that $Na > Cl > K > Mg > NH_4 > F > Br$; Ca and CO_3 are compromised by calcite contamination. Mass spectrometric analyses of individual fluid inclusions or inclusion assemblages in ore-stage minerals, opened by thermal decrepitation, show that $CO_2 > CH_4 \approx N_2 > H_2S > SO_2$. Of particular importance for estimation of ore-forming solution pH and gold transport, CO_2 is between 1 and 4 mol%, and H_2S concentrations are commonly 10^{-2}–10^{-1} molal (Hofstra and Cline, 2000). Eocene reconstructions of Carlin-type districts suggest most deposits formed at depths of 1–3 km, with a few as deep as 5 km or as shallow as 300 m (Cline et al., 2005; and references therein). Such depths correspond to hydrostatic pressures of less than 300 bars.

13.15.3.6 Carbonate Dissolution

Carbonic acid appears to have been the major acid volatile in ore fluids responsible for carbonate dissolution and hydrolysis of feldspars to illite and kaolinite. **Figure 23** shows that dissolution of carbonate rocks generates CO_2 such that fairly high confining pressures (e.g., 250 bars) are required to prevent fluid immiscibility (boiling), for which there generally is little evidence. It also shows that high fluid–rock ratios (>550–775)

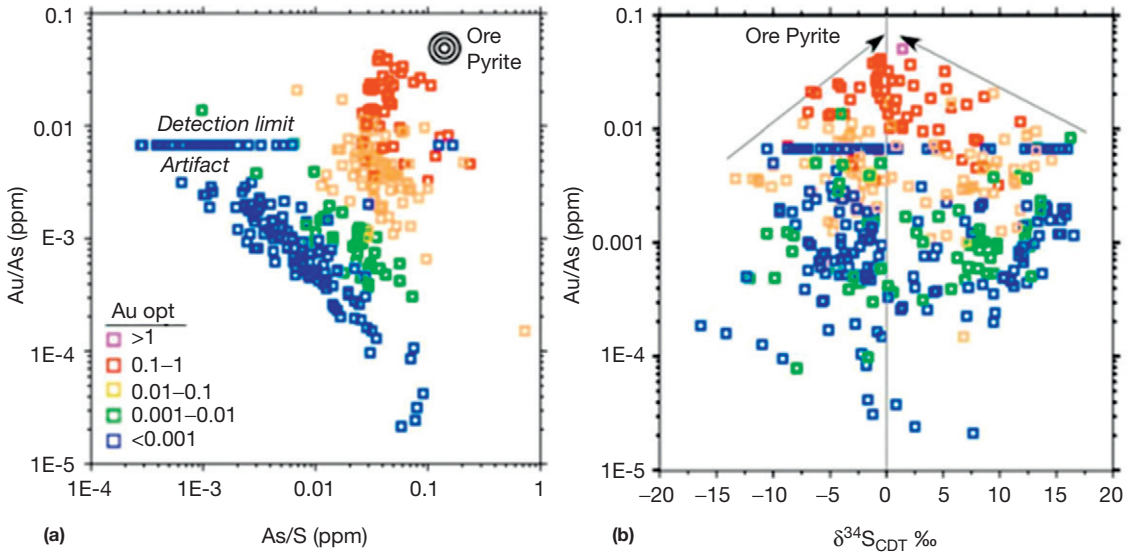

Figure 22 (a) Plot of whole rock Au/As and As/S ratios converge towards that of ore pyrite with increasing gold grade; (b) Plot of whole-rock $\delta^{34}S$ values and Au/As ratios converge towards that of ore pyrite from Hofstra et al. (2011). From the 'Screamer' sector of Betze-Post deposit, Carlin Trend.

are required to produce the central zones of calcite and dolomite absent argillic alteration. Any calcite precipitated in open fractures from such neutralized ore fluids contains a mixture of hydrothermal fluid and country rock carbonate, which can mask the stable isotopic composition of ore fluids.

13.15.3.7 Ore Fluid Composition and Precipitation Mechanisms

The sulfidation state of the ore fluids (log fS_2 −15 to −10) is constrained by the homogenization temperatures of fluid inclusions and the common occurrence of orpiment and realgar in the ore (Figure 24). The oxidation state of the ore fluids (log fO_2 −41 to −34) is constrained by the absence of hydrothermal hematite, ubiquitous presence of pyrite, and the predominance of CO_2 over CH_4 in fluid inclusions (Figure 25(a)). The pH of ore fluids was moderately low as indicated by the common occurrence of kaolinite or dickite, with or without sericite, and the general absence of adularia (Figure 25(a) and 25(b)). The dissolution of calcite and dolomite is further evidence that the early fluids were acidic with pH less than about 4.5 (Figure 23). Marcasite, which occurs in some ores, is only stable at pH less than 5 and temperatures less than 240 °C (Murowchick, 1992). The low pH of ore fluids and consequent increases in Al solubility explain the abundance of Al in dark or weakly cathodoluminescent bands of drusy quartz (Rusk et al., 2008). The alternation of Al-rich and Al-poor bands in drusy quartz with constant $\delta^{18}O$ values may reflect changes in pH related to the successive influx and neutralization of acidic fluids via carbonate dissolution.

The mineral evidence of a high sulfidation state (Figure 24) is consistent with the measured H_2S content of fluid inclusions (avg. 10^{-2} molal; Hofstra and Cline, 2000). Figure 25 shows that at the indicated range of H_2S activity and fO_2 that gold solubility as $Au(HS)_2^{1-}$ and $AuHS^o$ complexes are in the 100–1000 ppb range over a wide range of near neutral to acidic pH. Such high gold contents have actually been detected in quartz-hosted fluid inclusions from CTD in the Dian-Qian-Gui area of China (Su et al., 2009a, 2009b). To attain such high gold solubilities, the activity of H_2S must be greater than that along the pyrite–hematite or pyrite–magnetite buffers (Figure 25(b)). The paucity of hematite and magnetite in the suboxic to euxinic seafloor depositional environment of carbonaceous pyritic sedimentary rocks may be one reason that ore fluids evolved to such high sulfidation states. Perhaps another reason is that H_2S in early stage ore fluids replaces any hematite, magnetite, or other iron-bearing minerals in the host rocks with pyrite, causing successive aliquots of ore fluid to be more H_2S rich.

Quartz, stibnite, realgar, orpiment, gold, and cinnabar all have prograde solubility and precipitate from ore fluids during cooling (Hofstra, 1994; Hofstra et al., 1991). In contrast, calcite has retrograde solubility and dissolves as ore fluids cool or are neutralized by carbonate rocks. Calcite may precipitate as neutralized ore fluids lose CO_2 to the vapor phase. Barite forms as Ba in reduced ore fluids and mixes with external fluids containing marine sulfate derived from sedimentary rocks (Cline et al., 2005).

Equilibrium chemical modeling of isothermal reactions between H_2S-rich ore fluids and host rocks containing different amounts of reactive iron rationalize several key features of the ores (Figure 21). First, the gold grade and extent of mineralization vary as a function of the amount of reactive iron in the host rocks (Figure 26), with large, low-grade ore bodies in host rocks with small amounts of reactive Fe (e.g., 0.25 wt%) and small, high-grade ore bodies in host rocks with large amounts of reactive Fe (e.g., 5 wt%). Second, regardless of the iron content of the host rocks, the gold/pyrite ratio is relatively constant, corresponding to about 1000–1500 ppm Au in pyrite. Such concentrations are similar to the average abundance of Au in ore pyrite from several Nevada CTD (Reich et al., 2005).

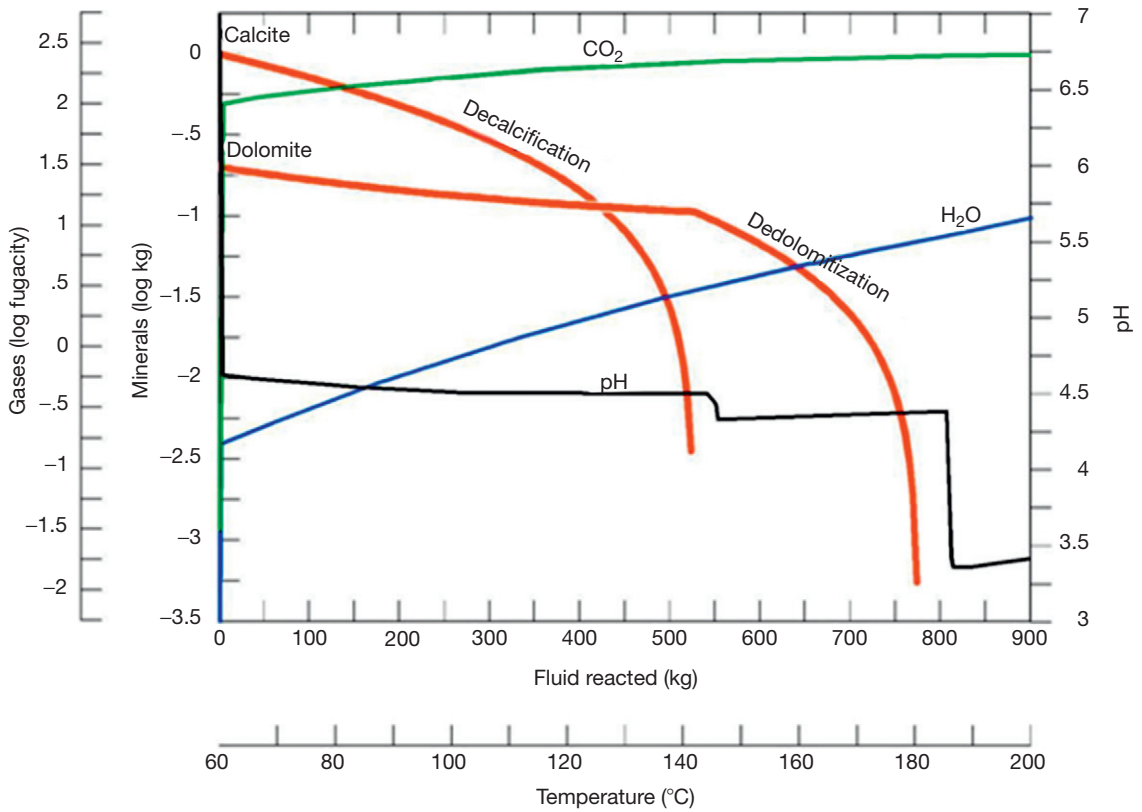

Figure 23 Plot of chemical reaction between a 200 °C ore fluid containing 4 mol% CO_2 and 6 wt% NaCl (equiv.) with a typical carbonate rock comprised of calcite (1 kg) and dolomite (0.2 kg) containing a dilute, pH 7, 60 °C pore fluid (e.g. local ground water at 2 km depth). The model shows how the abundance of calcite and dolomite, pH, and the fugacity of H_2O and CO_2 vary during fluid–rock reaction. During decalcification, pH remains near 4.5. During dedolomitization, pH drops to 4.3. Following dolomite dissolution, pH drops to about 3.5 (i.e., central zone of carbonate absent argillic alteration). About 525 kg of ore fluid is required to dissolve 1 kg of calcite, and an additional 250 kg is required to dissolve the remaining 0.2 kg of dolomite from Cline et al., (2005).

13.15.3.8 Element Substitution in Pyrite

Despite the apparent correspondence between equilibrium chemical models and the amount of Au and pyrite precipitated by sulfidation in the ores, experimental studies show that the solubility of Au in stoichiometric pyrite is only about 3 ppm (Tauson, 1999). In contrast, the solubility of Au in arsenopyrite is much greater at about 30 000 ppm (Fleet et al., 1997). These experiments suggest that entry of Au into the pyrite lattice is facilitated by As. Microanalytical studies (electron microprobe analyzer (EMPA), secondary ion mass spectrometry (SIMS), x-ray absorbance near edge structure (XANES) and high resolution transmission electron microscopy (HRTEM)) of arsenian pyrite from several CTD (Hough et al., 2011; Kesler et al., 2011; Reich et al., 2005; and references therein) show that as As^{1-} substitutes into the S site, there is significant substitution of Au^{1+} into pyrite (Figure 27). These studies also demonstrate that arsenian pyrite with discrete Au^{o} nanoparticles (see Hough et al. 2011) is actually rare and only present in samples with Au/As molar ratios greater than about 0.02 (Figure 27). An exemplary sample with abundant gold nanoparticles is from the Screamer sector of the Betze-Post deposit (Kesler et al., 2011), where arsenian pyrite precipitated by sulfidation of an external Fe-bearing fluid (Kesler et al., 2003). Thus, the rare formation of gold nanoparticles in arsenian pyrite may be an indication of fluid mixing.

Most importantly, the microanalytical results indicate that most of the gold in CTD precipitated in solid solution in arsenian pyrite (Kesler et al., 2011; Reich et al., 2005). The correspondence between the modeled proportion of gold and pyrite produced by sulfidation of host-rock Fe and the abundance of Au actually present in solid solution in arsenian pyrite suggest ore fluids could not have been highly undersaturated with respect to native gold. It also allows that the ore fluids would have been saturated with native gold if arsenic had not been present in sufficient amounts to form arsenian pyrite.

Regardless of whether ore fluids were saturated with native gold and pyrite or auriferous arsenian pyrite, the consumption of H_2S during sulfidation of host-rock Fe (±external Fe-bearing fluids) was the driving mechanism for their precipitation. Furthermore, the assemblage of trace elements typically detected in ore pyrite (As, Sb, Cu, Tl, Pb, Hg, and Ag; Figure 22) all form sulfide complexes. The fixation of such sulfide-complexed trace elements in ore pyrite may be an indication of the relatively low temperatures or ore formation and the rapid rate of pyrite precipitation during sulfidation, which also is suggested by the small grain size and anhedral morphology of ore pyrite (Figure 15).

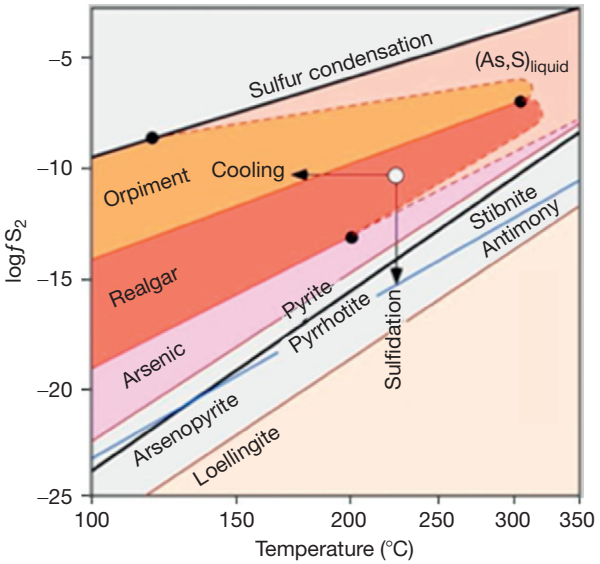

Figure 24 Log fS_2 versus T diagram showing stability fields of Fe minerals (bold black line), As minerals (colored fields), Sb minerals (blue line), and As–S liquid (dashed lines). The white dot corresponds to the modeled ore fluid and the black arrows shifts induced by cooling and sulfidation from Simon et al. (1999).

Arsenian pyrite is present in other gold deposit types, including LS and HS epithermal deposits and orogenic gold deposits, and can be classified into two types: As^{-1} pyrite where As substitutes into the S site under reducing conditions and As^{+3} pyrite where As substitutes into the Fe site under more oxidizing conditions (Deditius et al., 2008; Kesler et al., 2011). Such pyrites plot in different domains on an As–Au plot (Figure 27). Pyrites from orogenic, Carlin-type, and LS epithermal gold deposits mostly occur in the As^{-1} pyrite field where Au^{+1} substitutes into the pyrite lattice. In contrast, pyrites from HS epithermal deposits plot in the As^{+3} pyrite field and may contain native gold (Figure 27). This difference indicates that pyrite in orogenic, Carlin-type, and LS epithermal gold deposits formed under more reducing conditions than pyrite in HS epithermal gold deposits. Thus, despite the presence of high sulfidation state As-minerals in CTD, the predominance of As^{-1} pyrite suggests they are geochemically more like orogenic and LS epithermal gold deposits and not simply Cu-poor, sediment-hosted, analogues of HS epithermal gold deposits.

13.15.3.9 Source(s) of Ore Fluid Components

Water: H and O isotopic data from each district are usually suggestive of either two or, in a few districts, three sources of water (Cline et al., 2005; Hofstra and Cline 2000; Hofstra et al., 2005; Hu et al., 2002). Evidence for groundwater that plots near the meteoric-water line is typically obtained from analyses of late ore-stage minerals and inclusion fluids. Evidence for exchanged meteoric water that plots well away from the meteoric-water line is generally obtained on main ore-stage kaolinite, quartz, and inclusion fluids. Evidence for a more deeply sourced magmatic or metamorphic fluid detected in some deposits (Deep Star) and districts (Getchell Trend and West Qinling) is from main ore-stage kaolinite as well as inclusion fluids in main and later ore-stage minerals.

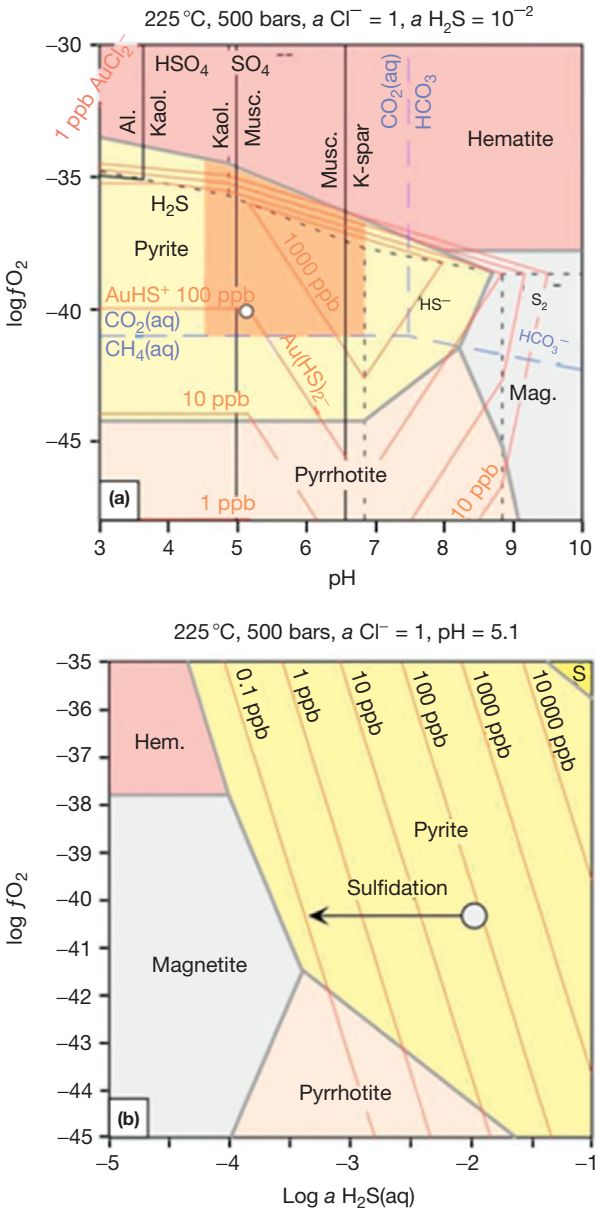

Figure 25 (a) Log fO_2 versus pH diagram showing solubility contours for gold (thin red lines) relative to stability fields of Fe minerals (colored fields), Al silicates (vertical black lines), predominance fields of sulfur species (black dashed lines) and carbon species (blue dashed lines), and the model ore fluid (white dot). (b) Log fO_2 versus log a H_2S(aq) diagram showing the solubility of gold (thin red lines) relative to the stability fields of Fe minerals (shaded fields) and liquid sulfur (S). The white dot corresponds to the modeled ore fluid and the black arrow shifts induced by sulfidation (adapted from Hofstra AH and Cline JS (2000).

CO_2: As described earlier, CO_2 is the principal acid volatile in ore fluids, and CO_2 metasomatism of marine carbonate rocks liberates additional CO_2 that may mask the isotopic signature of the source. Consequently, the C and O isotopic data on altered rock with recrystallized carbonate minerals and late ore-stage calcite often reflect the isotopic composition of

variably exchanged meteoric water and carbonate host rocks (Hofstra and Cline, 2000; Hofstra et al., 2005; Hu et al., 2002). A few districts (e.g., Getchell) exhibit data arrays that extend to lower C and O values that may reflect a deeper magmatic or metamorphic source.

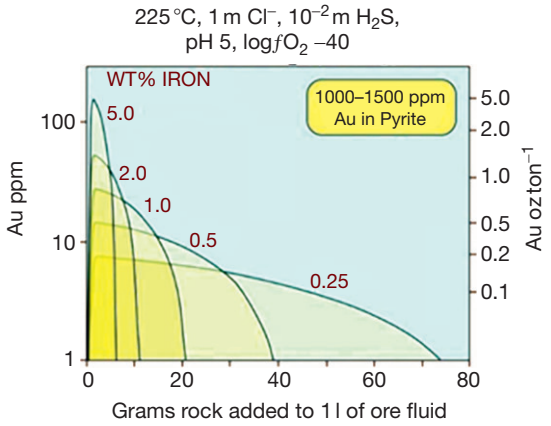

Figure 26 Plot showing the modeled gold grade and mass of ore produced by sulfidation of rocks with different iron contents. In each reaction path, the gold/pyrite ratio corresponds to 1000–1500 ppm gold in pyrite (reproduced from Hofstra AH and Cline JS (2000).

H_2S: As shown in the preceding text, H_2S is the main ligand for Au transport in CTD. If it were derived solely from a magmatic source, ore pyrite from the heart of each ore zone should have $\delta^{34}S$ values near 0‰ and late ore-stage orpiment, realgar, and stibnite should have complimentary values that differ by their lower temperatures of formation and fractionation factors. Whereas the Getchell Trend has some data that fits this model, most districts yield much higher or lower $\delta^{34}S$ values that require a sedimentary source (Cline et al., 2005). Some districts, such as the northern Carlin Trend, exhibit high $\delta^{34}S$ values (10‰) in the heart of large high-grade deposits (Meikle and Betze) and low $\delta^{34}S$ values (0‰) in peripheral ore zones (Screamer). This may indicate that the isotopic composition of S in ore fluids evolved due to fluid–rock reactions (particularly considering the abundance of pre-ore pyrite in sedimentary host rocks) or mixing with external H_2S-bearing fluids (Hofstra et al., 2011).

He: Helium isotope data of inclusion fluid extracted from ore and late ore-stage minerals are suggestive of a mixture of crustal and mantle-derived He with R/Ra of 0.33–1.41 in the Carlin Trend and Jerritt Canyon district (Hofstra et al., 2010) and R/Ra of 0.14–1.47 in the Getchell Trend (Cline et al., 2005). The He isotope data resemble those of Eocene felsic intrusions with R/Ra of 0.11–0.76 that also contain mixtures of He from crustal and mantle sources (Hofstra et al., 2010). With such data, it is difficult to discriminate between He from felsic magmas and He in convecting fluids that obtained

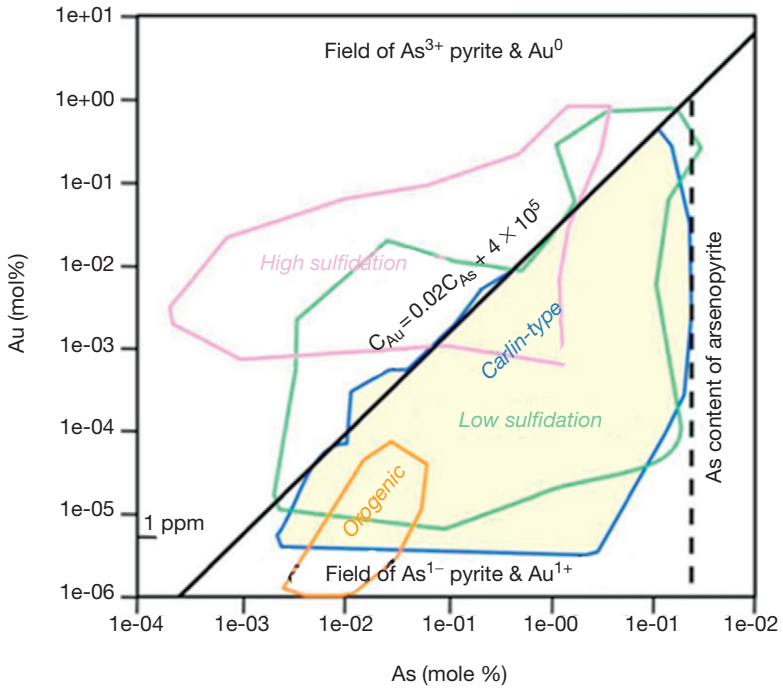

Figure 27 Plot of EMPA and SIMS data showing mol% Au versus As analyses of pyrite from Carlin-type (yellow field), low sulfidation (LS) (green line), high sulfidation (HS) (magenta line), and orogenic (orange line) gold deposits. The solubility limit for Au^{1+} in arsenian pyrite determined by Reich et al. (2005) is indicated by the black diagonal line. Carlin-type pyrite that plots below the line contains As^{1-} that substitutes into the S site and Au^{1+} that may substitute into the Fe site, whereas the few data that plot above the line contain nanoparticles of native gold (Au^0). Arsenian pyrite from orogenic and LS gold deposits is similar to Carlin-type pyrite, whereas that from HS deposits is distinct with As^{3+} substitution into the Fe site. This difference indicates that pyrite in orogenic, Carlin-type and LS gold deposits formed under more reducing conditions than pyrite in HS gold deposits (adapted from Kesler et al., (2011) and data in Zacharias et al. (2004), and Large et al. (2009)).

components from crustal and mantle sources. The greater mantle He component in ore fluids permits that there were mafic magmas at depth and deep fracture systems, such as the Getchell fault.

Pb: While the abundance of Pb in ore pyrite and late ore-stage sulfides is low, there is enough to analyze by conventional methods on well-prepared separates. SIMS can measure ^{206}Pb, ^{207}Pb, and ^{208}Pb, but the reference isotope ^{204}Pb is generally below detection. Such data (Hofstra et al., 2010; Tosdal et al., 2003) suggest the Pb in ore pyrite in Nevada CTD is derived from Neoproterozoic siliciclastic sedimentary rocks that underlie the host Paleozoic carbonate rocks. In contrast, late ore-stage sulfides commonly contain Pb derived from the Paleozoic host rocks.

Sr, Nd, and Os: These isotopes tend to reflect the isotopic composition of the marine carbonate, terrigenous detritus, or sulfides in the host rocks and thus far have been of limited value (Hofstra and Cline, 2000).

Summary: The isotopic data generally support models in which meteoric water convects to sufficient depths and temperatures to promote substantial isotopic exchange between the fluids and sedimentary rocks from which S, Pb, and perhaps Au and As(?) were scavenged. Such isotopically exchanged fluids mixed with unexchanged groundwaters during the late ore stage as the systems collapsed. The deposits and districts with evidence for more deeply sourced water and metasedimentary S (e.g., Chinese CTD) permit an epizonal orogenic model, while those with deeply sourced water and 0‰ $\partial^{34}S$ permit a magmatic-hydrothermal model (e.g., some in Nevada and perhaps in West Qinling CTD). Despite the clear evidence for a deeply sourced fluid in some well-studied deposits (e.g., Getchell), there also are well-studied high-grade deposits that lack any evidence for such deeply sourced water or magmatic sulfur (e.g., Meikle in the Carlin Trend). Consequently, at this writing, one single integrated model does not appear to account for the variability of observed geochemical and mineralogical data; this leads to continual debate on the origin of these deposits.

13.15.4 Orogenic Gold Deposits

13.15.4.1 Introduction

Orogenic gold deposits are most readily defined as those in deformed metamorphic rocks. As their name implies, orogenic gold deposits represent regional fluid flow that is inherent to orogeny. The gold-bearing ore bodies typically form in host rocks between 20 and 200 m.y. after deposition of the rocks and relatively late in their deformation history. Historically, these were thought of as a relatively high-grade type of gold deposits, with gold-bearing quartz veins mined underground at grades of at least 5 g t^{-1} and commonly at >10 g t^{-1}. With rising metal prices, improved mining methodologies, and more efficient gold extraction techniques, the character of the ores has dramatically changed during the past few decades. Many of these deposits are now mined by large open-pit operations, recovering both high-grade veins and surrounding lower-grade hydrothermally altered wall rock that had been considered waste, or even just distal geochemical anomalies, in the past. Thus, present-day open-pit mining of orogenic gold deposits allows for much lower ore grades, including some examples of large ore bodies grading between 0.45 and 1.0 g t^{-1} Au (e.g. northern Sonora, Mexico; Morro do Ouro, Brazil).

13.15.4.1.1 General geologic setting and genetic model

The orogenic gold deposits are found in three different broad temporal/geotectonic settings (Goldfarb et al., 2001). First, ores hosted in Late Archean greenstone were mainly formed between 2750 and 2520 Ma in granitoid–greenstone terranes worldwide. This group of deposits includes those of the Yilgarn craton (Western Australia), Superior province (Canada), Slave province (Canada), Tanzania craton (central Africa), Dharwar craton (India), Zimbabwe–Kaapvaal craton (southern Africa), and São Francisco craton (Brazil). Second, ores dated between 2100 and 1730 Ma are hosted by Paleoproterozoic sedimentary and volcanic rocks deposited on the margins to the granitoid–greenstone terranes. Banded iron formation and ferruginous chert are commonly favorable host lithologies in the Paleoproterozoic terranes. Examples include the ores of western Africa, northern South America, and Homestake (USA).

A final group of ores formed between c.650 and 50 Ma in marine sedimentary rocks adjacent to active continental margins. These include the Mesozoic to Tertiary gold deposits of the North American Cordilleran orogen, Colombian Andes, eastern Russia, and the Otago area of New Zealand, and the latest Neoproterozoic–Paleozoic gold deposits of the Tasman orogen, Central Asia orogenic belt, Pan African orogen, and Eastern Cordillera of the main Andean range. Although processes that form orogenic gold deposits are continuing today, the lack of significant ore systems younger than c.50 Ma reflects the absence of required time for uplift and unroofing of ores formed typically at midcrustal depths (see succeeding text). Most Phanerozoic orogenic gold deposits occur in the fore-arc terranes adjacent to a subduction-related continental arc (Figure 1); however, some may occur in deformed back-arc basins (Sukhoi Log, Russia; Bendigo, Australia).

The temporal distribution of the orogenic gold deposits correlates with periods of supercontinent growth, including Kenorland, Columbia, Gondwana, Pangea, and ongoing Amasia (Goldfarb et al., 2010). Juvenile crust added to the cratons represents a favorable source reservoir for gold, related metals, and volatiles that are concentrated to form the eventual ore deposits. The thick, buoyant, and low-density subcontinental lithospheric mantle, characteristic of Paleoproterozoic and older cratonic blocks, has tended to prevent uplift and erosion of many Precambrian terranes. The Mesoproterozoic to early Neoproterozoic orogenic belts of Rodinia generally lack economically significant gold deposits. This reflects uplift and erosion of these older accretionary-type orogens, such that almost all orogenic gold deposits that would have formed between c.1730–650 Ma were lost to the geologic record once the presently exposed, mainly deep-crustal high-grade metamorphic rocks reached the surface. In addition, the growth of Rodinia subsequent to the breakup of Columbia was likely a gradual reconfiguration, rather than two distinct events. During such a reconfiguration, the Cordilleran-type orogenic belts were dominated by mature sediments shed from the adjacent cratons, rather than by more volatile- and metal-rich accreted oceanic sediments. This too may have hindered development

of significant gold resources during the Mesoproterozoic to Neoproterozoic 'Boring Billion' year gap.

Structure plays the major role in localization of most orogenic gold provinces, with ores typically being formed relatively late within an evolving orogen. Deposits are near steeply dipping transcrustal fault systems that are parallel to the strike of the orogen or the greenstone belt. The first-order structures are many hundreds of kilometers in length and several hundred meters wide, often being defined by a series of closely spaced distinct faults that reflect a cumulatively broad zone of deformation. Ores are interpreted to have been deposited between 3 and 20 km depth, and thus subclassifications of ores as epizonal (<6 km), mesozonal (6–12 km), and hypozonal (>12 km) have been proposed by Groves et al. (1998). Irrespective of depth, a complex kinematic history is commonly represented by earlier reverse motion and later strike-slip events. The shift to a more transpressional to transtensional stress regime, and related seismicity, correlates with the majority of the gold-forming events (e.g., Goldfarb et al., 1991a, 1991b).

Whereas the transcrustal fault zones are the main fluid conduits that focus fluid flow (Cox, 1999; Fyfe, 1987), gold ore bodies are situated along second- and third-order subsidiary faults. These lower-order faults are dominated by brittle–ductile to ductile shear zones, but less commonly gold-bearing extensional veins and vein arrays may also develop. Rheologic heterogeneities result in a variety of lithologies in greenstone belts and metasedimentary rock-dominant terranes serving as favorable ore host rocks, particularly in areas of minimum mean stress, such as fault jogs, fault bends, and fold hinges. Ore-bearing quartz–carbonate veins are commonly laminated or contain breccia fragments, which reflect repeated fracturing and fracture sealing in the hydrothermal systems (e.g., Cox et al., 2001) over periods of a few million years (e.g., Miller et al., 1994). Larger ore bodies have extensive down-plunge continuity of as much as 1–2.5 km.

Geologists have long recognized that most orogenic ores occur in greenschist facies rocks (e.g., Boyle, 1979; Buryak, 1964; Groves et al., 1998). Barrovian metamorphic sequences, with inverted geothermal gradients reflecting the contraction-related thrust faulting of high-grade rocks over lower-grade rocks, are inherently characterized by an abundance of auriferous quartz ± carbonate veins in greenschist zones (**Figure 28**). Where large veins exhibit high densities along major transcrustal structures, giant gold districts exist; where generally smaller vein systems are scattered throughout the greenschist facies, without any apparent relationship to the first-order faults, lode deposits are smaller and commonly subeconomic (e.g., Klondike placer district; MacKenzie et al., 2008). Rocks with different metamorphic grades may be exposed at different locations along the length of a major fault system, and gold is restricted to the greenschist environments. For example, in southeastern Alaska, deposits of the Juneau gold belt are hosted by greenschist facies rocks along the northern quarter of a transcrustal fault system (Goldfarb et al., 1988). Amphibolite and granulite facies rocks exposed along the same structure to the south are cut by quartz veins, but these lack anomalous gold concentrations (Goldfarb et al., 1997).

Almost all orogenic gold deposits formed subsequent to the development of the metamorphic mineral assemblages within the immediate country rocks and thus on the retrograde metamorphic curve. A few, particularly Precambrian, large gold deposits hosted by high-grade metamorphic rocks (e.g., Hemlo, Challenger, Big Bell) formed during greenschist facies events on a prograde metamorphic path (Phillips and Powell, 2009). These may reflect a complex and less common P–T path type such that perhaps multiple or overlapping metamorphic events affected the same region.

The genetic model most widely accepted for the orogenic gold deposits is that they are a product of metamorphic devolatilization (see summary in Phillips and Powell, 2010). During greenschist to amphibolite facies metamorphic reactions involving most sedimentary and volcanic rock sequences, mainly at temperatures of approximately 440–520 °C (Elmer et al., 2006, Phillips and Powell, 2010), perhaps 3–5 vol% of the rock is converted to a liberated fluid (e.g., Fyfe et al., 1978); the fluid volumes mainly depend on abundances of hydrous and carbonate minerals. The produced fluid rapidly generates its own elevated transitory permeability (e.g., Tenthorey and Cox, 2003) and is focused by resulting fluid pressure gradients into nearby deep-seated faults. The prograde metamorphic fluid moves upward along these major structural channelways during episodic seismic events (e.g., Sibson et al., 1988). Gold and associated metals are carried with the fluid phase to shallower deposition sites in rocks already on a retrograde metamorphic path (e.g., Stuwe, 1998), commonly located in greenschist facies brittle–ductile regimes.

Gold is sourced and released from elevated concentrations in preexisting pyrite, which is syngenetic to diagenetic in origin in sedimentary rocks (Goldfarb et al., 1997), during the prograde desulfidation to form pyrrhotite. In greenstone belts, the pyrite might be present in altered areas of metabasic rocks or within minor, but widely distributed chert beds; for example, near the Golden Mile deposit, Western Australia, the highest gold background measurements are associated with seafloor-altered serpentinite (16–87 ppb Au) and interflow sedimentary rocks (16–420 ppb Au) (after Golding, 1978, as shown in Table 5 of Shackleton et al., 2003). The widely disseminated pyrite grains contain a few hundred ppb to a few thousand ppb gold (Boyle, 1979; Thomas et al., 2011). Some workers have argued for the need for metamorphism of a gold-enriched protolith to form large gold provinces, such as proposed buried 'fertile' volcanic sequences below the turbidite-hosted ores in the Victorian goldfields (e.g., Bierlein et al., 1998; Willman et al., 2010), but it appears that adequate fluid and sulfur budgets should ensure that such a model may characterize most typical active margin lithologies and a specific favorable Au-enriched source horizon is not required.

Supporting evidence for the metamorphic model includes the following: (1) the common H_2O–CO_2–CH_4–N_2–H_2S, low-salinity fluid that is typical of a product formed during devolatilization; (2) the isotopically heavy $\delta^{18}O$ and δD values for hydrothermal minerals (Goldfarb et al., 1991a; Kerrich, 1989); (3) the variable $\delta^{34}S$ values that reflect variable host terranes undergoing a regional metamorphism (e.g., Goldfarb et al., 1997); and (4) the general lack of ores in high-grade metamorphic rocks because at relatively high temperatures, most mobile sulfur and gold have already been removed from the rock sequence. A gradual decrease in ore-related metals at increasing metamorphic grades in a Barrovian sequence (e.g., Pitcairn et al., 2006; **Figure 29**) supports a model where the ore-forming materials are derived from the accreted crustal

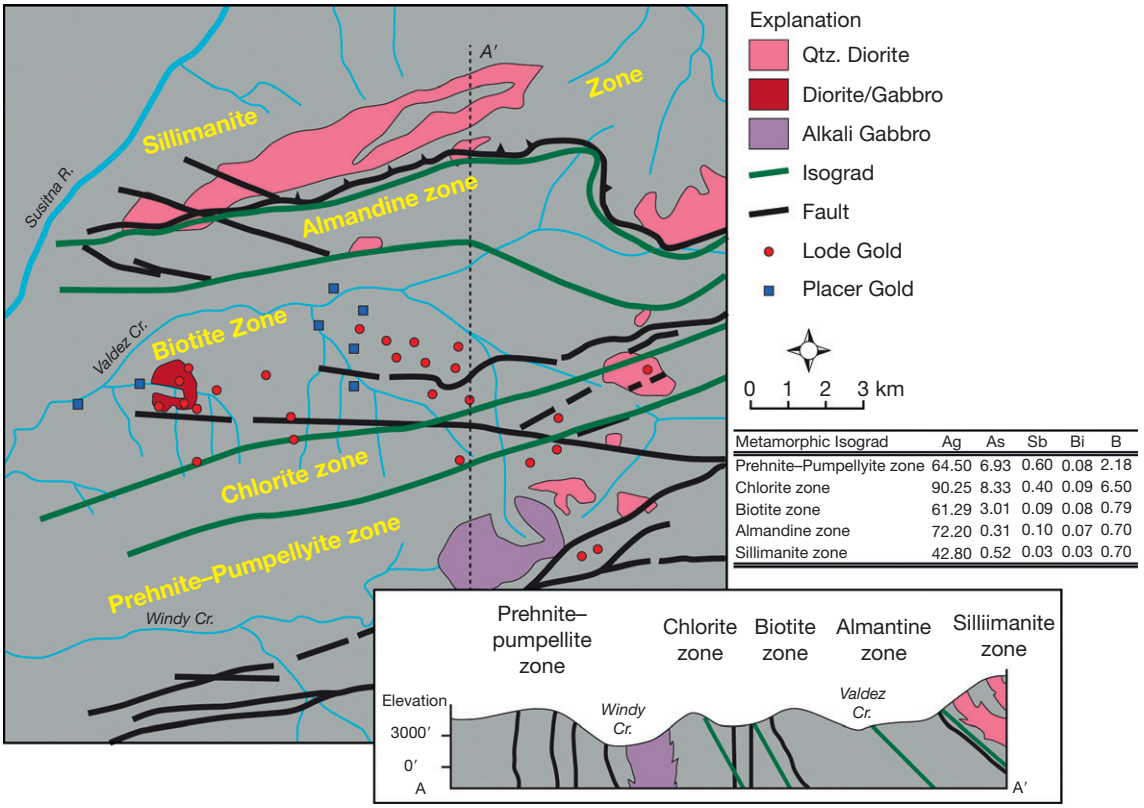

Metamorphic Isograd	Ag	As	Sb	Bi	B
Prehnite–Pumpellyite zone	64.50	6.93	0.60	0.08	2.18
Chlorite zone	90.25	8.33	0.40	0.09	6.50
Biotite zone	61.29	3.01	0.09	0.08	0.79
Almandine zone	72.20	0.31	0.10	0.07	0.70
Sillimanite zone	42.80	0.52	0.03	0.03	0.70

Figure 28 Map and cross section showing the spatial relation of the Valdez Creek district in central Alaska, which contains a series of small orogenic gold deposits and associated placers, to an inverted metamorphic sequence within a clastic sedimentary rock terrane (after Smith, 1981). Similar to the majority of orogenic gold deposits, those in the Valdez Creek district are spatially associated with the greenschist facies rocks (Goldfarb et al., 1997). The source for the gold and related metals is the sequence itself, with pyrite to pyrrhotite conversion at temperatures above middle greenschist, releasing sulfur and metals into an evolving fluid. Geochemical analyses of trace elements in the country rocks indicate a gradual decline in As, B, Bi, Sb, and, to a lesser degree, Ag, as metamorphic grade of the rocks increases; similar patterns would be expected for Au and W, but in this study most analyses for these elements were below analytical detection limits (E. Marsh, unpub. data).

allochthons tens of millions of years to a couple of hundred million years after the rocks were initially deposited. However, orogenic gold deposits in the North China craton and Sonora, Mexico, which are hosted by high-grade metamorphic rocks billions of years older than Cretaceous gold lodes, indicate in some circumstances that aqueous-carbonic fluid and ore components must be derived from metamorphosing slabs or their overlying sediments being subducted below reactivated craton margins. This is consistent with models that indicate a significant volume of CO_2 flux is derived from decarbonation of subducting slabs (Gorman et al., 2006).

13.15.4.2 Geochemistry and Mineralogy of Alteration and Ores

13.15.4.2.1 Ore mineral assemblages

The geochemistry of orogenic gold deposits is well defined. Gold, most consistently present in electrum, occurs in veins as grains within quartz, as grains in contact with country rock laminations or within altered wall rock fragments, or as remobilized veinlets cutting originally coeval sulfide minerals. In altered wall rock, gold may be chemically bound along the outer parts of arsenopyrite or arsenian pyrite grains. The fineness of most ore bodies is relatively high, with gold:silver ratios of 1:1–10:1, which contrasts with more Ag-rich LS epithermal type deposits. In addition to electrum, gold may be present in maldonite, calaverite, petzite, or aurostibite, reflecting enrichments of Bi, Te, or Sb in many hydrothermal systems. The typical range of 1–20 ppm Au, which is representative of most economic ore bodies, indicates three orders of magnitude of enrichment of gold relative to the 1–5 ppb Au range of most crustal source rocks. If one assumes that juvenile or sedimentary pyrite with background concentrations of a few hundred ppb to be the source of the gold in the ore deposits (see preceding text), gold in the veins is enriched 10–20 times that in source minerals themselves.

Gold-bearing quartz ± carbonate veins typically contain 2–5% sulfide minerals. These are dominantly pyrite in igneous rocks and arsenopyrite in metasedimentary rocks. Pyrrhotite becomes more abundant in higher temperature deposits or in relatively reduced ore host rocks, including most banded iron formations (BIFs). Trace element enrichments are most consistently As, Ag, Sb, B, Hg, Te, Bi, and/or W (**Figure 30**). Although arsenic is mainly in arsenopyrite, it also occurs less commonly in loellingite in hypozonal ores and realgar and orpiment in epizonal ores (e.g., Groves et al., 1998; see **Figure 24**). The epizonal ores may also be characterized by stibnite and traces of cinnabar, reflecting the solubility of Hg and Sb as sulfide

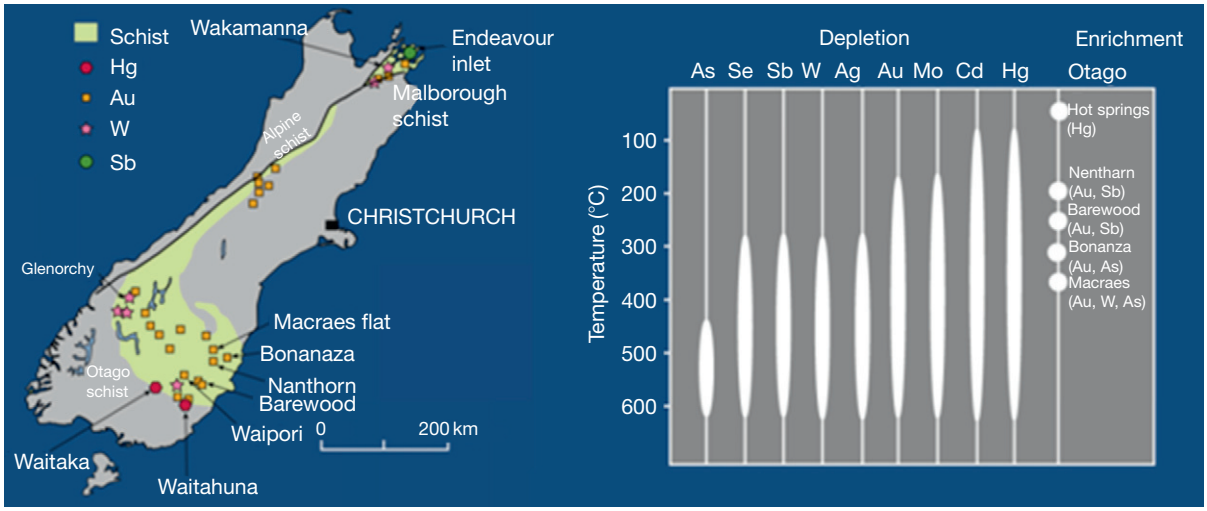

Figure 29 (Left) Map showing location of the Haast schist of the South Island, New Zealand, and that host orogenic gold and associated deposits. (Right) Plot showing elemental enrichments and depletions in various gold deposits within the metasedimentary rocks at metamorphic grades reflecting temperatures higher than gold ore formation (both diagrams are reproduced from Pitcairn IK, Teagle DAH, Craw D, Olivo GR, Kerrich R, and Brewer TS (2006) Source of metals and fluids in orogenic gold deposits. Insights from the Otago and Alpine schists, New Zealand. *Economic Geology* 101: 1525–1546).

complexes in hydrothermal fluids at relatively low temperatures and thus their selective transport into the upper few kilometers of the crust along the shallower levels of the regional fault systems. The presence of tourmaline in many veins is consistent with elevated B levels in many ore bodies. Tungsten is most consistently in scheelite, perhaps concentrated by CO_2 complexing. Tellurides may be the dominant ore-hosting phase in Precambrian (e.g., Golden Mile, Western Australia) or Phanerozoic (e.g., Kensington, Alaska) orogenic gold deposits. Bismuth may be present in solid solution in galena or in traces of Bi-rich mineral species (e.g., bismuthinite and maldonite). The majority of the deposits are characterized by Cu and/or Pb–Zn concentrations in the hundreds of ppm range, reflecting trace amounts of chalcopyrite, galena, sphalerite, or tetrahedrite. Limited base metals and a common Ag–As–Au–Sb–Hg geochemical signature reflect low-salinity ore-forming fluids (e.g., Kerrich, 1983) and auriferous hydrothermal systems dominated by sulfide complexing (see succeeding text). Zoning of ore-related minerals or gold grades is uncommon down-dip or along strike in these deposits, reflecting limited temperature variation (e.g., Kerrich, 1987; McCuaig and Kerrich, 1998).

13.15.4.2.2 Wall rock alteration

Visible wall rock alteration is well developed in many relatively reactive country rock types, but ore-hosting turbidite sequences typically show only weak alteration. The most extensive alteration zones are located where fluids reacted with granitoids and serpentinites in terranes dominated by metapelites or greenstones. Sulfidation, (de)-silicification, carbonization, and sericitization are the most consistent types of alteration, reflecting mobility of S, Si, K, and CO_2 within the hydrothermal systems.

Pyrite and arsenopyrite are the most common wall rock sulfide phases, with abundance decreasing away from ore zones. Sulfide precipitation in wall rocks destabilizes bisulfide complexes, causing deposition of wall rock gold in the

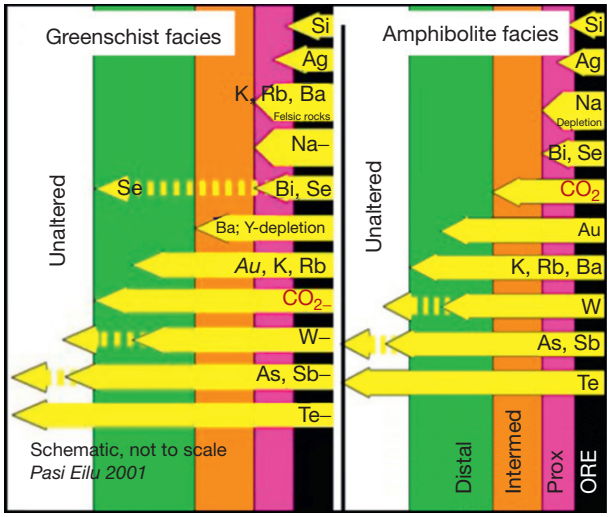

Figure 30 Summary diagram from Eilu and Groves (2001) for geochemical anomalies in ore bodies and surrounding mafic volcanic country rocks of the Yilgarn craton, western Australia. Most orogenic gold deposits are enriched to some degree in Ag, As, Au, B, Bi, Hg, Sb, Te, and W. Broader alteration halos for some trace elements relative to gold suggest they may be better pathfinders in the exploration for orogenic gold deposits.

alteration halos. Modern mining methods now consistently develop such auriferous-altered wall rocks as low-grade parts to the main ore bodies. Sulfidation and gold deposition in wall rocks reflect the sulfide/carbonate ratio of the hydrothermal fluid and the Fe/(Fe+Mg) ratios of the wall rocks (Böhlke, 1988). Silicification of wall rocks is represented by branching veinlets of quartz trending outward from the main ore zones. Silica depletion halos in country rocks surrounding most ore zones indicate some of the vein silica is locally derived. Sericite to coarser muscovite characterizes many alteration

assemblages, with visible bleaching as mafic minerals are replaced. In more mafic rocks, chlorite may be dominant at low temperatures and biotite at higher temperatures. Within ultramafic host rocks, fuchsite can be the most widespread mica phase. Slight increases in ratios of alkalis to hydrogen ion in the hydrothermal fluid can lead to significant amounts of K-feldspar or albite deposition. Hydrothermal carbonates include ankerite, siderite, calcite, dolomite, and magnesite, with compositions reflecting the bulk compositions of the rocks. In some districts, an early district-wide carbonization event has been reported to proceed the main period of ore formation.

There are some hypozonal deposits, particularly in the Yilgarn, Dharwar, and Superior cratons, where alteration minerals include biotite, Ca-amphiboles, plagioclase, pyroxene, and/or garnet. These reflect stable secondary hydrothermal silicate minerals deposited surrounding ore bodies formed at higher temperatures, which is explained in detail by the 'holistic continuum model' concept of Groves (1993). Also at relatively high temperatures and $X(CO_2)$, relatively oxidized mineral phases, such as hematite, magnetite, and anhydrite, may be stable (Evans et al., 2010).

13.15.4.2.3 Geochemistry of ore-forming fluids

The chemistry of the hydrothermal fluids responsible for formation of orogenic gold deposits is unique when compared to those that form other hypogene ores. The fluid, although H_2O-dominant, contains 5–25 mol% nonaqueous species dominated by CO_2 (**Figures 31** and **32**). The CO_2 contents tend to be near the low end of this range in Phanerozoic systems and the high range in Archean deposits, which could reflect slightly higher Archean temperatures for the ore fluids and/or greater relative CO_2 production via devolatilization from greenstone belts. In more reduced hydrothermal systems, methane and nitrogen are present at percent levels and, in some deposits, dominate over CO_2. Whether this reflects differences in source reservoirs or redox reactions at deposition sites is unclear. Salinities are usually low, in the range of 1–3 wt% NaCl (equiv.). There are some deposits where observed ore fluids are solely carbonic (e.g., Ashanti, West Africa, in Schmidt-Mumm et al., 1997; Carara, Guiana Shield, Brazil, in Klein and Fuzikawa, 2010). These are probably rare cases where fluid immiscibility has taken place somewhere along the hydrothermal flow path and gold has been transported to the site of deposition within the separate, more volatile unmixed component.

Gold solubility is clearly as a complex with reduced sulfur (e.g., Loucks and Mavrogenes, 1999; Mikucki, 1998; Seward, 1973). The main ligand is HS^- and the dominant species in solution is $AuHS^o$ in slightly acidic solutions (e.g., **Figures 10** and **25**). At typical hydrothermal temperatures of 250–400 °C, $AuHS^-$ becomes the more significant species in neutral to slightly alkaline fluids. Most estimates indicate neutral to slightly alkaline solutions of pH 5–6 (e.g., Reed, 1997) such that both gold species are probably important to varying degrees. In these relatively low-salinity fluids that typify orogenic gold deposits, $AuCl_2^-$ is not an important species except in rare higher temperature hydrothermal systems. Total sulfur concentrations may be as high as $10^{-3.5}$ molal for epizonal deposits or 1 molal for hypozonal ores (Mikucki, 1998). The gold itself is dissolved in the H_2S-bearing fluid as the fluid is being formed via devolatilization (Phillips and Powell, 2010), and pyrite is being converted to pyrrhotite (e.g., Ferry, 1981; Tomkins, 2010). About 3–15 t Au km^{-3} of rock may be dissolved assuming 80% efficiency of gold extraction (e.g., Phillips et al., 1987). The elevated CO_2 in these fluids forms a weak (carbonic) acid and may help buffer the ore fluid in a pH range where gold is most soluble in sulfide complexes (e.g., Phillips and Evans, 2004).

Oxygen isotopes ($\delta^{18}O$), most commonly measured on ore-hosted quartz, range between about +10 and +17‰, and calculated fluids are typically +5 to +10‰ (**Figure 33**). As a generalization, the slightly higher fluid values in the range are more characteristic of Phanerozoic deposits, reflecting either lower ore-forming temperatures and/or the metasedimentary

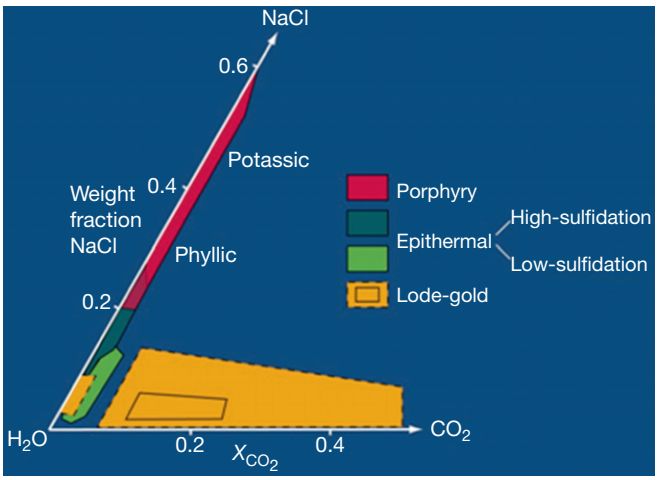

Figure 31 Plot showing general ranges of compositions of orogenic gold deposits and some other deposit types. Note that orogenic ores are characterized by a low to moderate salinity, CO_2-rich ore-forming fluid. Most commonly the nonaqueous volatile content is about 5–25 mol%. These contrast with fluids that are from epithermal and porphyry deposits that lack significant concentrations of nonaqueous volatiles and can be much more saline (reproduced from Ridley JR and Diamond LW (2000) Fluid chemistry of orogenic lode gold deposits and implications for genetic models. *Reviews in Economic Geology* 13: 141–162).

rather than metavolcanic rock source region. Hydrothermal flow along major fault zones is highly fluid dominated, but some exchange obviously takes place at sites of ore deposition. This is supported by the fact that in many districts where some veins are hosted in felsic intrusions, measurements of $\delta^{18}O$ are a few per millimeter lighter than those for auriferous quartz within other lithologies.

Hydrogen isotopes, when measured for hydrothermal micas, consistently indicate fluid δD of −20 to −35‰ (**Figure 33**). Most studies using δD values from bulk extraction of fluid inclusion waters yield much lighter ratios, but because of the typical multiple generations of fluid inclusions trapped in the ore bodies during tens of millions of years of postformational deformation and uplift, these measurements are meaningless (e.g., Pickthorn et al., 1987). In addition, hydrogen isotope fractionation between the hydrothermal fluid and structurally bound water adds further uncertainty to δD fluid inclusion measurements (Simon, 2001).

Sulfur isotopes are quite variable between deposits/districts of different ages and tend to reflect the sulfur signatures of the rocks undergoing devolatilization (e.g., Chang et al., 2008; Goldfarb et al., 1997; **Figure 34**). In individual large deposits, significant variation between ore bodies perhaps reflects multiple mechanisms of gold precipitation (Hodkiewicz et al., 2009).

Carbon isotopes for ore fluids have been determined from many deposits of all ages from measurements on hydrothermal carbonates. Most estimates for $\delta^{34}C$ are between 0 and −10‰ and are not diagnostic of a specific source; these data can reflect both mantle and many crustal carbon reservoirs.

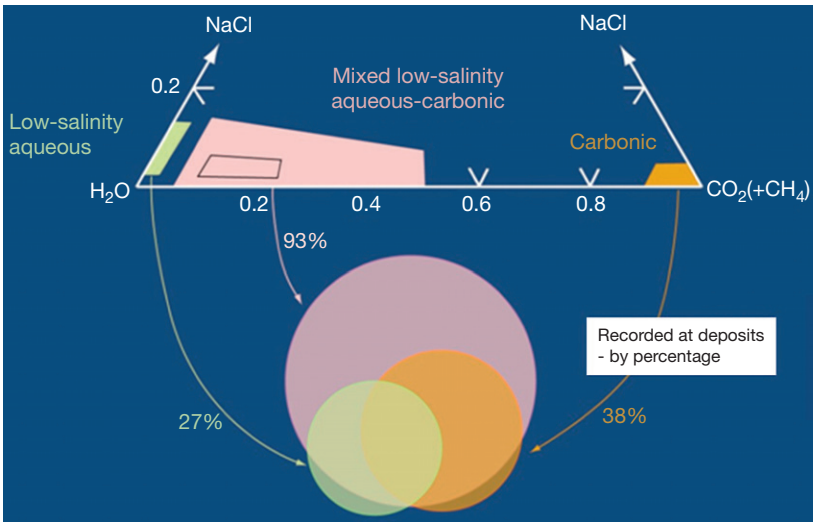

Figure 32 Compositional plot showing that most orogenic gold deposits form from low-salinity, mixed aqueous-carbonic fluids. Fluid immiscibility is recorded in about one-third of the deposits studied by fluid inclusion observations (Ridley and Diamond, 2000). More commonly, fluid immiscibility characterizes Precambrian rather than Phanerozoic deposits, likely reflecting slightly higher ore-forming temperatures or slightly more CO_2-rich ore fluids developed in earlier greenstone belts relative to younger accreted metasedimentary rock-dominant terranes.

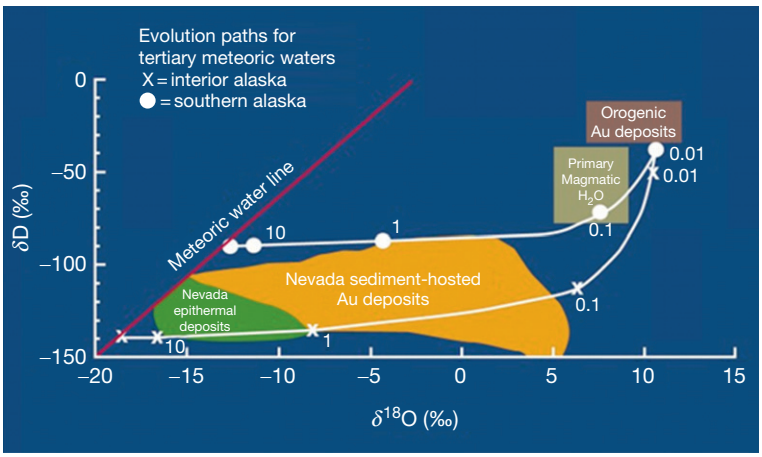

Figure 33 Plot of δD versus $\delta^{18}O$ of ore-forming fluids showing that orogenic gold deposits are formed from a unique fluid that is isotopically heavy in both oxygen and hydrogen as compared to epithermal and Carlin-type deposits. Most fluids are characterized by oxygen values of 5–10‰ and hydrogen values between −20 and −35‰. These are much heavier in hydrogen than meteoric or mixed meteoric and deep-crustal waters that form Carlin and epithermal gold deposits.

Measurements of $\delta^{15}N$ on hydrothermal micas cover a wide positive range and have been interpreted as consistent with metamorphic devolatilization processes (Jia and Kerrich, 1999; Jia et al., 2003).

Heavy radiogenic isotopes such as lead have proven to be less diagnostic of orogenic gold ore-forming processes than the stable isotopes. Many workers have tried to use such isotopes to suggest source rocks for the gold ores, assuming elements such as lead, strontium, and neodymium have followed the same evolutionary and hydrothermal path. Lead isotope data for gold deposits from the Alaskan Cordillera (Goldfarb et al., 1997; **Figure 35**) and from the Eastern Cordillera of Peru (Haeberlin et al., 2003, 2004) indicate signatures that reflect a strong lead contribution from sink (i.e., variable host-rock lithologies) areas, rather than from metal source areas. Mortensen et al. (2010), however, noted two distinct radiogenic Pb clusters for sulfides within auriferous veins of one general rock type, the Otago Schist on South Island, New Zealand. They interpreted these data to indicate mobilization of at least minor amounts of lead by the hydrothermal fluids, although both clusters were interpreted to reflect metals that were derived from the upper crustal schist belt and the isotopic differences being reflective of distinct earliest and latest Early Cretaceous ore-forming events. In the Precambrian greenstone belt, lead isotopes may better fingerprint metal source reservoirs because of the low lead concentrations in the greenstone sink areas. In the Yilgarn craton, lead isotopes for orogenic gold deposits suggest lead, and thus perhaps gold, was sourced from basement granite–gneiss terranes (Qiu and McNaughton, 1999). The usefulness of strontium as a metal source region tracer also appears to vary from one study to another (see discussion in Goldfarb et al., 2005).

Some other volatile species, such as boron and noble gases, have been measured within orogenic gold deposits to determine fluid sources, but the meaning of the resulting data are unclear. Boron isotopes in gold-related tourmaline in an Archean greenstone belt in India suggest boron was derived from both metamorphic devolatilization and I-type magmatism (Krienitz et al., 2008), but does not necessarily imply that gold and other volatiles have the same multiple-source characteristics. Noble gas data often show a mantle contribution but even in deposits where, in contrast, sulfur was clearly derived from the crust (e.g., Dongping, northern China, in Mao et al., 2003). Because many orogenic gold deposits are associated with first-order structures that reach down to the mantle, the presence of noble gases from the mantle, as well as lamprophyric magmas, within these conduits is not unexpected. However, this does not suggest that the main ore fluid components and the metals also have mantle sources. Fairmaid et al. (2011) used noble gas and halogen data from Ballarat, Victoria, to suggest signatures that were mixtures of deeper devolatilization-related fluids in a main source area and a more local contribution from near the site of ore deposition.

13.15.4.2.4 PTX constraints on ore deposition

Orogenic gold deposits reflect hydrothermal systems that precipitate gold over a wide range of temperatures and pressures. This is a consequence of the fact that these gold ores are products of regional geothermal gradients and not local magmatic heat engines, such as those that control most epithermal type gold deposits. Published ore formation temperature estimates are spread between about 225 and 600 °C, although most consistently fall in the 275–350 °C range, and pressures range from 1 to 5 kb. Continuous fluctuation between lithostatic and hydrostatic pressure regimes during flow migration

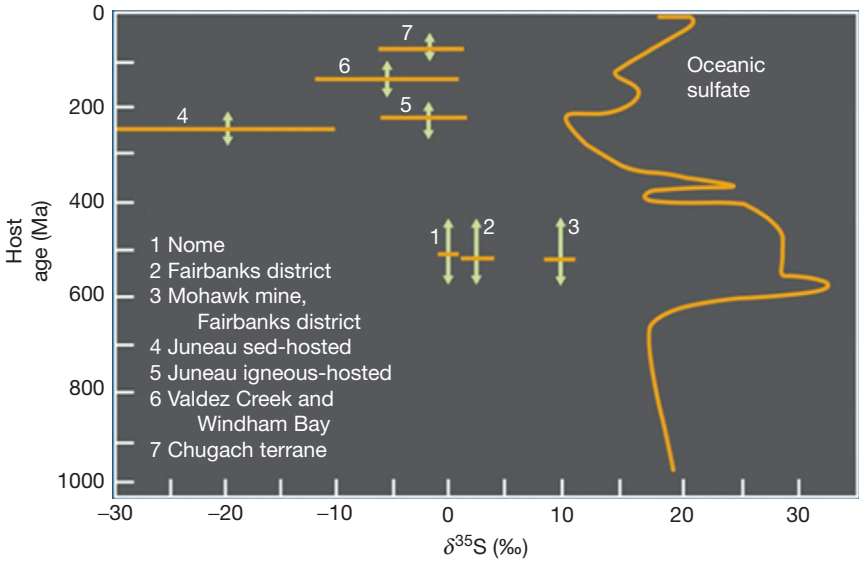

Figure 34 Plot of $\delta^{34}S$ values for sulfide minerals from orogenic gold deposits versus age of host-rock terranes for major gold districts in Alaska (reproduced from Goldfarb RJ, Miller LD, Leach DL, and Snee LW (1997) Gold deposits in metamorphic rocks of Alaska. *Economic Geology Monograph* 9: 151–190). Oceanic pyrite in these terranes would reflect the oceanic sulfate curve for the past billion years, but with values about 20‰ lighter. The sulfur isotopes of the minerals in the deposits reflect the signature of sulfur in the terranes such that heavy sulfur in sulfides reflects deposits formed in terranes consisting of rocks deposited when seawater sulfate was heavy and vice versa. This is consistent with the metamorphic devolatilization model for orogenic gold.

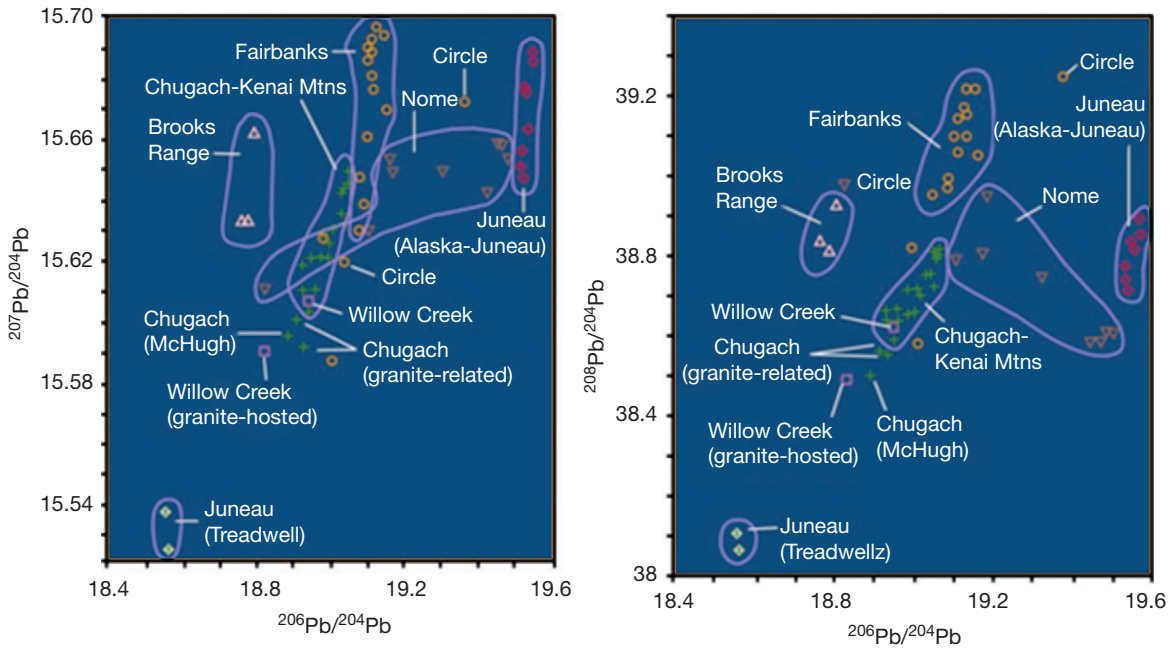

Figure 35 Plot of lead isotope analyses for sulfide minerals from orogenic gold deposits in Alaska. Within the same gold province (e.g., Alaska Juneau and Treadwell in Juneau gold belt; McHugh melange, S-type granite, and Chugach-Kenai Mountains metasediments of Chugach terrane), Pb isotope measurement vary with changing host-rock lithology. This indicates that much of the lead is being contributed at the site of ore formation and says little about the source of gold that has been transported to the deposit area by the hydrothermal fluid (reproduced from Goldfarb RJ, Miller LD, Leach DL, and Snee LW (1997) Gold deposits in metamorphic rocks of Alaska. *Economic Geology Monograph* 9: 151–190).

along fault zones is responsible for measurements of huge pressure fluctuations at sites of gold deposition. Where hydrothermal fluids reach levels shallower than about 3 km and thus temperatures less than about 225 °C, progressive water–wall rock interactions raise pH so that gold is no longer very soluble in reduced sulfur complexes; Hg- and Sb-rich sulfides predominate over Au in such epizonal environments (e.g., Goldfarb et al., 2004), and the mercury may be carried to very shallow levels in a vapor phase (e.g., Morteani et al., 2010). Ore formation has a maximum permissive temperature of about 600 °C, which is where fluids begin to become involved with partial melting (e.g., Tomkins and Grundy, 2009).

The main controls on ore deposition are pressure fluctuations and water–rock reaction. Drops in pressure are particularly significant in metasedimentary rock-hosted ore systems, where the highest ore grades are within the vein systems themselves. Loucks and Mavrogenes (1999) noted a 2 kb drop in pressure during hydrofracturing at 400 °C and 10 km depth will cause a 90% decrease in gold solubility. Such pressure drops may trigger CO_2 immiscibility (e.g., Naden and Shepherd, 1989), also increasing pH, which further destabilizes gold-bearing complexes. The common association of gold and tellurides in many orogenic gold deposits could be the result of Te also partitioning into the nonaqueous phase during immiscibility in the form of H_2Te (e.g., Tombros et al., 2010). However, in many fluid inclusion studies of Phanerozoic deposits, there is a lack of clear evidence of fluid immiscibility, reflecting a nonaqueous component of perhaps only 4–6 mol% and thus a fluid remaining in the one-phase field for relevant salinity and P–T solvi.

Fluid–wall rock interaction is a more common gold depositing process in the Archean, reflecting sulfidation of Fe-rich wall rocks in many greenstone belts (Lambeck et al., 2011) and abundant sulfide mineral and high-grade gold precipitation adjacent to quartz veins. Oxidation of the fluid during sulfidation may cause a drastic drop in gold solubility. In many Phanerozoic and Paleoproterozoic gold provinces, there is an association of ores with carbonaceous and organic material. Gold deposition in these environments may be related to reduction of the ore fluid by the carbon (e.g., Gize, 1999). Shifts in pH and temperature decreases are not important factors in the formation of orogenic gold (e.g., Phillips and Powell, 2010). Fluid mixing has been invoked by some workers (e.g., Neumayr et al., 2005, 2008) as important for orogenic gold formation based on observations of oxidized and reduced mineral phases in deposit halos. However, carbonation and sulfidation of ferric iron-rich minerals, such as magnetite, can produce alteration assemblages with pyrite in equilibrium with hematite and sulfate (Evans, 2010; Evans et al., 2006).

13.15.4.3 Geochemistry of Type Examples

13.15.4.3.1 Phanerozoic metasedimentary-hosted Muruntau

The Muruntau deposit, located in the eastern part of the Tien Shan of Uzbekistan, is the largest known orogenic gold deposit. Discovered in 1958, it has a total production and resource tonnage of about 5300 t Au at a grade of 3.5–4 g t^{-1}. It has been developed by open-pit methods since 1967. The ores are hosted by the Early Ordovician 'variegated' Besopan

carbonaceous phyllite, with numerous Late Carboniferous to Early Permian granitic stocks scattered throughout the region. Deposits mainly consist of relatively flat-lying quartz veinlets and stockworks, although there are also relatively steep central veins (Berger et al., 1994; Wilde et al., 2001). A Re–Os date on ore-stage arsenopyrite indicates mineralization at 287.5 ± 1.7 Ma (Morelli et al., 2007) and overlaps with a 279 ± 18 Ma Sm–Nd isochron age for hydrothermal scheelite (Kempe et al., 2001). There are many possibilities as to why Muruntau may be so large. These may include the following: (1) the occurrence of an exceptionally prominent jog in the main deep-crustal fault system, which separates the South and Central Tien Shan just to the north of Muruntau; (2) an inherent high background of syngenetic/diagenetic gold in the local stratigraphy, as stressed by various Russian workers (e.g., Dolzhenko, 1991; 280 ppb estimate in Yermolayev et al., 1995); and/or (3) a thick sequence of carbonate rocks in the local geology, which may have provided a pathway for hydrothermal fluids to the clastic rocks, in a manner suggested for many Carlin deposits. Additionally, Wilde et al. (2001) suggested that the thermochemical sulfate reduction of nearby anhydrite-bearing Devonian evaporites provided a large H_2S reservoir.

At Muruntau, gold is commonly associated with pyrite, arsenopyrite, and scheelite; the sulfides comprise 1.5–2 vol% of the more altered rock. This giant hydrothermal system is geochemically complex; there appears to be a zoning of stibnite- and cinnabar-rich mineralization surrounding the main gold ore body, and there is a very silver-rich ore body adjacent and to the southeast of Muruntau (e.g., Myutenbai). Gold ores average 39 ppm Bi, 30 ppm Te, 34 ppm Se, and 30 ppm W (Koneev et al., 2005). Traces of base metal sulfides, Bi-bearing phases, tellurides, and sulfosalts are common. The main stage of alteration is commonly described as albite–quartz–biotite–pyrrhotite–tourmaline, with later sericite, chlorite, and minor carbonate and K-feldspar (Bierlein and Wilde, 2010). Muruntau is the only major orogenic gold deposit known to also produce platinum. However, the recovered platinum is not associated with the gold-forming event. Rather, the platinum-group elements are locally enriched in the carbonaceous host rocks at levels of 0.30 ppm Pd and 0.61 ppm Pt (Yermolayev et al., 1995).

Ore-related fluid inclusions for Muruntau are of low to moderate salinity, are CO_2-rich with significant CH_4 and N_2, and show evidence of fluid immiscibility (Berger et al., 1994; Graupner et al., 1998, 2001; Zairi and Kurbanov, 1992). Most homogenization temperatures suggest ore formation somewhere between 270 and 400 °C, although it is unclear specifically from what part of this range are the most reliable estimates and good pressure estimates are lacking. At the silver-rich Myutenbai ore body, fluid inclusion temperatures and compositions are similar to those from the Muruntau ores, but there is no evidence of immiscibility (Graupner et al., 2001). Veins similar to those hosting ores, but distal to the Muruntau ore zones, are also CO_2-rich, but lack elevated CH_4, N_2, and H_2S compositions (Wilde et al., 2001).

Oxygen isotope values for ore-bearing quartz vein types range from 8 to 15‰, with fluid values calculated at mainly 400 °C between 4 and 9 per mil (Berger et al., 1994). Gold-related pyrite and arsenopyrite $\partial^{34}S$ values range between 2.8 and 5.5‰ (Berger et al., 1994). Helium in arsenopyrite indicates a mainly crustal origin and a much lesser mantle source, whereas Ne, Kr, and Xe in the sampled fluid inclusions are of atmospheric origin (Graupner et al., 2006). Bulk extraction fluid inclusion $\partial^{13}C$ carbon isotope values between −5.3 and −2.1‰ and log Br/Cl between −3.23 and −2.64 are both interpreted as suggestive of a juvenile contribution to the hydrothermal system (Graupner et al., 2006). There are, however, as described earlier, always concerns on the significance of the analyses of bulk extraction fluid inclusion waters and noble gases that may have different source reservoirs than other components in a hydrothermal system. The $\delta^{13}C$ values for carbonaceous matter in the unmineralized host rocks are −28.8 to −28.0‰, whereas in the ore bodies, the same material has only been enriched to values of −27.9 to −24.8‰ (Rusinova and Rusinov, 2003).

13.15.4.3.2 Paleoproterozoic BIF-hosted Homestake

The Homestake deposit in the Black Hills, SD, USA, is the second largest Proterozoic orogenic gold deposit, after Ashanti in West Africa. It was mined from 1876 to 2001 by underground operations to depths of 2.5 km. Total production was 1237 t Au from ore averaging 8.34 g t^{-1}. The ore-hosting sequence consists of dominantly intracontinental rift basin sediments that were deposited between c.2560 and 1870 Ma (Caddey et al., 1991; Dahl et al., 2006) and metamorphosed to upper greenschist to lower amphibolite facies. The deposit is essentially restricted to structurally deformed areas in the c.2.0 Ga Homestake Formation (Hark et al., 2008), which is a ≤125 m-thick carbonate–silicate–sulfide facies iron formation. Ore bodies occur as tabular replacement zones of pyrrhotite and arsenopyrite within the chemically reactive BIF, which contains 15–35% total iron, and vein-hosting shear zones. Dating of ore-related arsenopyrite by Re–Os methods indicates gold deposition in the BIF at 1736 ± 8 Ma (Morelli et al., 2010), but it is apparent that some gold was remobilized in response to Cretaceous magmatism.

Caddey et al. (1991) summarized geochemical patterns in the Homestake Formation. Sulfur, CO_2, Ag, As, and Au were enriched in the ores; this is consistent with the observed hydrothermal siderite and sulfide formation in and surrounding the ore bodies. Such sulfidic replacement of Fe-rich layers in BIF characterizes not only Homestake, but BIF-hosted orogenic gold deposits in general (e.g., Geita, Morro Velho). Less commonly, enrichments in Co, Cr, Cu, Ni, Pb, Se, Te, V, and Zn have been measured. Unlike most orogenic gold deposits, there is no increase in W concentrations in the ore zones. Gold:silver ratio is 5:1, and silver was also recovered during mining. Trace element and REE data, in conjunction with Pb isotope data for ore-stage sulfides, have shown the replacement style ore and the shear zone-related ore likely has a similar origin (Frei et al., 2009). Sulfur isotope $\partial^{34}S$ data range from 5.6 to 9.8‰ for ore-related sulfides within the ore bodies (Rye and Rye, 1974), which were interpreted to indicate a seawater sulfate source for the sulfur. Rye and Rye (1974) also showed that, locally, sulfur values of sulfides decreased toward the ore bodies within the Homestake Formation. Data were interpreted as consistent with a syngenetic model for a gold source, although more recent structural (Caddey et al., 1991) and geochronologic data (Morelli et al., 2010) confirm an epigenetic formation. Oxygen isotope $\partial^{18}O$ data for hydrothermal quartz in the ore bodies range from 11.7 to 15.9‰. Rye and

Rye (1974) suggested a trend in these data, with isotopically lighter measurements in areas of the deposit that were of highest metamorphic grade. They also report δD values of −56 to −112‰ and $\delta^{13}C$ values of −1.3 to −8.4‰, but these data are from fluid inclusions in crushed vein material, and the meaning of such bulk extraction measurements is questionable. Lead isotopes of sulfide minerals have been interpreted to indicate an epigenetic mixture of magmatic and host-rock leads (Frei et al., 2009), although the 1713 ± 10 Ma age for local magmatism postdates the Re–Os mineralization age (see preceding text).

Fluid inclusion data were determined for arsenopyrite-bearing quartz veins (Groen et al., 1989; Kath, 1990; Rye and Rye, 1974). Two- and three-phase H_2O–CO_2 fluid inclusions were related to the ore-forming event. A fluid inclusion homogenization temperature mode of 248–274 °C, with trapping pressure estimates of 3.5–4 kb from metamorphic conditions, yields trapping temperature estimates of 400–450 °C. Microthermometric data indicate as much as 8 mol% CH_4 in a fluid with salinities between 3.8 and 6.5 equiv. wt% NaCl (equiv.).

13.15.4.3.3 Late Archean Greenstone-hosted Golden Mile

The Golden Mile deposit in the Yilgarn craton of Western Australia is the largest Archean orogenic gold deposit. It was mined from the late 1890s through the late 1980s by underground operations and with ores averaging about 11.5 g t^{-1} Au. Since 1989, gold has been recovered from the giant Fimiston open-pit and has averaged about 1.5–2 g t^{-1} Au. Total production has exceeded 1600 t Au and significant resources remain. The deposit occurs along the regional Boulder-Lefroy fault system. The greenstone belt volcanic-sedimentary rock succession is c.2.69 Ga in age and was intruded by the ore-hosting Golden Mile dolerite (diabase) dike at c.2675 Ma. The absolute age of gold formation has been controversial, but recent data suggest that the ductile–brittle Fimiston-type replacement/shear mineralization, the brittle–ductile Oroya-type veinlet mineralization, and the brittle Mt. Charlotte-type stockwork mineralization formed relatively coeval at c.2640 Ma (Vielreicher et al., 2010). The reason for the large size of the Golden Mile has been suggested to be the combination of favorable structural and geologic characteristics (Phillips et al., 1996), with the total gold and volatile content of the ore bodies able to be explained by devolatilization of a greenstone block 8 km × 8 km × 5 km in volume (Phillips et al., 1987). The gold ore is defined by an Ag–Au–Te–W geochemical signature, with wall rock enrichments in CO_2, K, S. B, V, Ba, As, Sb, and Rb (Bateman et al., 2001; Phillips and Gibb, 1993). Pyrite is the dominant sulfide phase in the ores, but there are minor amounts of arsenopyrite, tetrahedrite, and base metal sulfides. About 25% of the ores are hosted by a wide variety of telluride minerals (e.g., Shackleton et al., 2003), with Te concentrations locally exceeding 1000 ppm. Gold fineness throughout the deposit is >900 °C. Silver and Sb both increase relative to gold with a depth (Bateman et al., 2001), which is atypical of most hydrothermal systems. Within a few meters of the Fimiston lodes, high-grade altered dolerite is dominated by an ankerite–siderite–sericite–quartz–hematite–pyrite–telluride ± albite, tourmaline, magnetite, and anhydrite assemblage. Similar high-grade ore zones in dolerite surrounding the Oroya veinlets are altered to vanadium mica–ankerite–quartz–siderite–hematite–pyrite–telluride (Bateman et al., 2001; White et al., 2003).

Ho et al. (1990a, 1990b) interpreted the Fimiston ores to have formed from an aqueous-carbonic fluid with 15–25 mol% CO_2 and a salinity of <5.5 wt% NaCl (equiv.). The Oroya style of mineralization showed a significant methane component in the hydrothermal fluids, which was interpreted to reflect the interaction with lesser carbonaceous metasedimentary rocks within the overall metamafic sequence. Temperature-corrected fluid inclusion trapping pressures were estimated to be 1.5–4 kb at about 280–330 °C. Clout (1989) suggested conflicting P–T estimates of ore formation of 100–260 bars and 170–250 °C, also from fluid inclusion interpretations, but such shallow pressures are atypical of most orogenic gold deposits (e.g., Groves et al., 1998), and the low temperatures are not consistent with the mineral assemblages (e.g., White et al., 2003). Log fS_2 was estimated as −12.6 to −5.5 and log fTe_2 at −11.4 to −6.8 for the ore-forming fluids (Shackleton et al., 2003). Most vein quartz measurements of $\partial^{18}O$ ranged from 14 to 15‰ with calculated fluids of 6.6 ± 2.0‰, and δD values for hydrothermal muscovite were generally −25 to −50‰ (Clout, 1989; Golding et al., 1990). The widespread hematitic alteration, coupled with the anomalously light $\delta^{34}S$ (−2 to −10‰) for Archean orogenic gold pyrites (Phillips et al., 1986), has led to controversies in the ore genesis model in trying to explain the relatively oxidized hydrothermal fluids. Many workers have stressed a mixing of fluids or two distinct fluids to help explain assemblages with coexisting hematite, magnetite, siderite, ankerite, pyrite, and anhydrite (e.g., Neumayr et al., 2008). However, thermodynamic modeling by Evans et al. (2006) shows how hematite precipitation and a sulfate-bearing fluid could form via reaction of a typical reduced orogenic gold hydrothermal fluid with the Golden Mile dolerite.

13.15.5 Summary and Conclusions

Gold is transported by aqueous complexes formed with dissolved H_2S in the ore-forming fluids in all of the ores discussed here. The H_2S can come from igneous rocks, magmas, rocks undergoing metamorphism, and even sedimentary rocks. Other elements with strong affinity to make aqueous complexes with H_2S are transported along with gold, particularly As, but also Hg, Sb, Se, Te, Tl, and locally Ag. Silver may decouple from these by forming earlier Ag–S minerals during transport or perhaps remains in the solution as stable Ag–Cl complexes in some settings. Temperatures, salinities, of ore-forming fluids in all ores discussed here are generally similar, and all can locally be enriched in CO_2. Orogenic gold deposits formed at higher temperature and deeper than the other deposit types have higher dissolved CO_2 contents, and the pH of the ore-forming fluids may be different from CTD and epithermal deposits. Some combination of boiling, cooling, and fluid mixing cause deposition of most epithermal ores, whereas reactions with Fe-rich carbonate host rocks are most important for CTD, whereas pressure drops (typically caused by hydrofracturing) are important in orogenic deposits. Perhaps gold nanoparticles can form in any of these deposits (less likely in orogenic?) when dissolved contents are elevated, and

they are physically transported to the site of deposition. However, evidence of this is preserved only in the highest grade deposits, and the formation of nanoparticles implies a gold-rich fluid evolves to form them along its flow path.

Acknowledgments

This research was supported in part by funding from the US National Science Foundation to J. Saunders (EAR-0838208), US Geological Survey's Mineral Resource External Research Program (MRERP #05HQGR0153). Thanks to Samuel B. Romberger and Erin E. Marsh who reviewed and edited an earlier version of this paper. The authors also thank Newmont and Barrick mining companies for allowing access to their data and some of the ores discussed here.

References

Ahmad M, Solomon M, and Walshe JL (1987) Mineralogical and geochemical studies of the Emperor gold telluride deposit, Fiji. *Economic Geology* 82: 345–370.

Arribas A, Hedenquist J, Itaya T, Okada T, Concepcion R, and Garcia J (1995) Contemporaneous formation of adjacent porphyry and epithermal Cu–Au deposits over 300Ka in northern Luzon, Philippines. *Geology* 23: 337–340.

Bakken, BM (1990) Gold mineralization, wall-rock alteration, and the geochemical evolution of the hydrothermal system in the main orebody, Carlin Mine, Nevada: Ph.D. dissertation, Stanford University, Stanford, CA, United States (USA), 256pp.

Barker SLL, Hickey KA, Cline JS, et al. (2009) Uncloaking invisible gold; use of NanoSIMS to evaluate gold, trace elements, and sulfur isotopes in pyrite from Carlin-type gold deposits. *Economic Geology* 104: 897–904.

Bateman RJ, Hagemann SG, McCuaig TC, and Swager CP (2001) Protracted gold mineralization throughout Archean orogenesis in the Kalgoorlie camp, Yilgarn craton, Western Australia: Structural, mineralogical, and geochemical evolution. *Geological Survey of Western Australia Record* 2001(17): 63–98.

Berger BR, Drew LJ, Goldfarb RJ, and Snee LW (1994) An epoch of gold riches: The late Paleozoic in Uzbekistan, Central Asia. *Society of Economic Geologists Newsletter* 16: 7–11.

Berger BR and Henley RW (2011) Magmatic-vapor expansion and the formation of high-sulfidation gold deposits: Structural controls on hydrothermal alteration and ore mineralization. *Ore Geology Reviews* 39: 75–90.

Bethke P, Rye R, Stoffregen R, and Vikre P (2005) Evolution of the magmatic-hydrothermal acid-sulfate system at Summitville, Colorado: Integration of geological, stable-isotope, and fluid-inclusion evidence. *Chemical Geology* 215: 281–315.

Bierlein FP, Arne DC, Broome JMN, and Ramsay WRH (1998) Metatholeiites and interflow sediments from the Cambrian Heathcote greenstone belt, Australia: Sources for gold mineralization in Victoria? *Economic Geology* 93: 84–101.

Bierlein FP and Wilde AR (2010) New constraints on the polychronous nature of the giant Muruntau gold deposit from wall-rock alteration and ore paragenetic studies. *Australian Journal of Earth Sciences* 57: 839–854.

Böhlke JK (1988) Carbonate-sulfide equilibria and "stratabound" disseminated epigenetic gold mineralization; a proposal based on examples from Alleghany, California, U.S.A. *Applied Geochemistry* 3: 499–516.

Boyle RW (1979) The geochemistry of gold and its deposits. *Geological Survey of Canada, Bulletin* 280, 584pp.

Brown KL (1986) Gold deposition from geothermal discharges in New Zealand. *Economic Geology* 81: 979–983.

Buryak VA (1964) The process of regional metamorphism influencing development of gold-sulfide mineralization in the central part of the Lena goldfield: Physical–chemical conditions of magmatism and metasomatism. *All-union Petrographic Symposium* 3: 184–189.

Caddey SW, Bachman RL, Campbell TJ, Reid RR, and Otto RP (1991) The Homestake gold mine, an early Proterozoic iron formation-hosted gold deposit, Lawrence County, South Dakota. *U.S Geological Survey Bulletin* 1857-J, pp. J1–J67.

Cail TL and Cline JS (2001) Alteration associated with gold deposition at the Getchell, Carlin-type gold deposit, north-central Nevada (abs.). *Geological Society of America, Abstracts with Program* 31(6): A-42.

Castor SB, Boden DR, Henry CD, et al. (2003) The Tuscarora Au–Ag district: Eocene volcanic-hosted epithermal deposits in the Carlin gold region, Nevada. *Economic Geology* 98: 339–366.

Chamberlain VE and Lambert RJ (1994) Lead isotopes and the sources of the Columbia River Basalt Group. *Journal of Geophysical Research* 99: 11805–11817.

Chang Z, Large RR, and Maslennikov V (2008) Sulfur isotopes in sediment-hosted orogenic gold deposits: Evidence for an early timing and a seawater sulfur source. *Geology* 36: 971–974.

Chen M, Mao J, Qu W, et al. (2007) Re–Os dating of Arsenian pyrites from the Lannigou gold deposit, Zhenfeng, Guizhou Province, and its geological significances. *Dizhi Lunping Geological Review* 53(3): 0371–5736.

Chesley JT and Ruiz J (1998) Crust–mantle interaction in large igneous provinces: Implications from the Re–Os isotope systematics in large igneous provinces: Implications from the Re–Os isotope systematics of the Columbia River flood basalts. *Earth and Planetary Science Letters* 154: 1–11.

Chitwood RA (2012) *Geochemistry and Mineralogy of the Eastern Ag-rich Epithermal Veins in the Midas District, Nevada*, USA, 117 p. Unpublished MS Thesis, Auburn University.

Chouinard A, Paquette J, and Williams-Jones A (2005a) Crystallographic controls on trace-element incorporation in auriferous pyrite from the Pascua epithermal high-sulfidation deposit, Chile–Argentina. *The Canadian Mineralogist* 43: 951–963.

Chouinard A, Williams-Jones A, Leonardson R, et al. (2005b) Geology and genesis of the multistage high-sulfidation epithermal Pascua Au–Ag–Cu deposit, Chile and Argentina. *Economic Geology* 100: 463–490.

Cline JS, Hofstra AH, Muntean JL, Tosdal RM, and Hickey KA (2005) Carlin-type gold deposits in Nevada: Critical geologic characteristics and viable models. *Economic Geology* 100th Anniversary Volume: 451–484.

Clout JM (1989) *Structural and Isotopic Studies of the Golden Mile Gold–telluride Deposit, Kalgoorlie, Western Australia*, 352 p. Unpublished PhD Thesis, Monash University, Victoria, Australia.

Cook HE (2005) Carbonate sequence stratigraphy: An exploration tool for sediment-hosted, disseminated gold deposits in the Great Basin. In: Rhoden HN, Steininger RC, and Vikre PG (eds.) *Geological Society of Nevada Symposium 2005. Window to the World*, pp. 19–24. Reno, NV: Geological Society of Nevada.

Cox SF (1999) Deformational controls on the dynamics of fluid flow in mesothermal gold systems. *Geological Society Special Publication* 155: 123–140.

Cox SF, Knackstedt MA, and Brown J (2001) Principles of structural control on permeability and fluid flow in hydrothermal systems. *Reviews in Economic Geology* 14: 1–24.

Dahl PS, Hamilton MA, Wooden JL, et al. (2006) 2480 Ma mafic magmatism in the northern Black Hills, South Dakota: A new link connecting the Wyoming and Superior cratons. *Canadian Journal of Earth Sciences* 43: 1579–1600.

Deditius AP, Utsunomiya S, Renock D, et al. (2008) A proposed new type of arsenian pyrite; composition, nanostructure and geological significance. *Geochimica et Cosmochimica Acta* 72: 2919–2933.

Deen JA, Rye RO, Munoz JL, and Drexler JW (1994) The magmatic hydrothermal system at Julcani, Peru; evidence from fluid inclusions and hydrogen and oxygen isotopes. *Economic Geology* 89: 1924–1938.

Deyell C, Leonardson R, Rye R, Thompson J, Bissig T, and Cooke D (2005) Alunite in the Pascua-Lama high-sulfidation deposit: Constraints on alteration and ore deposition using stable isotope geochemistry. *Economic Geology* 100: 131–148.

Dolzhenko VN (1991) Gold in siliceous pre-Mesozoic sediments of the eastern Tian Shan. *Geokhimiya* 1: 67–74 (in Russian).

Drummond SE and Ohmoto H (1985) Chemical evolution and mineral deposition in boiling hydrothermal systems. *Economic Geology* 80: 126–147.

Eilu P and Groves DI (2001) Primary alteration and geochemical dispersion haloes of Archaean orogenic gold deposits in the Yilgarn Craton: The pre-weathering scenario: Geochemistry. *Exploration, Environment, Analysis* 1: 183–200.

Elmer FL, White RW, and Powell R (2006) Devolatilization of metabasic rocks during greenschist-amphibolite facies metamorphism. *Journal of Metamorphic Geology* 24: 497–513.

Emsbo P, Groves DI, Hofstra AH, and Bierlein FP (2006) The giant Carlin gold province: A protracted interplay of orogenic, basinal, and hydrothermal processes above a lithospheric boundary. *Mineralium Deposita* 41: 517–525.

Emsbo P, Hofstra AH, Lauha EA, Griffin GL, and Hutchinson RW (2003) Origin of high grade gold ore, source of ore fluid components, and genesis of Meikle and neighboring Carlin-type deposits, northern Carlin trend, Nevada. *Economic Geology* 98: 1069–1106.

Etoh J, Izawa E, Watanabe K, Taguchi S, and Sekine R (2002) Bladed quartz and its relationship to gold mineralization in the Hishikari low-sulfidation epithermal gold deposit, Japan. *Economic Geology* 97: 184–1851.

Evans KA (2010) A test of the viability of fluid–wall rock interaction mechanisms for changes in opaque phase assemblage in metasedimentary rocks in the Kambalda-St. Ives goldfield, Western Australia. *Mineralium Deposita* 45: 207–213.

Evans KA, Phillips GN, and Powell R (2006) Rock-buffering of auriferous fluids in altered rocks associated with the golden mile-style mineralization, Kalgoorlie gold field, Western Australia. *Economic Geology* 101: 805–817.

Evans KA, Powell R, and Holland TJB (2010) Internally consistent data for sulphur-bearing phases and application to the construction of pseudosections for mafic greenschist facies rocks in Na_2O–CaO–K_2O–FeO–MgO–Al_2O_3–SiO_2–CO_2–O–S–H_2O. *Journal of Metamorphic Geology* 28: 667–687.

Fairmaid AM, Kendrick MA, Phillips D, and Fu B (2011) The origin and evolution of mineralizing fluids in a sediment-hosted orogenic-gold deposit, Ballarat East, Southeastern Australia. *Economic Geology* 106: 653–666.

Ferry JM (1981) Petrology of graphitic sulfide-rich schists from south-central Maine: An example of desulfidation during prograde regional metamorphism. *American Mineralogist* 66: 908–930.

Fleet ME, Mumin E, and Hamid A (1997) Gold-bearing arsenian pyrite and marcasite and arsenopyrite from Carlin trend gold deposits and laboratory synthesis. *American Mineralogist* 82: 182–193.

Frei R, Dahl PS, Frandsson MM, et al. (2009) Lead-isotope and trace-element geochemistry of Paleoproterozoic metasedimentary rocks in the Lead and Rochford basins (Black Hills, South Dakota, USA): Implications for genetic models, mineralization ages, and sources of leads in the Homestake gold deposit. *Precambrian Research* 172: 1–24.

Fyfe WS (1987) Tectonics, fluids and ore deposits: Mobilization and remobilization. *Ore Geology Reviews* 2: 21–36.

Fyfe WS, Price NJ, and Thompson AB (1978) *Fluids in the Earth's crust*. Amsterdam: Elsevier.

Getahun A (1994) *Fluid–Rock Reaction and Mineralization in Two High-level Volcanic Settings: Augustine Fumaroles and the Summitville Acid-sulfate Copper–Gold Deposit*. Unpublished PhD Dissertation, University of Oregon.

Gize AP (1999) A special issue on organic matter and ore deposits: Interactions, applications, and case studies [introduction]. *Economic Geology* 94: 963–965.

Goldfarb RJ, Ayuso R, Miller ML, et al. (2004) The Late Cretaceous Donlin Creek deposit, Southwestern Alaska – controls on epizonal formation. *Economic Geology* 99: 643–671.

Goldfarb RJ, Baker T, Dube B, et al. (2005) Distribution, character, and genesis of gold deposits in metamorphic terranes. *Economic Geology* 100th Anniversary Volume: 407–450.

Goldfarb RJ, Bradley D, and Leach DL (2010) Secular variation in economic geology. *Economic Geology* 105: 459–465.

Goldfarb RJ, Groves DI, and Gardoll S (2001) Orogenic gold and geologic time; a global synthesis. *Ore Geology Reviews* 18: 1–75.

Goldfarb RJ, Leach DL, Pickthorn WJ, and Paterson CJ (1988) Origin of lode–gold deposits of the Juneau gold belt, southeastern Alaska. *Geology* 16: 440–443.

Goldfarb RJ, Miller LD, Leach DL, and Snee LW (1997) Gold deposits in metamorphic rocks of Alaska. *Economic Geology Monograph* 9: 151–190.

Goldfarb RJ, Newberry RJ, Pickthorn WJ, and Gent CA (1991a) Oxygen, hydrogen, and sulfur isotope studies in the Juneau gold belt, southeastern Alaska – constraints on the origin of hydrothermal fluids. *Economic Geology* 86: 66–80.

Goldfarb RJ, Snee LW, Miller LD, and Newberry RJ (1991b) Rapid dewatering of the crust deduced from ages of mesothermal gold deposits. *Nature* 354: 296–299.

Golding L (1978) *Mineralogy, Geochemistry, and Origin of the Kalgoorlie Gold Deposits, Kalgoorlie*, 402 p. Unpublished PhD Thesis, University of Melbourne, Victoria, Australia.

Golding SD, Groves DI, McNaughton NJ, Mikucki EJ, and Sang J-H (1990) Source of ore fluid and ore components: sulphur isotope studies. *Gold deposits of the Archaean Yilgarn Block, Western Australia: nature, genesis and exploration guides*. Publication 20: 259–262.

Goldstrand PM and Schmidt KW (2000) Geology, mineralization, and ore controls at the Ken Snyder gold-silver mine, Elko County, Nevada. In: John DA and Wallace AR (eds.) *Geology and Ore Deposits 2000. The Great Basin and Beyond*, pp. 265–287. Reno, NV: Geological Society of Nevada.

Gorman PJ, Kerrick DM, and Connolly JAD (2006) Modeling open system metamorphic decarbonation of subducting slabs. *Geochemistry, Geophysics, and Geosystems* 7 (4): Q04007.

Grant JA (1986) The isocon diagram – a simple solution to Gresens' equation for metasomatic alteration. *Economic Geology* 81: 1976–1982.

Graupner T, Kempe U, Spooner ETC, Bray CJ, Kremenetsky AA, and Irmer G (2001) Microthermometric, laser Raman spectroscopic, and volatile-ion chromatographic analysis of hydrothermal fluids in the Paleozoic Muruntau-Au-bearing quartz vein ore field, Uzbekistan. *Economic Geology* 96: 1–23.

Graupner T, Niedermann S, Kempe U, Klemd R, and Bechtel A (2006) Origin of ore fluids in the Muruntau gold system: Constraints from noble gas, carbon isotope and halogen data. *Geochimica et Cosmochimica Acta* 70: 5356–5370.

Graupner T, Spooner ET, Kempe U, Bray CJ, and Kremenetsky AA (1998) Characterization of hydrothermal fluids from the Giant Muruntau Au-quartz vein ore field, Uzbekistan: Initial results. *APIFIS [Asian and Pacific International Fluid Inclusion Society] Newsletter*, Special Issue – *Mineral Forming Fluids and Ore Genesis*, 49–52

Gray J and Coolbaugh M (1994) Geology and geochemistry of Summitville, Colorado: An epithermal acid-sulfate deposit in a volcanic dome. *Economic Geology* 89: 1906–1923.

Groen JC, Bodnar RJ, and Campbell TJ (1989) Fluid inclusions in the Homestake iron formation of the northern Black Hills of South Dakota and their relationship to metamorphism. Program and Abstracts: PACROFI II, Second Biennial Pan-American Conference on Research on Fluid Inclusions, January 4–7, 1989, Virginia Polytechnic Institute & State University, Blacksburg, Virginia, vol. 2, p. 27.

Groves DI (1993) The crustal continuum model for late-Archaean lode-gold deposits of the Yilgarn Block, Western Australia. *Mineralium Deposita* 28: 366–374.

Groves DI, Goldfarb RJ, Gebre-Mariam M, Hagemann SG, and Robert F (1998) Orogenic gold deposits: A proposed classification in the context of their crustal distribution and relationship to other gold deposit types. *Ore Geology Reviews* 13: 7–27.

Gu XX, Zhang YM, Li BH, and Dong SY (2010) The relationship between gold mineralization and hydrocarbon accumulation in the Youjiang Basin, south China. *Geochimica et Cosmochimica Acta* 74 (12, supplement 1): A360.

Gustafson LB and Hunt JP (1975) The porphyry copper deposit at El Salvador, Chile. *Economic Geology* 70: 857–912.

Haeberlin Y, Moritz R, and Fontbote L (2003) Paleozoic orogenic gold deposits in the eastern Central Andes and its foreland, South America. *Ore Geology Reviews* 22: 41–59.

Haeberlin Y, Moritz R, Fontbote L, and Cosca M (2004) Carboniferous orogenic gold deposits at Pataz, eastern Andean Cordillera, Peru—geological and structural framework, paragenesis, alteration, and $^{40}Ar/^{39}Ar$ geochronology. *Economic Geology* 99: 73–112.

Hames W, Brueseke M, Kamenov G, Marma J, Saunders J, and Unger DL (2010) Geochemical and geochronologic constraints for evolution of the epithermal Au–Ag veins of the northern Great Basin: New evidence from Midas, Nevada. *Geological Society of America Abstracts with Programs* 40(5): 581

Hames WE, Unger DL, Saunders JA, and Kamenov GD (2009) Metallogeny and magmatism in the early Yellowstone hotspot. *Journal of Volcanology and Geothermal Research* 188: 214–224.

Hark JS, Frei R, Whitehouse MJ, Dahl PS (2008) New evidence for 2.01Ga rifting of the easternmost Wyoming craton (Black Hills, SD): Implications for breakup of a supercraton (Superia). *Geological Society of America Abstracts with Programs* 40(6): 145.

Hedenquist JW (1991) Boiling and dilution in the shallow portion of the Waiotapu geothermal system, New Zealand. *Geochimica et Cosmochimica Acta* 55: 2753–2765.

Hedenquist J, Arribas A, and Reynolds J (1998) Evolution of an intrusion-centered hydrothermal system: Far Southeast-Lepanto porphyry and epithermal Cu–Au deposits, Philippines. *Economic Geology* 93: 337–404.

Hedenquist JW, Arribas A Jr., and Urien E (2000) Exploration for epithermal gold deposits. *Reviews in Economic Geology* 13: 245–277.

Hedenquist JW and Henley RW (1985) Effects of CO_2 on freezing point depression measurements on fluid inclusions: Evidence from active geothermal systems and implications for epithermal ore deposition. *Economic Geology* 80: 1379–1406.

Hedenquist JW and Lowenstern JB (1994) The role of magmas in the formation of hydrothermal ore deposits. *Nature* 370: 519–527.

Hedenquist JW, Matsuhisa Y, Izawa E, White N, Giggenbach W, and Aoki M (1994) Geology, geochemistry, and origin of high sulfidation Cu–Au mineralization in the Nansatsu District, Japan. *Economic Geology* 89: 1–30.

Heinrich CA (2005) The physical and chemical evolution of low-salinity magmatic fluids at the porphyry to epithermal transition: A thermodynamic study. *Mineralium Deposita* 39: 864–889.

Heinrich CA (2006) How fast does gold trickle out of volcanoes? *Science* 314: 163–264.

Heinrich CA, Driesner T, Stefanosson A, and Seward TM (2004) Magmatic vapor contraction and the transport of gold from the porphyry environment to epithermal ore deposits. *Geology* 32: 761–764.

Heinrich CA, Gunther D, Audetat A, Ulrich T, and Frischknect R (1999) Metal fractionation between magmatic brine and vapor, determined by microanalysis of fluid inclusions. *Geology* 27: 755–758.

Henley RW, Mavrogeneses J, and Tanner D (2011) Sulfosalt melts and heavy metal (As–Sb–Bi–Sn–Pb–Tl) fractionation during volcanic gas expansion: The

El Indio (Chile) Paleo-Fumarole. *Geofluids* http://dx.doi.org/10.1111/j.1468-8123.2011.00357.x.

Ho SE, Groves DI, and Phillips GN (1990a) Fluid inclusions in quartz veins associated with Archaean gold mineralization: Clues to ore fluids and ore depositional conditions and significance to exploration. In: Herbert HK and Ho SE (eds.) *Stable Isotopes and Significance to Exploration, University of Western Australia, Western Australia, Publication 23*, pp. 35–50. Perth: Geology Department and University Extension.

Ho SE, Bennett JM, Cassidy KF, Hronsky JMA, Mikucki EJ, and Sang JH (1990a) Nature of ore fluid and transportational and depositional conditions in sub-amphibole facies deposits. In: Ho SE, Groves DI, and Bennett JM (eds.) *Gold Deposits of the Archaean Yilgarn Block*. University of Western Australia, Western Australia, Publication, vol. 20, pp. 198–211. Perth: Geology Department and University Extension.

Hodkiewicz PF, Groves DI, Davidson GJ, Weinberg RF, and Hagemann SG (2009) Influence of structural setting on sulphur isotopes in Archean orogenic gold deposits, Eastern Goldfields province, Yilgarn, Western Australia. *Mineralium Deposita* 44: 129–150.

Hofstra AH (1994) *Geology and Genesis of the Carlin-type Gold Deposits in the Jerritt Canyon District, Nevada*, 709 p. Unpublished PhD Dissertation, University of Colorado.

Hofstra AH, Christiansen WD, Zohar PB, and Tousignant G (2011) Lithogeochemistry of the Devonian Popovich Formation in the northern Carlin Trend, Nevada. In: Steininger R and Pennell B (eds.) *Great Basin Evolution and Metallogeny*, pp. 63–96. Reno, NV: Geological Society of Nevada.

Hofstra AH and Cline JS (2000) Characteristics and models for Carlin-type gold deposits, Chapter 5. In: Hagemann SG and Brown PE (eds.) *Gold In 2000*. *Reviews in Economic Geology* 13: 163–220. Colorado: Society of Economic Geologists.

Hofstra AH, Landis GP, Premo WR, Ressel MW, and Henry CD (2010) Evaluation of the role of magmatic volatiles from Eocene mafic to felsic igneous rocks in the formation of Carlin-type gold deposits in the Carlin trend and Jerritt Canyon district as constrained by He, Pb, Sr, and Nd isotopic data: In: Steininger R, and Pennell W (eds.) *Great Basin Evolution and Metallogeny*, pp. 63–96. Reno: Geological Society of Nevada.

Hofstra AH, Leventhal JS, Northrop HR, et al. (1991) Genesis of sediment-hosted disseminated gold deposits by fluid mixing and sulfidization: Chemical-reaction-path modeling of ore-depositional processes documented in the Jerritt Canyon district, Nevada. *Geology* 19: 36–40.

Hofstra AH, Zhang X-C, Emsbo P, et al. (2005) Source of ore fluids in Carlin-type gold deposits in the Dian-Qian-Gui area and West Qinling belt, P.R. China: Implications for genetic models. In: Mao J and Bierlein FP (eds.) *Mineral Deposit Research: Meeting the Global Challenge, Proceedings of the 8th Biennial SGA Meeting*, pp. 533–536. Beijing, China

Hough RM, Noble RRP, and Reich M (2011) Natural gold nanoparticles. *Ore Geology Reviews* 42: 55–61.

Hu R-Z, Su W-C, Bi X-W, Tu G-Z, and Hofstra AH (2002) Geology and geochemistry of Carlin-type gold deposits in China. *Mineralium Deposita* 37: 78–392.

Izawa E and Cunningham CG (1989) Hydrothermal breccia pipes and gold mineralization in the Iwashita orebody, Iwato deposit, Kyushu Japan. *Economic Geology* 84: 715–724.

Izawa E, Urashima Y, Ibaraki K, et al. (1990) The Hishikari gold deposit: High grade epithermal veins in quaternary volcanics of southern Kyushu, Japan. *Journal of Geochemical Exploration* 36: 1–56.

Jensen EP (2003) Magmatic and hydrothermal evolution of the Cripple Creek gold deposit Colorado, and comparisons with regional and global magmatic-hydrothermal systems associated with alkaline magmatism. Unpublished PhD Thesis, University of Arizona, Tuscon.

Jensen EP and Barton MD (2000) Gold deposits related to alkaline magmatism. *Reviews in Economic Geology* 13: 210–314.

Jia Y and Kerrich R (1999) Nitrogen isotope systematics of mesothermal lode gold deposits – metamorphic, granitic, meteoric water, or mantle origin? *Geology* 27: 1051–1054.

Jia Y, Kerrich R, and Goldfarb RJ (2003) Metamorphic origin of ore-forming fluids for orogenic gold-bearing quartz vein systems in the North American Cordillera; constraints from a reconnaissance study of $\delta^{15}N$, δD, and $\delta^{18}O$. *Economic Geology* 98: 109–123.

John DA (2001) Miocene and early Pliocene epithermal gold silver deposits in the in the northern Great Basin, western USA: Characteristics, distribution, and relationship to magmatism. *Economic Geology* 96: 1827–1853.

John DA, Hofstra AH, Fleck RJ, Brummer JE, and Saderholm EC (2003) Geologic setting and genesis of the Mule Canyon low-sulfidation epithermal gold–silver deposit, north-central Nevada. *Economic Geology* 98: 425–464.

John D, Thomason R, and McKee E (1989) Geology and K–Ar geochronology of the Paradise Peak Mine and the relationship of pre-basin and range extension to early Miocene precious metal mineralization in west-central Nevada. *Economic Geology* 84: 631–649.

Kamenov GD, Saunders JA, Hames WE, and Unger D (2007) Mafic magmas as sources for gold in middle-Miocene epithermal deposits of northern Great Basin, USA: Evidence from Pb isotopic compositions of native gold. *Economic Geology* 102: 1191–1195.

Kath RL (1990) *Petrogenesis of the Homestake Iron Formation and Associated Pelitic Rocks, Lead, South Dakota: Implications for P–T Paths, Fluid Evolution, and Gold Mineralization*, 228 p. Unpublished PhD Dissertation, South Dakota School of Mines and Technology.

Kempe U, Belyatsky BV, Krymsky RS, Kremenetsky AA, and Ivanov PA (2001) Sm–Nd and Sr isotope systematics of scheelite from the giant Au(–W) deposit Muruntau (Uzbekistan) – implications for the age and sources of Au mineralization. *Mineralium Deposita* 36: 379–392.

Kerrich R (1983) Geochemistry of gold deposits in the Abitibi greenstone belt. *Canadian Institute of Mining and Metallurgy* Special Volume 27: 75

Kerrich R (1987) The stable isotope geochemistry of Au–Ag vein deposits in metamorphic rocks. *Mineralogical Association of Canada, Short Course Handbook* 13: 287–336.

Kerrich R (1989) Lithophile element systematics of gold vein deposits in Archean greenstone belts; implications for source processes. *Economic Geology Monograph* 6: 508–519.

Kesler SE, Ewing RC, Deditius A, Reich MM, Utsunomiya S, and Chryssoulis S (2011) Role of arsenian pyrite in hydrothermal ore deposits: A history and update. In: Steiniger R and Pennell B (eds.) *Great Basin Evolution and Metallogeny*, pp. 233–245. Reno: Geological Society of Nevada.

Kesler SE, Fortuna J, Ye Z, et al. (2003) Evaluation of the role of sulfidation in deposition of gold, screamer section of the Betze-post Carlin-type Deposit, Nevada. *Economic Geology* 98: 1137–1157.

Kesler SE, Riciputi LC, and Ye Z (2005) Evidence for a magmatic origin for Carlin-type gold deposits; isotopic composition of sulfur in the Betze-post-Screamer Deposit, Nevada, USA. *Mineralium Deposita* 41: 127–136.

Kesler S, Russell N, Seaward M, et al. (1981) Geology and geochemistry of sulfide mineralization underlying the Pueblo Viejo gold–silver oxide deposit, Dominican Republic. *Economic Geology* 76: 1096–1117.

Klein EL and Fuzikawa K (2010) Origin of the CO_2-only fluid inclusions in the Palaeoproterozoic Carará vein-quartz gold deposit, Ipitinga Auriferous District, SE-Guiana Shield, Brazil. Implications for orogenic gold mineralization. *Ore Geology Reviews* 37: 31–40.

Koneev RI, Turesebekov AH, Ignatikov EN, Vasilevsky BB, and Rakhimov RR (2005) Au–Ag–Se–Te mineral and geochemical systems in black shale hosted deposits, Uzbekistan. In: Mao J-W and Bierlein FP (eds.) *Mineral Deposit Research: Meeting the Global Challenge*, pp. 1403–1405. Heidelberg: Springer.

Kouzmanov K, Pettke T, and Heinrich CA (2010) Direct analysis of ore-precipitating fluids: Combined IR microscopy and LA-ICP-MS study of fluid inclusions in opaque ore minerals. *Economic Geology* 105: 351–373.

Krienitz MS, Trumball RB, Hellmann A, Kolb J, Meyer FM, and Wiedenbeck M (2008) Hydrothermal gold mineralization at the Hira Buddini gold mine, India: Constraints on fluid evolution and fluid sources from boron isotopic compositions of tourmaline. *Mineralium Deposita* 43: 421–434.

Lambeck Alexis, Mernagh TP, and Wyborn L (2011) Are iron-rich sedimentary rocks the key to the spike in orogenic gold mineralization in the Paleoproterozoic? *Economic Geology* 106: 321–330.

Langmuir D (1997) *Aqueous Environmental Geochemistry*. New York: Prentice Hall 600 p.

Large RR, Bull SW, and Gilbert S (2011a) Multiple syngenetic metalliferous horizons enriched in V, As, Mo, Se, Ni, Ag, Zn, and Au in the Northern Carlin Trend: Implications for the genesis of world class gold–arsenic deposit. In: Steiniger R and Pennell B (eds.) *Great Basin Evolution and Metallogeny*, pp. 1–16. Reno: Geological Society of Nevada.

Large RR, Bull SW, and Maslennikov VV (2011b) A carbonaceous sedimentary source-rock model for Carlin-type and orogenic gold deposits. *Economic Geology* 106: 331–358.

Large RR, Danyushevsky L, Hollit C, et al. (2009) Gold and trace element zonation in pyrite using a laser imaging technique; implications for the timing of gold in orogenic and Carlin-style sediment-hosted deposit. *Economic Geology* 104: 635–668.

Leavitt ED and Arehart GB (2005) Alteration, geochemistry, and paragenesis of the Midas epithermal gold–silver deposit, Elko County, Nevada. In: Rhoden HN, Steinenger RC, and Vikre PG (eds.) *Window to the World*, pp. 527–563. Reno, NV: Geological Society of Nevada.

Leavitt ED, Spell TL, Goldstrand PM, and Arehart GG (2004) Geochronology of the Midas low-sulfidation gold-silver deposit, Elko County Nevada. *Economic Geology* 99: 1665–1686.

Levinson AA (1974) *Introduction to Exploration Geochemistry*. Wilmette, IL: Applied Publishing Ltd. 614 p.

Lindgren W (1933) *Mineral Deposits*, 4th ed. New York: McGraw-Hill.

Longo AA, Dilles JH, Grunder A, and Duncan R (2010) Evolution of calc-alkaline volcanism and associated hydrothermal gold deposits at Yanacocha, Peru. *Economic Geology* 105: 1191–1241.

Loucks RR and Mavrogenes JA (1999) Gold solubility in supercritical hydrothermal brines measured in synthetic fluid inclusions. *Science* 284: 159–2163.

Lund K (2008) Geometry of the Neoproterozoic and Paleozoic rift margin of western Laurentia: Implications for mineral deposit settings. *Geosphere* 4: 429–444.

Mackenzie DJ, Craw D, and Mortensen J (2008) Structural controls on orogenic gold mineralization in the Klondike goldfield, Canada. *Mineralium Deposita* 46: 435–448.

Mao J, Li Y, Goldfarb RJ, He Y, and Zaw K (2003) Fluid inclusion and noble gas studies of the Dongping gold deposit, Hebei province, China: A mantle connection for mineralization? *Economic Geology* 98: 517–534.

Mao J, Yumin Q, Goldfarb R, Zhang Zaochong, Garwin S, and Ren F (2002) Geology, distribution, and classification of gold deposits in the western Qinling belt, central China. *Mineralium Deposita* 37: 352–377.

Matsuhisa Y, Morishita Y, and Sato T (1985) Oxygen and carbon isotope variations in gold-bearing hydrothermal veins in the Kushikino mining area, southern Kyushu, Japan. *Economic Geology* 80: 283–293.

McCuaig TC and Kerrich R (1998) P–T–t-deformation-fluid characteristics of lode gold deposits; evidence from alteration systematics. *Ore Geology Reviews* 12: 381–454.

Meyer C, Shea E, and Goddard C (1968) Ore deposits at Butte, Montana. In: Ridge JD (ed.) *Ore Deposits of the United States 1933–1967 [Graton-sales volume]*, vol. 2, pp. 1363–1416. New York: American Institute of Mining, Metallurgical, and Petroleum Engineers.

Mikucki EJ (1998) Hydrothermal transport and depositional processes in Archean lode-gold systems; a review. *Ore Geology Reviews* 13: 307–321.

Miller LD, Goldfarb RJ, Gehrels GE, and Snee LW (1994) Genetic links among fluid cycling, vein formation, regional deformation, and plutonism in the Juneau gold belt, southeastern Alaska. *Geology* 22: 203–207.

Morelli RM, Bell CC, Creaser RA, and Simonetti A (2010) Constraints on the genesis of gold mineralization at the Homestake gold deposit, Black Hills, South Dakota, from rhenium-osmium sulfide geochronology. *Mineralium Deposita* 45: 461–480.

Morelli RM, Creaser RA, Seltmann R, Stuart FM, Selby D, and Graupner T (2007) Age and source constraints for the giant Muruntau gold deposit, Uzbekistan, from coupled Re–Os–He isotopes in arsenopyrite. *Geology* 35: 795–798.

Morteani G, Ruggieri G, Moller P, and Preinfalk C (2010) Geothermal mineralized scales in the pipe system of the geothermal Piancastagnaio power plant (Mt. Amiata geothermal area): A key to understand the stibnite, cinnabar and gold mineralization of Tuscany (central Italy). *Mineralium Deposita* 46: 197–210.

Mortensen JK, Craw D, MacKenzie DJ, Gabites JE, and Ullrich T (2010) Age and origin of orogenic gold mineralization in the Otago Schist Belt, South Island, New Zealand: Constraints from lead isotope and $^{40}Ar/^{39}Ar$ dating studies. *Economic Geology* 105: 777–793.

Muntean JL, Cline JS, Simon AC, and Longo AA (2011) Magmatic-hydrothermal origin of Nevada's Carlin-type gold deposits. *Nature Geoscience* 4: 122–127.

Muntean J, Kesler S, Russell N, and Polanco J (1990) Evolution of the Monte Negro acid-sulfate Au–Ag deposit, Pueblo Viejo, Dominican Republic; important factors in grade development. *Economic Geology* 85: 1738–1758.

Murowchick JB (1992) Marcasite inversion and the petrographic determination of pyrite ancestry. *Economic Geology* 87: 1141–1152.

Naden J and Shepherd TJ (1989) Role of methane and carbon dioxide in gold deposition. *Nature* 342: 793–795.

Nagayama T (1993) Precipitation sequence of veins at the Hishikari deposits, Kyushu, Japan. *Resource Geology* Special Issue 14(Japan): 13–28.

Nash JT (1972) Fluid inclusion studies of some gold deposits in Nevada. *U.S. Geological Survey Professional Paper* 800C: C15–C19.

Nash JT, Utterback WC, and Trudel WS (1995) Geology and geochemistry of Tertiary volcanic host rocks, Sleeper gold-silver deposit, Humboldt County, Nevada. *U.S. Geological Survey Bulletin* 2090, 63pp.

Neumayr P, Petersen KJ, Gauthier L, et al. (2005) Mapping of hydrothermal alteration and geochemical gradients as a tool for conceptual targeting: St. Ives Gold Camp, Western Australia. In: Bierlein FP and Mao J (eds.) *Mineral Deposit Research: Meeting the Global Challenge*, pp. 1479–1482. Berlin: Springer.

Neumayr P, Walshe J, Hagemann S, et al. (2008) Oxidized and reduced mineral assemblages in greenstone belt rocks of the St. Ives gold camp, Western Australia: Vectors to high-grade ore bodies in Archaean gold deposits? *Mineralium Deposita* 43: 363–371.

Phillips GN and Evans KA (2004) Role of CO_2 in the formation of gold deposits. *Nature* 429: 860–863.

Phillips GN and Gibb HFC (1993) *A Century of Gold Mining at Kalgoorlie*. *Economic Geology Research Unit Contribution 45*, 68 p. Townsville: Key Centre in Economic Geology.

Phillips GN, Groves DI, and Brown IJ (1987) Source requirements for the Golden Mile, Kalgoorlie – significance to the metamorphic replacement model for Archean gold deposits. *Canadian Journal of Earth Sciences* 24: 1643–1651.

Phillips GN, Groves DI, and Kerrich R (1996) Factors in the formation of the giant Kalgoorlie gold deposit. *Ore Geology Reviews* 10: 295–317.

Phillips GN, Groves DI, Neall FB, Donnelly TH, and Lambert IB (1986) Anomalous sulfur isotope compositions in the Golden Mile, Kalgoorlie. *Economic Geology* 81: 2008–2015.

Phillips GN and Powell R (2009) Formation of gold deposits: Review and evaluation of the continuum model. *Earth-Science Reviews* 94: 1–21.

Phillips GN and Powell R (2010) Formation of gold deposits: A metamorphic devolatilization model. *Journal of Metamorphic Geology* 28: 689–718.

Pickthorn WJ, Goldfarb RJ, and Leach DL (1987) Dual origins of lode gold deposits in the Canadian Cordillera—discussion. *Geology* 15: 471–473.

Pitcairn IK, Teagle DAH, Craw D, Olivo GR, Kerrich R, and Brewer TS (2006) Source of metals and fluids in orogenic gold deposits. Insights from the Otago and Alpine schists, New Zealand. *Economic Geology* 101: 1525–1546.

Qiu Y and McNaughton NJ (1999) Source of Pb in orogenic lode–gold mineralisation; Pb isotope constraints from deep crustal rock from the southwestern Archaean Yilgarn Craton, Australia. *Mineralium Deposita* 34: 366–381.

Ransome FL (1909) Geology and ore deposits of goldfield, Nevada. *U.S. Geological Survey Professional Paper* 66: 258

Redak S (2005) *Colorado Grande (Midas) Trace Element Zonation Study*, 21 p. Unpublished Internal Report Prepared for Newmont Mining Company.

Reed MH (1997) Hydrothermal alteration and its relationship to ore fluid composition. In: Barnes HL (ed.) *Geochemistry of Hydrothermal Ore Deposits*, 3rd, pp. 303–366. New York: John Wiley & Sons.

Reed M and Palandri J (2006) Sulfide mineral precipitation from hydrothermal fluids. *Reviews in Mineralogy and Geochemistry* 60: 609–632.

Reed M, Rusk B, and Palandri J (2013) The Butte magmatic-hydrothermal system: One fluid yields all alteration and veins. *Economic Geology* (in press).

Reich M, Kesler SE, Utsunomiya S, Palenik CS, Chryssoulis SL, and Ewing RC (2005) Solubility of gold in arsenian pyrite: *Geochimica et Cosmochimica Acta* 69: 2781–2796.

Ressel MW and Henry CD (2006) Igneous geology of the Carlin Trend, Nevada; development of the Eocene plutonic complex and significance for Carlin-type gold deposits. *Economic Geology* 101: 347–383.

Richards JP (1995) Alkalic-type epithermal gold deposits – a review. In: Thompson JFH (ed.) *Magmas, Fluids, and Ore Deposits*. Mineralogic Association of Canada Short Course 23: 367–400.

Richards JP (2009) Postsubduction porphyry Cu–Au and epithermal Au deposits: Products of remelting of subduction-modified lithosphere. *Geology* 37: 247–250.

Ridley JR and Diamond LW (2000) Fluid chemistry of orogenic lode gold deposits and implications for genetic models. *Reviews in Economic Geology* 13: 141–162.

Riederer MJ (2007) *Fluid Inclusion Study of the Midas Low-sulfidation Epithermal Au/Ag Mine, Elko County, Nevada*, 131 p. Unpublished MSc Thesis, University of Wisconsin, Madison.

Romberger SB (1988) Geochemistry of gold in hydrothermal deposits. *U.S. Geological Survey Bulletin* 1857-A: A9–A25.

Rusinova OV and Rusinov VL (2003) Metasomatism in the Muruntau ore field, Western Uzbekistan. *Geology of Ore Deposits* 45: 66–85.

Rusk BG, Reed MH, and Dilles JH (2008) Fluid inclusion evidence for magmatic-hydrothermal fluid evolution in the porphyry copper–molybdenum deposit at Butte, Montana. *Economic Geology* 103: 307–334.

Rye R, Bethke P, and Wasserman M (1992) The stable isotope geochemistry of acid sulfate alteration. *Economic Geology* 87: 225–262.

Rye DM and Rye RO (1974) Homestake Gold Mine, South Dakota; I, stable isotope studies. *Economic Geology* 69: 293–317.

Saito M and Sato E (1978) On the recent exploration at the Iwato gold mine. *Mining Geology* 28: 191–202.

Sales R and Meyer C (1948) Wall rock alteration at Butte, Montana. *American Institute Mining and Metallurgical Engineers, Technical Publication* 2400: 1–25.

Saunders JA (1986) *Petrology, Mineralogy, and Geochemistry of Representative Gold Telluride Ores from Colorado*, 171 p. Unpublished PhD Thesis, Colorado School of Mines, Golden, CO.

Saunders JA (1988) Textural and geochemical characteristics of gold mineralization from the Cresson Mine, Cripple Creek district, Colorado, U.S.A. *Institution of Mining and Metallurgy (London) Transactions* 97: B36–B39.

Saunders JA (1990) Colloidal transport of gold and silica in epithermal precious metal systems: Evidence from the Sleeper deposit, Humboldt County, Nevada. *Geology* 18: 757–760.

Saunders JA (1991) Gold deposits of the Boulder County gold district, Colorado. *U.S. Geological Survey Bulletin* 1857-I: 137–148.

Saunders JA (1994) Silica and gold textures at the Sleeper deposit, Humboldt County, Nevada. Evidence for colloids and implications for ore-forming processes. *Economic Geology* 89: 628–638.

Saunders JA (2010) Geologic time and epithermal ore formation. *Society of Economic Geologist's Newsletter* 2010: 10–11.

Saunders JA (2012) Textural evidence of episodic introduction of metallic nanoparticles into bonanza epithermal ores. *Minerals* 2: 228–243.

Saunders JA and Brueseke ME (2012) Volatility of Te and Se and the geochemistry of epithermal Au–Ag ores in western USA. *Economic Geology* 107: 165–172.

Saunders JA and May ER (1986) Bessie G: A high-grade epithermal gold telluride deposit, La Plata County, Colorado. In: Macdonald AJ (ed.) *GOLD'86, An International Symposium on the Geology of Gold*, pp. 436–444. Toronto: Konsult International Inc.

Saunders JA and Schoenly PA (1995) Boiling, colloid nucleation and aggregation, and the genesis of bonanza gold mineralization at the Sleeper deposit, Nevada. *Mineralium Deposita* 30: 199–211.

Saunders JA, Schoenly PA, and Cook RB (1996) Electrum disequilibrium crystallization textures in volcanic-hosted bonanza epithermal gold deposits. In: Coyner AR and Fahey PL (eds.) *Geology and Ore Deposits of the America Cordillera Symposium*, pp. 173–179. Reno, NV: Geological Society of Nevada.

Saunders JA, Unger DL, Kamenov GD, Fayek M, Hames WE, and Utterback WC (2008) Genesis of Middle Miocene Yellowstone-hotspot-related bonanza epithermal Au–Ag deposits, Northern Great Basin Region, USA. *Mineralium Deposita* 43: 715–734.

Saunders JA, Kamenov GD, Brueseke ME, Hames W, and Mathur R (2011a) Hydrothermal precious-metal and sulfide nanoparticle transport and deposition and the genesis of bonanza epithermal ores (abs). *Geological Society of America Abstracts with Programs* 43(5): 514.

Saunders JA, Vikre P, Unger DL, and Beasley L (2011b) Colloidal and physical transport textures exhibited by electrum and naumannite in bonanza epithermal veins from western USA, and their significance. In: Steininger R and Pennell W (eds.) *Great Basin Evolution and Metallogeny*, pp. 825–832. Reno: Geological Society of Nevada.

Saunders JA, Kamenov GD, Hofstra AH, Unger DL, Creaser RA, and Barra F (2011c) "Forensic" geochemical approaches to constrain the source of Au–Ag in low-sulfidation epithermal ores. In: Steininger R, and Pennell W (eds.) *Great Basin Evolution and Metallogeny*, pp. 693–700. Reno, NV: Geological Society of Nevada.

Schmidt-Mumm A, Oberthuer T, Vetter U, and Blenkinsop TG (1997) High CO_2 content of fluid inclusions in gold mineralization in the Ashanti belt, Ghana—a new category of ore forming fluids? *Mineralium Deposita* 32: 107–118.

Seward TM (1973) Thio complexes of gold and the transport of gold in hydrothermal ore solutions. *Geochimica et Cosmochimica Acta* 37: 379–399.

Shackleton JM, Spry PG, and Bateman R (2003) Telluride mineralogy of the Golden Mile deposit, Kalgoorlie, Western Australia. *The Canadian Mineralogist* 41: 1503–1524.

Shelton KL, So CS, Haeussler GT, Hi SJ, and Lee KY (1990) Geochemical studies of the Tongyoung gold–silver deposits, Republic of Korea: Evidence of meteoric water dominance in a Te-bearing epithermal system. *Economic Geology* 85: 1114–1132.

Sherlock RL, Tosdal RM, Lehrman NJ, et al. (1995) Origin of the McLaughlin mine sheeted vein complex: Metal zoning, fluid inclusion and isotopic evidence. *Economic Geology* 90: 2156–2181.

Shikazono N and Nagayama T (1993) Origin and deposition mechanisms of the Hishikari gold–quartz–adularia mineralization. *Resource Geology* Special Issue 14(Japan): 47–56

Shimizu T, Matsueda H, Ishiyama D, and Matsubaya O (1998) Genesis of epithermal Au–Ag mineralization of the Koryu Mine, Hokkaido, Japan. *Economic Geology* 93: 303–325.

Sibson RH, Robert F, and Poulsen KH (1988) High-angle reverse faults, fluid-pressure cycling, and mesothermal gold–quartz deposits. *Geology* 16: 551–555.

Sillitoe RH (1997) Characteristics and controls on the largest porphyry copper-gold and epithermal gold deposits in the circum-Pacific region. *Australian Journal of Earth Sciences* 44: 373–388.

Sillitoe RH (2010) Porphyry copper systems. *Economic Geology* 105: 3–41.

Sillitoe RH and Hedenquist JW (2003) Linkages between volcanotectonic settings, ore-fluid compositions, and epithermal precious metal deposits. *Society of Economic Geologists* Special Publication, 10: 315–343.

Sillitoe RH and Lorson R (1994) Epithermal gold–silver–mercury deposits at Paradise Peak, Nevada; ore controls, porphyry gold association, detachment faulting, and supergene oxidation. *Economic Geology* 89: 1228–1248.

Simmons SF and Brown KL (2006) Gold in magmatic hydrothermal solutions and the rapid formation of a giant gold deposit. *Science* 314: 288–291.

Simmons SF and Christensen BW (1994) Origins of calcite in a boiling geothermal system. *American Journal of Science* 294: 361–400.

Simmons SF, White NC, and John DA (2005) Geological characteristics of epithermal precious and base metal deposits. *Economic Geology* 100th Anniversary Volume: 485–522.

Simon K (2001) Does δD from fluid inclusions in quartz reflect the original hydrothermal fluid? *Chemical Geology* 177: 483–495.

Smith TE (1981) Geology of the Clearwater Mountains, south-central Alaska: *Alaska Division of Geological and Geophysical Surveys Report* 60, 72 p.

So C-S, Dunchenko VY, Yun S-T, Park M-S, Choi S-G, and Shelton KL (1995) Te- and Se-bearing epithermal Au–Ag mineralization, Prasolovskoye, Kunashir Island, Kuril island arc. *Economic Geology* 90: 105–117.

So C-S and Yun S-T (1996) Geochemical evidence of progressive meteoric water interaction in epithermal Au–Ag mineralization, Jeonju-Buan District, Republic of Korea. *Economic Geology* 91: 636–646.

Spycher NF and Reed MH (1989) Evolution of a Broadlands-type epithermal ore fluid along alternate paths: Implication for the transport and deposition of base, precious, and volatile metals. *Economic Geology* 84: 328–359.

Steven TA and Ratte JC (1960) Geology and ore deposits of Summitville district, San Juan Mountains, Colorado. *U.S. Geological Survey Professional Paper* 487: 1–9.

Stoffregen R (1987) Genesis of acid-sulfate alteration and Au–Cu–Ag mineralization at Summitville, Colorado. *Economic Geology* 82: 1575–1591.

Stuwe K (1998) Tectonic constraints on the timing relationships of metamorphism, fluid production and gold-bearing quartz vein emplacement. *Ore Geology Reviews* 13: 219–228.

Su W, Heinrich CA, Pettke T, Zhang X, Hu R, and Xia B (2009a) Sediment-hosted gold deposits in Guizhou, China; products of wall-rock sulfidation by deep crustal fluids. *Economic Geology* 104: 73–93.

Su W, Hu R, Xia B, Xia Y, and Liu Y (2009b) Calcite Sm/Nd isochron age of the Shuiyindong Carlin-type gold deposit, Guizhou, China. *Chemical Geology* 258: 269–274.

Symonds RB, Rose WI, Bluth G, and Gerlach T (1994) Volcanic gas studies: Methods, results, and applications. In: Carroll MR and Holloway JR (eds.) *Volatiles in Magmas. Reviews in Mineralogy* 30: 1–66.

Tauson VL (1999) Gold solubility in the common gold-bearing minerals; experimental evaluation and application to pyrite. *European Journal of Mineralogy* 11: 937–947.

Taylor BE (2007) Epithermal gold deposits. In: Goodfellow WD (ed.) *Mineral Deposits of Canada: A synthesis of major Deposit Types, District Metallogeny, The Evolution of Geological Provinces, and Exploration Methods*. Geological Association of Canada, Mineral Deposits Division, Special Publication No. 5: 113–139.

Teal L and Benavides A (2010) History and overview of the Yanacocha Mining District, Cajamarca, Peru. *Economic Geology* 105: 1173–1190.

Tenthorey E and Cox SF (2003) Reaction-enhanced permeability during serpentinite dehydration. *Geology* 31: 921–924.

Thomas HV, Large RR, Bull SW, et al. (2011) Pyrite and pyrrhotite textures and composition in sedimentary rocks, laminated quartz veins, and gold reefs at the Bendigo mine, Australia: Insights for ore genesis. *Economic Geology* 106: 1–31.

Thompson TB (2005) Carlin-type gold deposits - Products of magmatism? SME-AIME Annual Meeting and Exhibition, Feb. 28-Mar. 2, Salt Lake City, Utah, Technical Program, p. 50. (abstract)

Tohma Y, Imai A, Sanematsu K, et al. (2010) Characteristics and mineralization age of the Fukusen No. 1 Vein, Hishikari epithermal gold deposits, southern Kyushu, Japan. *Resource Geology* 60: 348–358.

Tombros S, St. Seymour K, and Williams-Jones AE (2010) Controls on tellurium in base, precious, and telluride minerals in the Panormos Bay Ag–Au–Te deposits, Tinos Island, Cyclades, Greece. *Economic Geology* 105: 1097–1111.

Tomkins AG (2010) Windows of metamorphic sulfur liberation in the crust: Implications for gold deposit genesis. *Geochimica et Cosmochimica Acta* 74: 3246–3259.

Tomkins AG and Grundy C (2009) Upper temperature limits of orogenic gold deposit formation: Constraints from the granulite-hosted Griffin's Find deposit, Yilgarn craton. *Economic Geology* 104: 669–685.

Tosdal RM, Cline JS, Fanning C, and Wooden JL (2003) Lead in the Getchell-Turquoise Ridge Carlin-type gold deposits from the perspective of potential igneous and sedimentary rock sources in northern Nevada; implications for fluid and metal sources. *Economic Geology* 98: 1189–1211.

Urashima Y (1975) Gold–silver deposits of Japan. *Mining and Metallurgical Institute of Japan* 1: 1–42.

Vielreicher NM, Groves DI, Snee LW, Fletcher IB, and McNaughton NJ (2010) Broad synchroneity of three gold mineralization styles in the Kalgoorlie Gold Field: SHRIMP, U-Pb, and $^{40}Ar/^{39}Ar$ geochronological evidence. *Economic Geology* 105: 187–227.

Vielreicher RM, Vielreicher NM, Hagemann SG, and Jones G (2002) Fault zone evolution and its controls on ore-grade distribution at the Jian Cha Ling gold deposit, western Qinling region, central China. *Mineralium Deposita* 38: 538–554.

Vikre PG (1985) Precious metal vein system in the National district, Humboldt County, Nevada. *Economic Geology* 80: 360–393.

Vikre PG (1989) Ledge formation at the Sandstorm and Kendall gold mines, Goldfield, Nevada. *Economic Geology* 84: 2115–2138.

Wallace AR (2003) Geology of the Ivanhoe Hg–Au district, Northern Nevada: Influence of Miocene volcanism, lakes, active faulting on epithermal mineralization. *Economic Geology* 98: 409–424.

White RW, Powell R, and Phillips GN (2003) A mineral equilibria study of the hydrothermal alteration in mafic greenschist facies rocks at Kalgoorlie, Western Australia. *Journal of Metamorphic Geology* 21: 455–468.

Wilde AR, Layer P, Mernagh T, and Foster J (2001) The giant Muruntau gold deposit: Geologic, geochronologic, and fluid inclusion constraints on ore genesis. *Economic Geology* 96: 633–644.

Williams-Jones AE and Heinrich CA (2005) Vapor transport of metals and the formation of magmatic-hydrothermal ore deposits. *Economic Geology* 100: 1287–1312.

Willman CE, Korsch RJ, Moore DH, et al. (2010) Crustal-scale fluid pathways and source rocks in the Victorian gold province, Australia: Insights from deep seismic reflection profiles. *Economic Geology* 105: 895–915.

Yermolayev NP, Sozinov NA, Chinenov VA, Goryachkin NI, and Nikiforov AV (1995) Forms taken by platinum metals in gold ores from black shales. *Geochemistry International* 32: 81–90.

Yuningsih ET, Matsueda H, Rosana MF, and Aryani SC (2011) Physicochemical conditions o f the Se- and Te-rich epithermal deposits of western Java, Indonesia (abs). *Geological Association of Canada/Mineralogical Association of Canada Abstracts* 34: 237–238.

Zacharias J, Fryda J, Paterova B, and Mihaljevic M (2004) Arsenopyrite and As-bearing pyrite from the Roudny deposit, Bohemian Massif. *Mineralogical Magazine* 68: 31–46.

Zairi NM and Kurbanov NK (1992) Isotopic-geochemical model of ore genesis in the Muruntau ore field. *International Geology Review* 34: 88–94.

Zhang X and Spry PG (1994) Petrological, mineralogical, fluid inclusion, and stable isotope studies of the Gies gold–silver telluride deposit, Judith Mountains, Montana. *Economic Geology* 89: 602–627.